Chapter 9. LARGE-SCALE BIOGEOCHEMICAL–PHYSICAL INTERACTIONS IN ELEMENTAL CYCLES

NICOLAS GRUBER

University of California, Los Angeles

JORGE L. SARMIENTO

Princeton University

Contents

1. Introduction

Why is the distribution of most chemicals not uniform within the ocean (Fig. 9.1)? In the absence of sources and sinks the effect of ocean circulation and mixing would be to smooth the distribution of chemicals. An important reason for nonuniformity is the increase in concentration that occurs in regions of evaporation, and the reduction in concentration that occurs in regions of rainfall or river input at the ocean atmosphere interface. Evaporation, precipitation, and river input lead to concentration ranges usually well below 10%, as evidenced in the oceanic variability of salinity. However, as Fig. 9.1 shows, many chemicals have concentration ranges much greater than this. The concentration of inorganic nitrogen, for example, is more than five times smaller near the surface than in the deep ocean. Dissolved inorganic carbon shows a surface depletion that is also substantially larger than the 10% variation that could be induced by freshwater fluxes.

The primary mechanism that drives such large concentration gradients is the use of dissolved inorganic chemicals by living organisms for formation of organic matter

The Sea, Volume 12, edited by Allan R. Robinson, James J. McCarthy, and Brian J. Rothschild
ISBN 0-471-18901-4

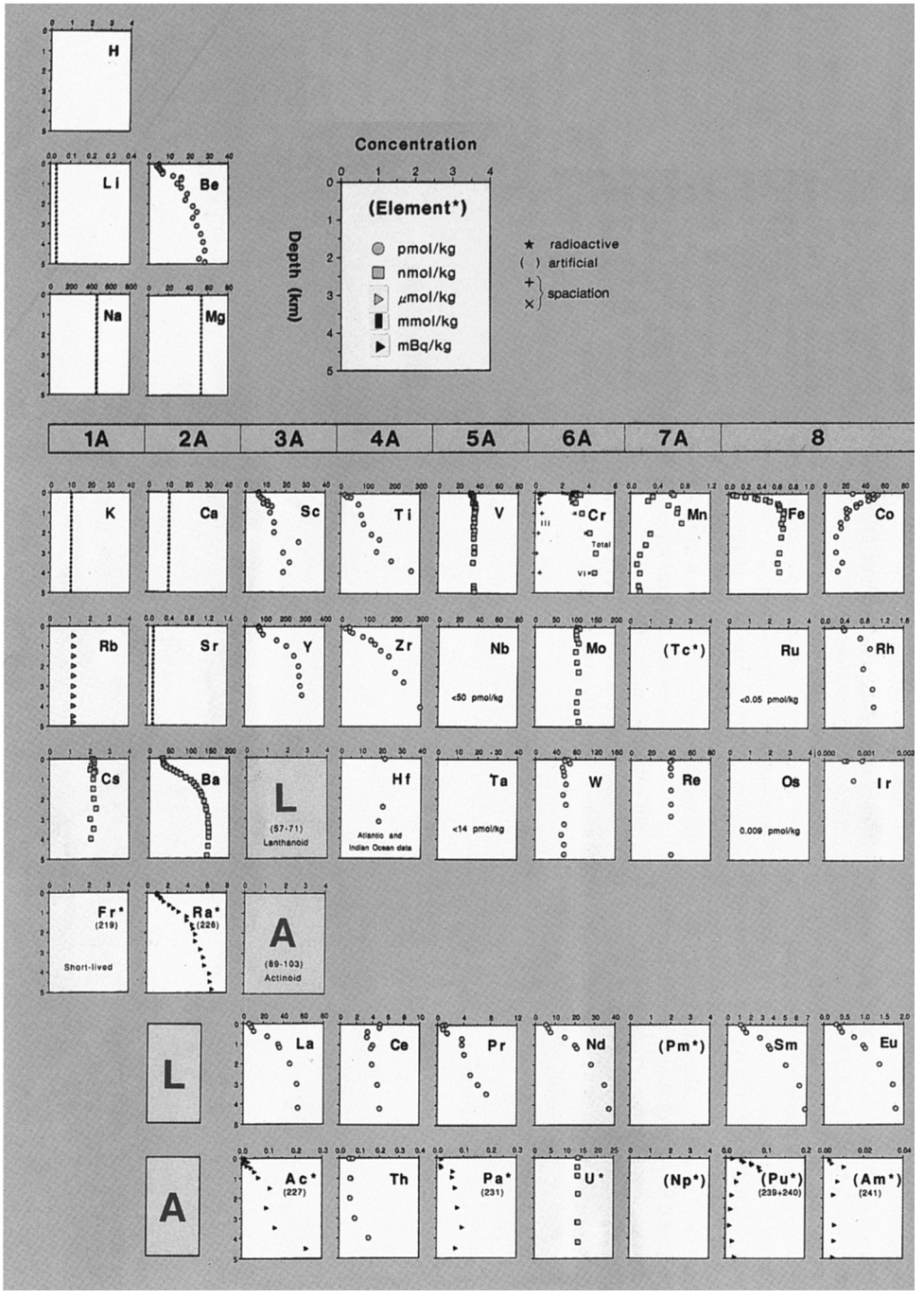

Fig. 9.1. Plots of vertical profiles of elements in the North Pacific

in the North Pacific Ocean

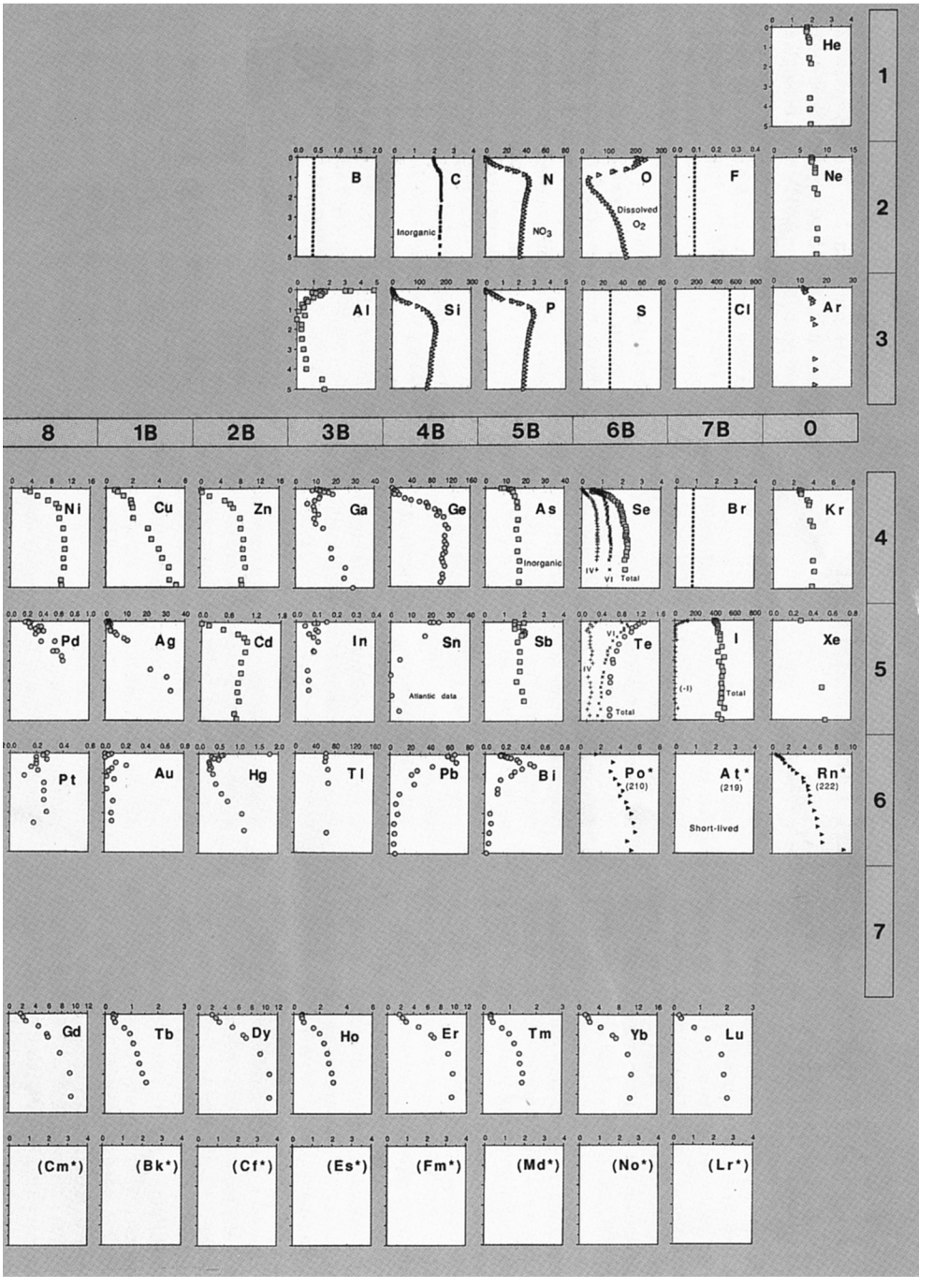

arranged as in the periodic table of elements. (From Nozaki, 1997.)

and inorganic solids. Photosynthetic organisms use the energy from light in the upper part of the ocean to produce both particulate and dissolved organic matter and a wide range of inorganic solids as well. These biogenic materials are often transported long distances before being converted back to dissolved inorganic chemicals by processes such as remineralization and dissolution. The largest such transports are vertical, giving rise to greatly reduced concentrations in the surface ocean and enhanced concentrations in the abyss. A few chemicals, the most important being oxygen, are affected by these processes in the opposite direction. They are released during photosynthesis and consumed during remineralization. The wide range of biological and associated processes that affect such chemicals are referred to as biogeochemical processes.

The view that therefore emerges with regard to the large-scale distribution of chemicals in the ocean is one where biogeochemical processes are constantly creating spatial and temporal gradients in the chemicals, whereas ocean circulation and mixing are in general attempting to homogenize these gradients. The resulting distribution of the chemicals in the ocean can thus be understood as the result of a complex interplay between biogeochemical cycles and ocean physics. These large-scale biogeochemical/physical interactions are the focus of this chapter. In particular, we are interested in determining the relative roles of the various gradient makers in creating the large-scale distribution of chemicals in the ocean. We focus our discussion on the two most important biogeochemical elements, carbon and nitrogen. We include the cycling of phosphorus and oxygen since they allow us to gain much additional information about carbon and nitrogen.

We start our discussion with a very simple model that highlights many of the concepts that will be applied and discussed in this chapter. The simplest model that can be devised to understand the spatial distribution of chemicals in the ocean (especially the vertical) is a two-box model as depicted in Fig. 9.2. We apply this model first to nitrogen.

Photosynthesis in the surface box reduces the surface inorganic nitrogen concentration (N_s) and forms organic matter. A fraction of this organic matter is exported to the deep box (Φ^N), where it gets remineralized, leading to an increase in the deep inorganic nitrogen concentration (N_d). This process is often termed the *soft tissue pump* (Volk and Hoffert, 1985), since it leads to the net removal of tracers in the surface waters and a net addition in deep waters. The movement of water between the surface and deep ocean is complicated, but it often suffices to represent it very simply by a volume exchange rate ν between two well mixed boxes. We can thus write the inorganic nitrogen budget in the deep box as the balance between the addition of material from remineralization (Φ^N) and the loss of material by mixing with the surface waters [$\nu(N_s - N_d)$]:

$$V_d \frac{dN_d}{dt} = \nu(N_s - N_d) + \Phi^N \tag{1}$$

where V_d is the volume of the deep box. The steady-state solution [i.e., when the time rate of change is zero ($dN_d/dt = 0$)] is simple. The downward transport of nitrogen by organic matter is equal to the physical transport of nitrate from the abyss into the surface box.

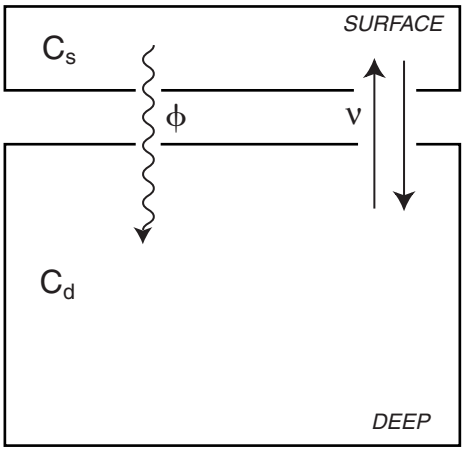

Fig. 9.2. Schematic of a two-box model of the ocean. Both the surface and the deep boxes are assumed to be mixed homogeneously. Biological uptake of inorganic constitutents in the surface box reduces surface concentrations (C_s) and leads to the export of organic material into the deep box (Φ). This organic material is remineralized in the deep box, thereby increasing deep concentrations (C_d). The two boxes exchange water at a volume rate ν).

$$\Phi^N = \nu(N_d - N_s) \tag{2}$$

Although great care must be taken to avoid generalization from a two-box model to the real world, this simple steady-state condition is fundamental for understanding large-scale biogeochemical/physical interactions in the oceans. It states that for a given ocean circulation, the vertical gradient in nitrate reflects the magnitude of the downward flux of organic nitrogen. That is, the stronger the biological export, the stronger the resulting gradient. Conversely, for a given biological flux Φ^N, the stronger the volume exchange rate ν, the weaker the vertical gradient. Thus, we see that on a large scale, the effect of ocean biological processes represented by Φ^N is to enhance gradients, while the effect of ocean circulation and mixing, represented by ν, is to homogenize the ocean.

A second insight from this simple model arises from the observation that nitrate is often severely depleted in the surface ocean (i.e., $N_s \approx 0$). This implies that the strength of the export of organic nitrogen is controlled by the deep nitrate concentration, which is equivalent to saying that the inventory of nitrate in the ocean controls the magnitude of the surface export. We will see later that this conclusion must be modified somewhat due to the supply of nitrate from the atmosphere and by fixation of N_2 gas at the surface.

The first major theme of this chapter is to explore the large-scale distribution of tracers in the ocean and infer from this the nature of the biogeochemical–physical interactions. This can readily be seen by moving ν in equation 2 to the left side. The resulting equation states that the large-scale structure of N as represented by $(N_d - N_s)$ is shaped by the biogeochemical–physical interactions represented by Φ^N/ν. We use knowledge of the circulation represented by ν to separate out the biogeochemical processes represented by Φ^N.

If we assume for the moment that inorgnic carbon in the ocean is, like nitrogen, only affected by the photosynthesis/remineralization cycle (soft tissue pump), we can write a conservation equation for inorganic carbon in the deep box that is analogous to equation 1. The steady-state solution for carbon in the deep box is then also analogous to equation 2; thus,

$$\Phi^C = \nu(C_d - C_s) \tag{3}$$

where Φ^C is the export of organic carbon from the surface to the deep and C_d and C_s are the deep and surface inorganic carbon concentrations, respectively.

An observation that is fundamental for understanding biogeochemical–physical interactions in the sea is the fact that the biological cycles of many elements are often closely linked to each other. This is a consequence of the relatively narrow stoichiometric requirements of these organisms at the biochemical and cellular level. This permits us to write the photosynthetic uptake of carbon and nutrients and the reverse reactions of respiration and remineralization as a simple reversible reaction:

$$106CO_2 + 16HNO_3 + H_3PO_4 + 78H_2O \Leftrightarrow C_{106}H_{175}O_{42}N_{16}P + 150O_2 \tag{4}$$

where we used the stoichiometric ratios of Anderson (1995) rather than those originally proposed by Redfield et al. (1963) (see Sidebar 9.1). This biological linkage between the ocean nitrogen and carbon cycles [$\Phi^C = (106/16) * \Phi^N$] enables us to combine equations 2 and 3 to give

$$C_d - C_s = (N_d - N_s)\ \frac{106}{16} \tag{5}$$

SIDEBAR 9.1
Stoichiometric Ratios

One of the most powerful tools for gaining insight into the marine biogeochemical cycles stems from the observation that marine phytoplankton tend to have relatively uniform elemental composition and that the average ratio of these elements in seawater tend to be very close to the requirements of these organisms. Redfield et al. (1963) was the first to suggest this idea based on the observations of Fleming (1940) and his own studies. This concept has become known since as the Redfield ratio concept. This concept states that the reactions of photosynthesis, respiration, and remineralization can be written as a single reversible reaction with a relatively fixed stoichiometry (see reaction 4).

The validity of the Redfield concept and the precise values of the stoichiometric ratios have been the subject of intense investigation over the last decade. The various studies can be differentiated into two approaches. The first strategy is to analyze the elemental composition of particulate organic matter (e.g., Redfield et al., 1963; Martin et al., 1987; Laws, 1991; Anderson, 1995; Honjo, 1996). The second method is to infer the stoichiometric ratios from the changes in nutrient, oxygen, and carbon concentrations that result from remineralization processes (remineralization ratios)

(e.g., Takahashi et al., 1985; Minster and Boulahdid, 1987; Boulahdid and Minster, 1989; Anderson and Sarmiento, 1994; Shaffer, 1996; Shaffer et al., 1999; Hupe and Karstensen, 2000). If the elemental composition of phytoplankton is indeed relatively constant (Falkowski, 2000) and no elemental fractionation occurs during remineralization (Knauer et al., 1979), the two approaches should give the same answer. Otherwise, either of these two mechanisms can lead to differences between the two methods.

There exist currently two distinct views about the stoichiometric ratios of photosynthesis, respiration, and remineralization. The first point of view, which is based mainly on the study of the composition of organic matter, suggests that there are considerable variations in the elemental stoichiometry [e.g., induced by variations in growth rates (Goldman et al., 1979), by varying nutrient concentrations (Goldman et al., 1979), or by variable stoichiometric uptake kinetics (Sambrotto et al., 1993; Arrigo et al., 1999)]. This view is supported by two recent studies of the stoichiometric ratios of remineralization, which showed considerable variations of these ratios with depth. These variations were interpreted as due to the preferential remineralization of certain elements as the organic matter particles are settling through the water column (Shaffer et al., 1999; Hupe and Karstensen, 2000).

The second view is one of relatively constant stoichiometric ratios, on the basis of the results of an analysis of remineralization ratios of isopycnal surfaces (Takahashi et al., 1985) and on neutral surfaces (Anderson and Sarmiento, 1994). Although this view is in line with the original Redfield ratio concept (Redfield et al., 1963), several modifications have been proposed relative to the originally suggested stoichiometric ratios. In particular, the newer studies propose substantially lower oxygen and hydrogen contents (see Table I).

We adopt here the second view, of relatively constant stoichiometric ratios, for two reasons. First, the most comprehensive and only global study so far by Anderson and Sarmiento (1994) revealed relatively uniform values, independent of depth and ocean basin. Second, as we show during the discussions below, the anomaly patterns that we find using constant stoichiometric ratios are entirely consistent with the expectations.

TABLE I
Stoichiometric Ratios of Phytoplankton Organic Matter and Oxygen Released during Synthesis of the Organic Matter or Consumed During Remineralization

	Organic Matter					Oxygen,
	C	H	O	N	P	O_2
Redfield et al. (1963)[a]	106	263	110	16	1	138
Anderson (1995)[b]	106	164–186	26–59	16	1	141–161
Anderson and Sarmiento (1994)[c]	117 ± 14	—	—	16 ± 1	1	170 ± 10

[a] Traditional Redfield ratios.
[b] Revised ratios based on a revision of the hydrogen and oxygen content in the Redfield ratio based on reevaluation of the range of composition of organic matter.
[c] Stoichiometry based on an analysis of the remineralization ratios in the deep ocean below 400 m.

We adopt the stoichiometric ratios of Anderson and Sarmiento (1994), which suggest that the organic matter remineralized in the deep ocean has ratios of $N/P/C_{org}/O_2 = 1:16 \pm 1:117 \pm 14:-170 \pm 10$ and therefore approximately the same composition as equation 4. However, there is considerable uncertainty associated with the fact that it was not possible to do the analysis in waters shallower than 400 m. We also recognize that these ratios might not entirely reflect the "true" ratios, since Anderson and Sarmiento (1994) did not take into account dianeutral mixing, which can distort the results (Shaffer et al., 1999). This effect seems to affect the C_{org}/P ratio strongest but has little influence on the N/P ratio. We therefore have to be careful when interpreting results that hinge on C_{org}/P but can be more confident about the use of a constant N/P ratio of 16 : 1.

This substitution has an important consequence. The assumption of constant stoichiometric ratios permits us to relate the spatial gradients of one tracer (here inorganic carbon) to the spatial gradients of another tracer (nitrate). This finding provides us with a powerful set of tools for the analysis of ocean biogeochemistry. It suggests first that the underlying distributions of carbon, nitrogen, phosphorus, and oxygen in the ocean should be fairly similar. We can therefore study the distribution of any one of these tracers and infer with reasonable accuracy what the distribution of any other one should look like. However, as we begin to compare the actual tracer distributions with those that we would expect if the stoichiometry of ocean biogeochemical processes were actually as depicted by equation 4, we will find remarkable divergences that clearly indicate the presence of biogeochemical processes that do not follow this stoichiometry.

The second major theme of this chapter is to define a set of tracers that would be conservative if equation 4 held everywhere in the ocean, and to use the divergence of these observed tracers from its expected distribution to focus our attention on these processes, such as nitrogen fixation, denitrification, and air–sea gas exchange that differentiate one chemical from another.

We begin this chapter with an investigation of the large-scale distribution of inorganic carbon, nitrate, phosphate, and dissolved oxygen in the ocean based on the most recent survey data obtained during the World Ocean Circulation Experiment (WOCE). As noted, the cycles of these elements are closely linked to each other through the soft tissue pump. However, as also noted, we will see that there are a number of processes that decouple the different tracers from each other. These decoupling processes and how they are controlled by physical–biogeochemical interactions constitute one of the major themes of this chapter. Discussion of the decoupling processes will concentrate on those acting on nitrogen and carbon, as these processes have received a lot of scientific attention over the last few years. The most important decoupling processes for nitrogen, N_2 fixation and denitrification, are the focus of Section 3. We discuss the distribution, rates, and controls of these processes, and particularly highlight the importance of them for maintaining the long-term inventory of biologically available nitrogen in the ocean and hence maintaining long-term biological productivity. We will see how critical phosphorus and oxygen and their interactions with ocean dynamics are in controlling this balance. In Section 4 we then turn to a discussion of carbon and the processes that control its distribution,

apart from the soft tissue pump. A major result of this investigation will be that the net impact of air–sea gas exchange on the distribution of inorganic carbon is relatively weak. By contrast, the effect of air–sea gas exchange is much stronger for oxygen, leading to a strong decoupling of its distribution from nitrate and phosphate. We find that this different behavior is due to the interaction of ocean biology with ocean circulation and the kinetics of air–sea gas exchange. We conclude with a summary of our main results.

2. Large-Scale Tracer Distributions

We first investigate the large-scale ocean distributions of nitrate (N), phosphate (P), oxygen (O_2), and dissolved inorganic carbon (DIC). Figures 9.3 and 9.4 show the distribution of these four tracers in vertical sections along a pathway that starts in the northern North Atlantic, goes southward until about 60°S, turns eastward and follows the Antarctic Circumpolar Current at this latitude circle until 150°E (Fig. 9.5), and then follows this longitude circle northward into the Pacific until the Alaskan coast is reached at approximately 60°N. These sections thus provide a good representation of the magnitude of the tracer variability observed in the global ocean. Inspection of these figures reveals that the distribution of these tracers in the global ocean is more variable and complex than the profiles in Fig. 9.1 might suggest. Note that the DIC concentration has been normalized to constant salinity in order to remove the effect of evaporation and precipitation. This normalization is not necessary for the other tracers, since their concentration range is large relative to their mean concentration. Therefore, variations induced by salinity changes contribute very little to the large-scale distribution of these tracers.

Two main observations emerge from inspection of Figs. 9.3 and 9.4. First, the surface depletions of nitrate, phosphate, and DIC are not uniform across the globe. Surface cncentrations of these tracers are low and very similar in the low latitudes of the Atlantic and Pacific, but the surface depletion is much less expressed in the Southern Ocean. Second, deep ocean concentrations of N, P, and DIC increase gradually from the Atlantic through the Southern Ocean and into the Pacific Ocean. The distribution of oxygen (Fig. 9.3*b*) shows to a large degree the same features, except with opposite sign (i.e., deep concentrations decrease from the Atlantic to the Pacific.

We learned from our analysis of the two-box model that the large-scale distribution of these chemicals can be understood in most simple terms as a balance between biogeochemical processes that create gradients and physical transport that tends to homogenize them. Thus, in order to understand the large-scale patterns exhibited by N, P, O_2, and DIC (Figs. 9.3 and 9.4), one first has to learn about large-scale ocean circulation.

Figure 9.6 shows vertical sections of potential temperature (θ) and salinity (S) along the same transects as the biogeochemical tracers. These two sections reveal that the high surface concentrations of DIC, N, and P in the Southern Ocean are the signal of surface exposure of deep waters. This exposure is the result of very weak vertical gradients in temperature and salinity caused by strong surface buoyancy forcing combined with upwelling. This upwelling is a consequence of a divergence induced by the northward Ekman transport of surface waters caused by the strong eastward-blowing winds over the Southern Ocean. This situation of very weak vertical stratification with large exchange between the deep and surface ocean is in contrast to the low

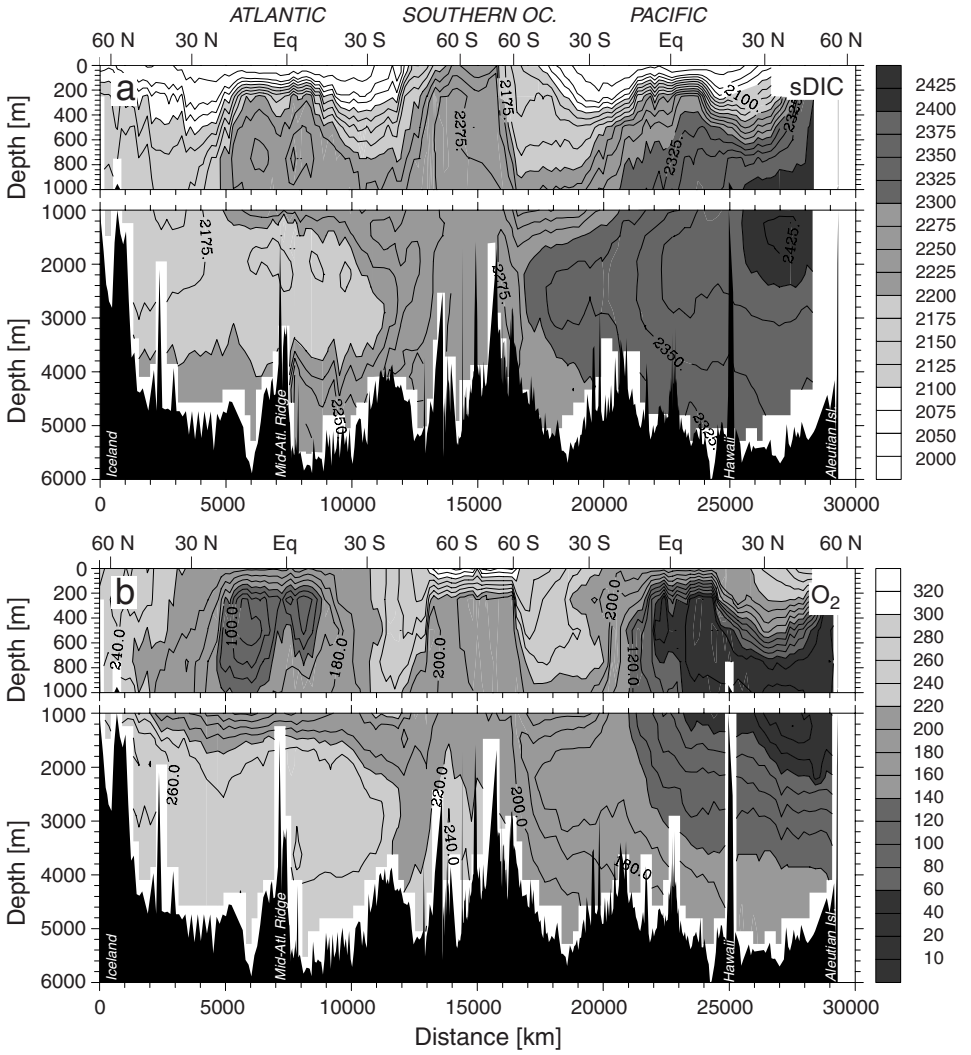

Fig. 9.3. Vertical sections of (*a*) salinity normalized dissolved inorganic carbon (DIC) (μmol kg^{-1}) and (*b*) oxygen (μmol kg^{-1}) along the station track shown in Fig. 9.5. Horizontal axis is distance in kilometers from the first station just south of Iceland at 63°N 20°W. The *x*-axis in the Southern Ocean (south of 57°S) has been compressed by a factor of 5.

latitudes, where strong stratification by temperature and salinity separates the upper ocean very effectively from the intermediate and deep ocean. Variations of the N, P, O_2, and DIC concentrations in the intermediate and deep oceans are determined primarily by the global *thermohaline circulation*, often called the great conveyor belt [Broecker (1991a) see Fig. 9.7 and Schmitz (1996) for a detailed overview].

The lower branch of this conveyor belt consists of the formation of deep water in the northern North Atlantic and the southward transport of these waters in the Atlantic, subsequent mixing in the Circumpolar Current with deep waters formed

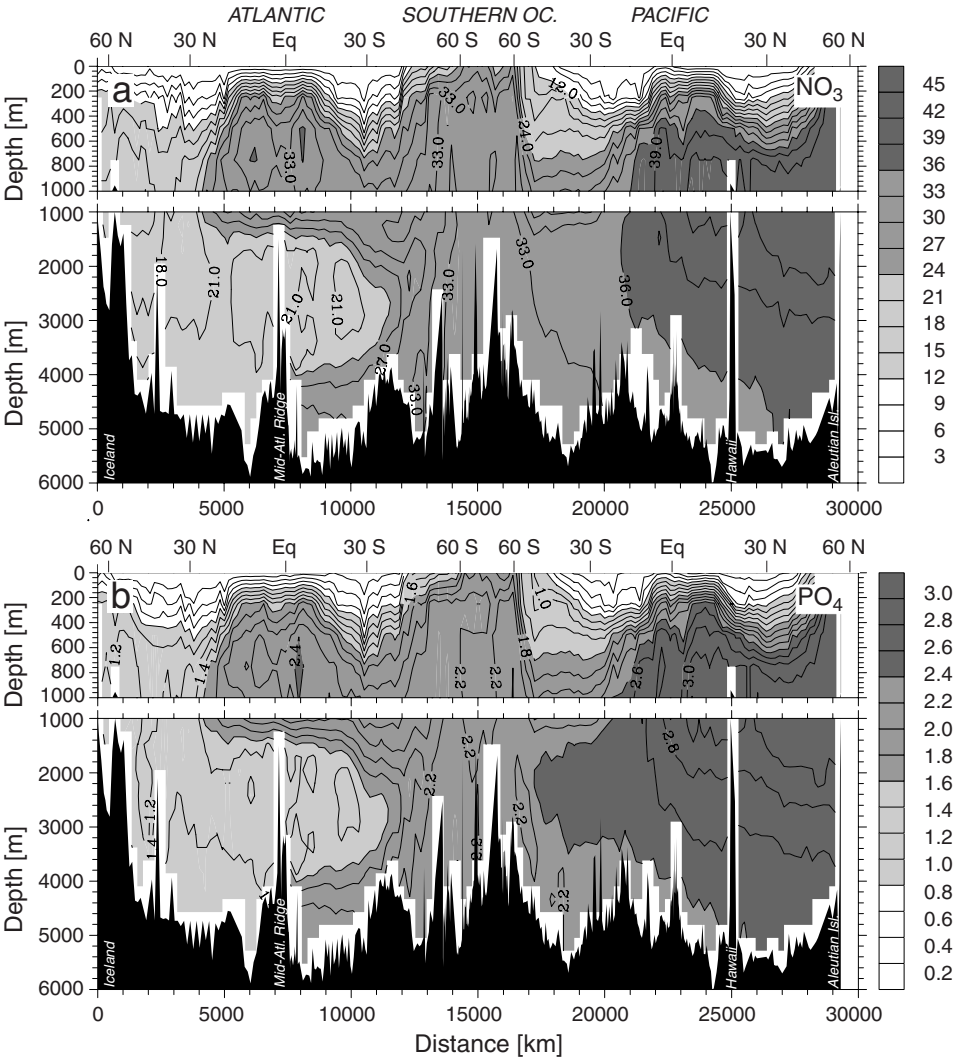

Fig. 9.4. Same as Fig. 9.3 except for (*a*) nitrate (μmol kg^{-1}) and (*b*) phosphate (μmol kg^{-1}).

around Antarctica, and northward transport of these common deep waters into the deep Indo-Pacific Oceans (Fig. 9.7). The two main deep-water masses can be distinguished by their θ and salinity properties. North Atlantic Deep Water is characterized by potential temperatures around 2 to 4°C and relatively high salinities between 34.9 and 35.0. The latter signature can be identified clearly as the southward-spreading salinity maximum in the deep waters of the Atlantic (Fig. 9.6*b*). The NADW loses its signature once it is mixed in with Circumpolar Deep Water (CDW) around Antarctica. Deep water formed around Antarctica, often called Antarctic Bottom Water (AABW), is comparably fresh (salinities between 34.6 and 34.7) and cool (θ between −1.0 and 0°C). Most of the waters that enter the deep Indo-Pacific return as middepth

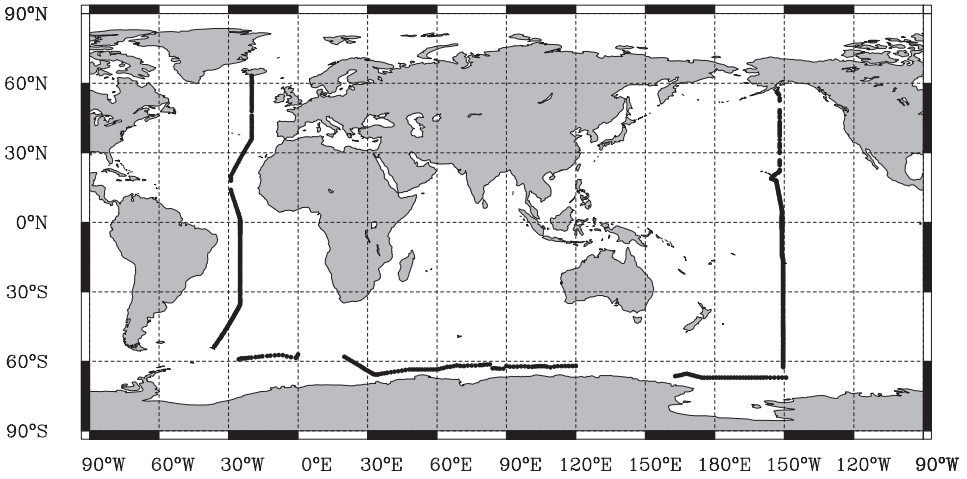

Fig. 9.5. Map showing the locations of the station used for the sections shown in Figs. 9.3, 9.4, 9.6, 9.8, 9.15, 9.21, and 9.11. Data from the following cruises are used: Ocean Atmosphere Carbon Exchange Study (OACES), North Atlantic 1993 (NATL93) cruise (R. Wanninkhof, personal communication), South Atlantic Ventilation Experiment (SAVE) (ODF, 1992a,b), Meteor 11-5 (WOCE S1/2 A21/A22) (Chipman et al., 1994), WOCE S41 (T. Whitworth III, personal communication), WOCE S4P (Chipman et al., 1997), WOCE P16S (Takahashi et al., 1996), WOCE P16C (Goyet et al., 1996), and WOCE P16N (J. Bullister, personal communication).

flows to the CDW and do not upwell back to the surface as some older depictions of the thermohaline circulation suggested (see, e.g., Broecker, 1991a). The final branch of this conveyor is formed by the return flow of upper and intermediate waters from the Southern Ocean northward into the northern North Atlantic, where the cycle starts over again. A second circulation cell of importance is the formation of intermediate waters near the Subantarctic Front at about 45°S and their subsequent spreading northward at depths of about 1000 m. The core of these waters, commonly referred to as Antarctic Intermediate Waters (AAIW), can readily be identified as a pronounced salinity minimum (Fig. 9.6*b*).

The concentrations of N, P, and DIC increase relatively gradually along the flow path of the lower branch of the great conveyor belt, while the concentration of O_2 decreases accordingly. These changes can best be understood by the continuous addition of products of the remineralization of organic matter as these waters move along the lower branch of this conveyor belt. As this organic material gets remineralized, it releases stoichiometric amounts of nitrate, phosphate, and inorganic carbon, while consuming stoichiometric amounts of oxygen (see Sidebar 9.1). This explains the very similar pattern exhibited by the four biogeochemical tracers. A closer comparison of the pattern seen in N, P, and O_2 reveals that the first two are very strongly correlated, whereas O_2 deviates from N and P in a number of places. The most striking difference exists in the surface ocean, where the strong surface depletion seen in N and P is not mirrored by high O_2 values. This is the consequence of the fact that O_2 exchanges at the surface with the atmosphere, whereas no such process exists for N and P. This allows the O_2 cycle to decouple from that of N and P.

Although this decoupling between N, P, and O_2 adds a level of complexity in our quest to understand the large-scale distribution of chemicals in the ocean, it offers

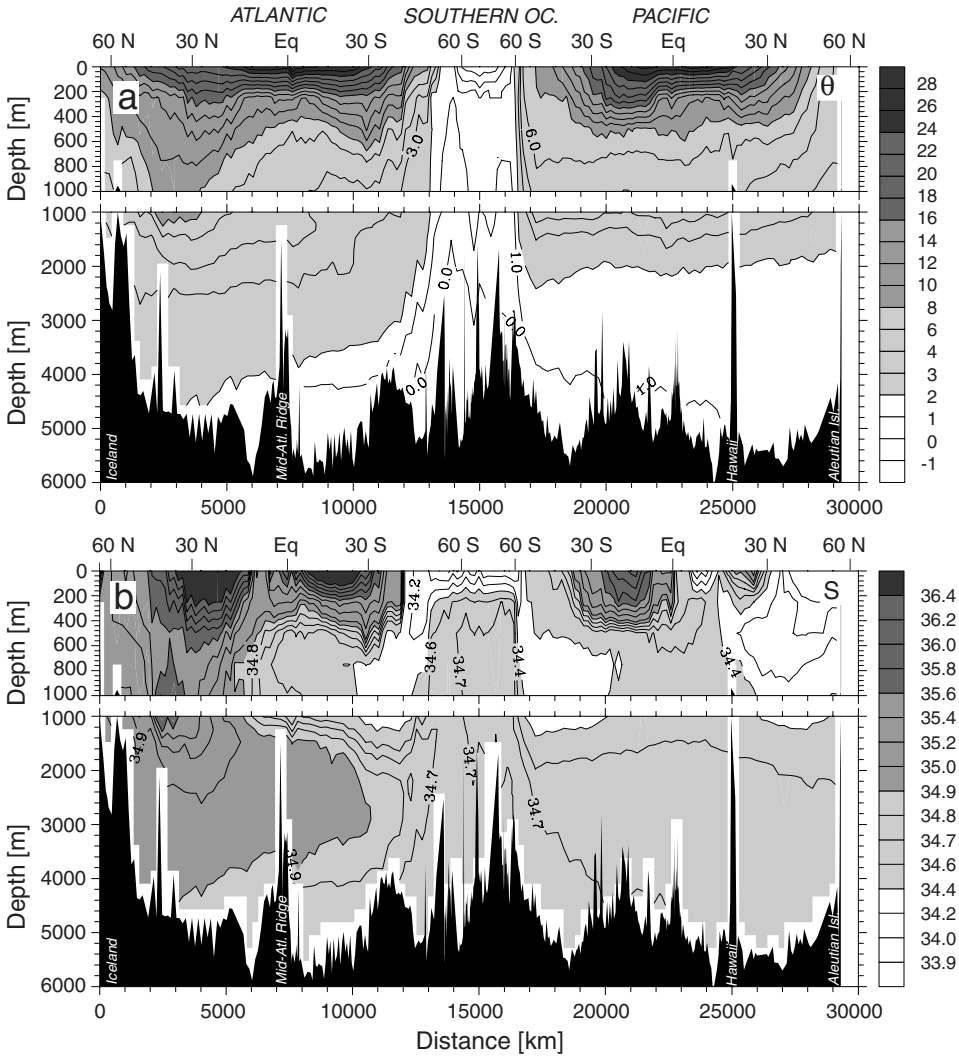

Fig. 9.6. Same as Fig. 9.3 except for (*a*) potential temperature (θ) (°C) and (*b*) salinity (on the practical salinity scale).

us at the same time the possibility to separate the observed distribution of N and P into a preformed and a remineralized component. The motivation for this separation is to determine how much of the variability seen in N and P stems from the addition of remineralized products since this water was last in contact with the atmosphere (*remineralized component*), and how much of the variability stems from the fact that not all nutrients were used up before this water parcel left the surface (*preformed component*).

We begin with the distribution of oxygen by defining an apparent oxygen utilization (AOU) as

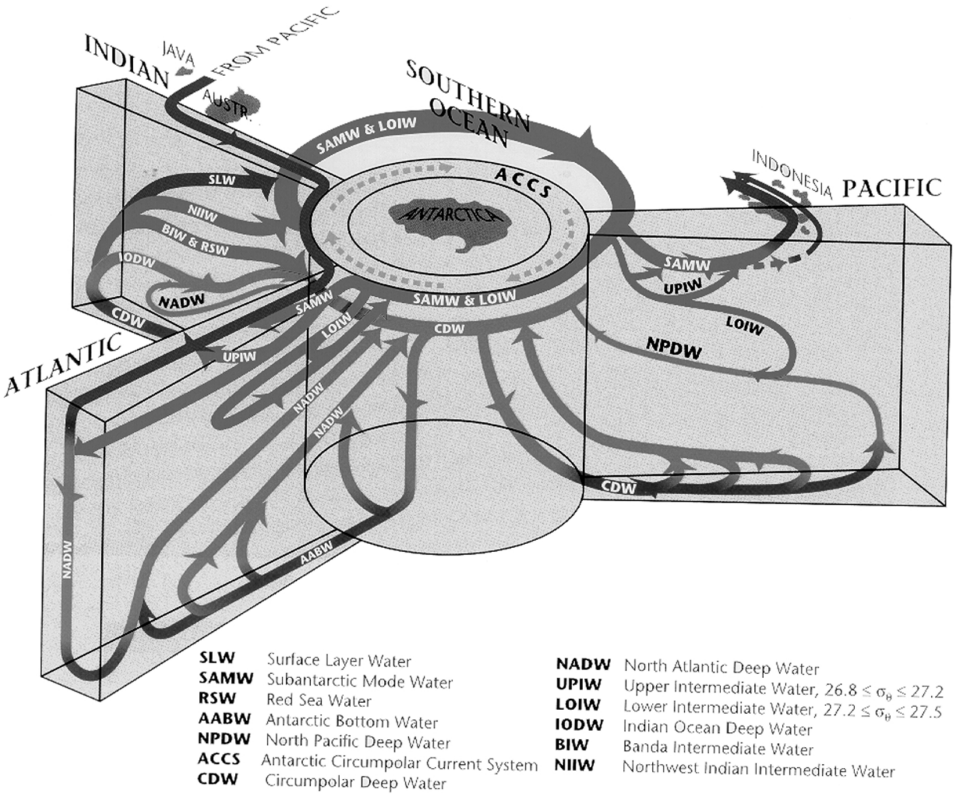

Fig. 9.7. Three-dimensional interbasin flow schematic with typical meridional-vertical sections for the oceans indicated, and their horizontal connections in the Southern Ocean and the Indonesian Passages. (From Schmitz, 1996.)

$$\mathrm{AOU} = \mathrm{O}_2^{\mathrm{sat}} - \mathrm{O}_2^{\mathrm{obs}} \tag{6}$$

The rationale behind this tracer is that water parcels leave the surface ocean with oxygen at or near saturation, with atmospheric oxygen at the temperature and salinity of the water parcel. Thus, the difference AOU between the saturation concentration, $\mathrm{O}_2^{\mathrm{sat}}$, calculated from the potential temperature and salinity of a given water parcel and the observed concentration, $\mathrm{O}_2^{\mathrm{obs}}$, is a measure of how much oxygen has been utilized by the process of remineralization.

When multiplied by the appropriate stoichiometric ratio, the AOU can be used to estimate the biological utilization of any tracer. Thus, the remineralized component of N and P can be estimated as

$$\Delta\mathrm{N}^{\mathrm{remin}} = -r_{\mathrm{N}:\mathrm{O}_2}\ \mathrm{AOU} \tag{7}$$

$$\Delta\mathrm{P}^{\mathrm{remin}} = -r_{\mathrm{P}:\mathrm{O}_2}\ \mathrm{AOU} \tag{8}$$

where r_{N/O_2} and r_{P/O_2} are the stoichiometric N/O_2 and P/O_2 ratios. The preformed component can then be obtained from

$$N^{preformed} = N^{obs} - \Delta N^{remin} \quad (9)$$

$$P^{preformed} = P^{obs} - \Delta P^{remin} \quad (10)$$

Figure 9.8 shows the distribution of preformed and remineralized phosphate along the same pathway from the North Atlantic to the North Pacific as shown in Fig. 9.4*b* for phosphate. Preformed P looks in many respects very similar to salinity. This is not surprising, since both salinity and preformed P act as conservative tracers, (i.e., tracers without sources and sinks in the interior of the ocean). Thus, once these tracers have left the surface, their concentration can only be changed by mixing.

The most striking aspect of the distribution of preformed P is that waters formed in the northern North Atlantic contain relatively small concentrations of preformed phosphate, whereas deep waters formed around Antarctica contain high concentrations. The second interesting feature is the strong uniformity of preformed P in the deep Pacific and the fact that its concentration lies between that of North Atlantic Deep Waters (NADW) (Fig. 9.7) and that of surface waters in the Southern Ocean. This observation is a consequence of the fact that there is no deep-water formation in the North Pacific and that the deep waters filling the deep Indo-Pacific originate from Circumpolar Deep Water that is formed by blending NADW with Antarctic Surface Waters (Fig. 9.7). The homogeneity of deep waters in the Pacific and the large dynamical difference of preformed P betweeen NADW and waters formed around Antarctica make this tracer (and derivatives of it) ideal for separating the contribution of these two water masses in the deep Atlantic (Broecker et al., 1985b, 1998, 1999).

The remineralized component of phosphate shows clearly the increase in concentrations as the waters move along the lower branch of the conveyor belt as a result of the continuous addition of remineralized phosphate (Fig. 9.8*b*). This figure also shows the increase in the remineralized component as the intermediate waters move equatorward, a fact that was masked partially in the P sections (Fig. 9.4*b*). The highest concentrations of remineralized P are found at relatively shallow depths close to the equator in the Atlantic and north of the equator in the Pacific. The preformed and remineralized components of nitrate exhibit an almost identical distribution and are therefore not shown.

If the soft tissue pump was the only process affecting the large-scale distribution of N, P, O_2, and DIC, we would expect that all data would lie on a straight line in a property versus property plot. Figure 9.9 shows that this is only partially the case for DIC and N, whereas O_2 clearly violates this expectation. One possible explanation for why there exist substantial deviations from a straight line is that our assumption of constant stoichiometric ratios during photosynthetic uptake, respiration, and remineralization is wrong. This is probably the cause of some variability, but investigations of deep-water variabaility in the stoichiometric ratios suggest that this is too small to explain these deviations (Takahashi et al., 1985; Anderson and Sarmiento, 1994), even taking the newer results of Shaffer et al. (1999) and Hupe and Karstensen (2000) into account. The main reason for these deviations appears to be that these chemicals are affected by processes other than the production/remineralization cycle.

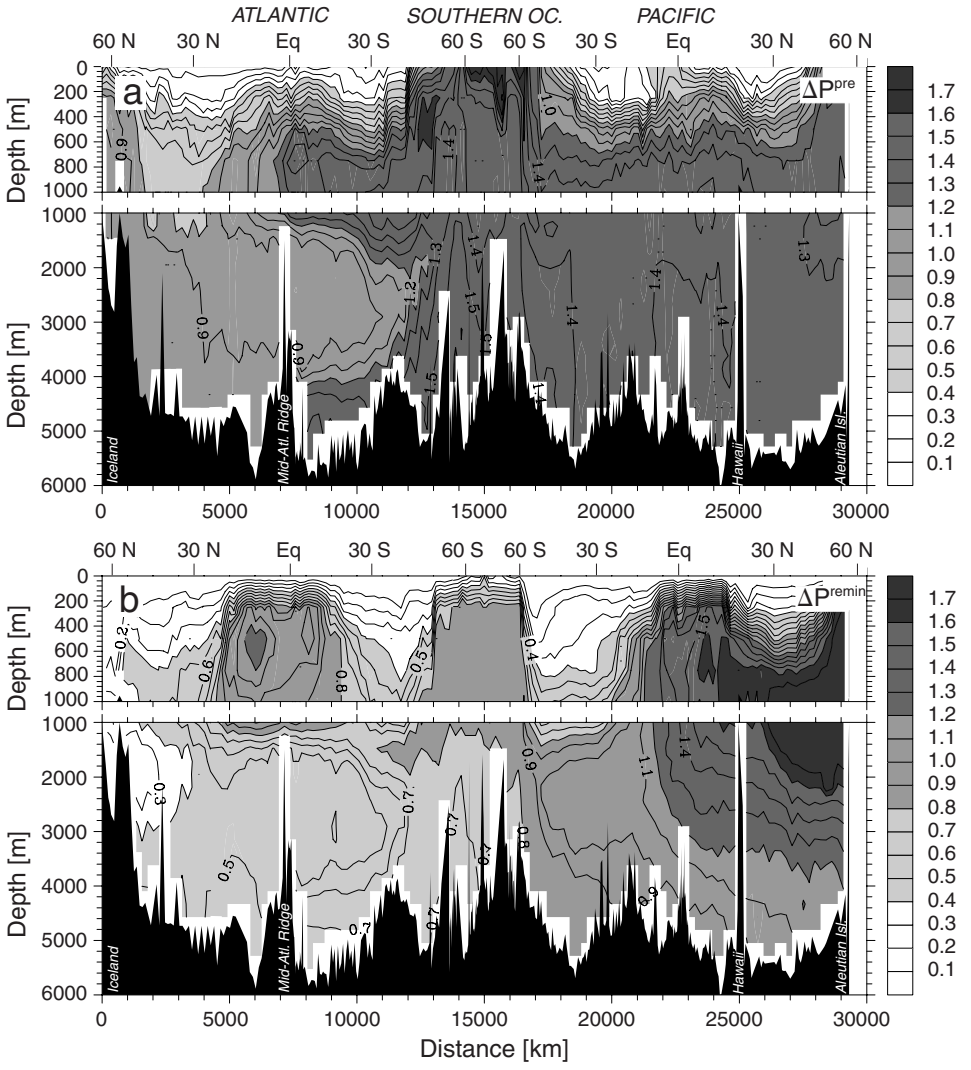

Fig. 9.8. Same as Fig. 9.3 except for (*a*) preformed phosphate ($P^{preformed}$) (μmol kg^{-1}) and (*b*) remineralized phosphate (ΔP^{remain}) (μmol kg^{-1}). See the text for definitions.

Although the latter is clearly the dominant process, we cannot understand the oceanic distribution of biogeochemical tracers wihout investigating these other processes as well. In the case of oxygen, we have learned already that air–sea gas exchange is responsible for the large deviations from the uniform relationship with phosphate. Since CO_2 is exchanging with the atmosphere as well, it is surprising to find that the relationship of DIC with P is much tighter than that of O_2. Obviously, there must be substantial differences in the manner by which air–sea gas exchange imprints the DIC and O_2 concentrations in the sea. Although air–sea gas exchange might explain the decoupling of O_2 and DIC from the cycling of P, it offers no explanation for the

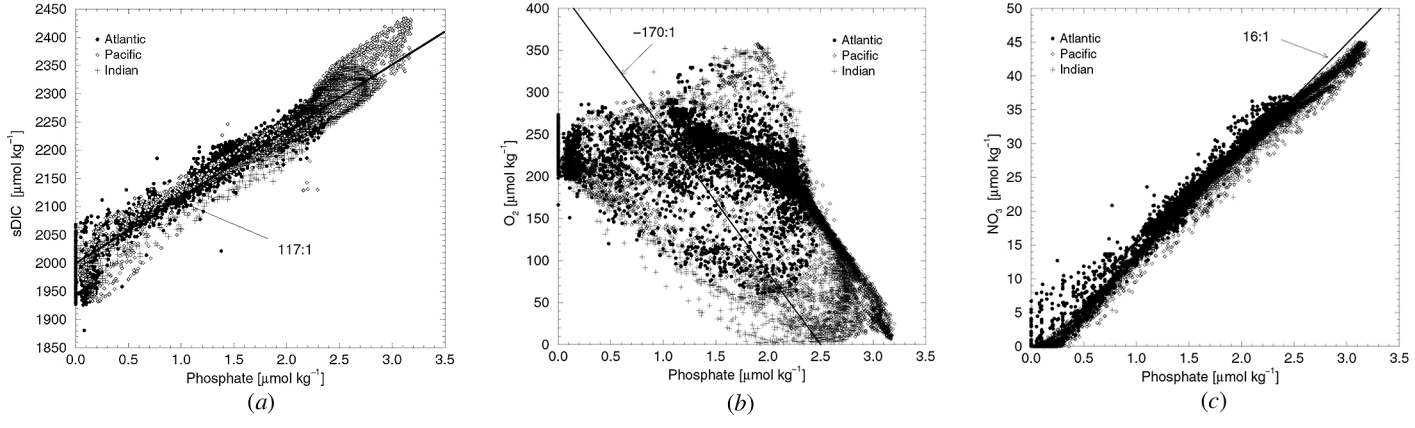

Fig. 9.9. Plots of (*a*) nitrate, (*b*) salinity normalized DIC, and (*c*) oxygen versus phosphate for data from all depths. Solid lines depict the expected slope between the tracers as a result of the photosynthesis/remineralization cycle. [Based on data from three long transects in the Atlantic (OACES NATL93, SAVE), Pacific (WOCE P16), and Indian (WOCE I9NI8S) Oceans.]

small, but significant decoupling between N and P. As we study in detail in the next section, this decoupling comes mainly from N_2 fixation and denitrification.

An important concept in our study of the role of the processes that lead to deviations from the Redfield stoichiometry in the oceans is that of quasiconservative tracers. This concept, which we use extensively in our investigations here, builds on the fundamental assumption that the soft tissue pump operates with a relatively fixed stoichiometric ratios. Using this assumption, we can remove the effect of this pump and focus on the contribution of the other processes. This concept is explained more thoroughly in Sidebar 9.2.

SIDEBAR 9.2
Quasiconservative Tracers

The power of the Redfield ratio concept lies in the fact that it relates variations caused by the soft tissue pump in one tracer to variations in another tracer originating from the same process. This permits us to derive *quasiconservtive tracers* (i.e., tracers that are unaffected by the soft tissue pump). Such tracers have contributed substantially to our understanding of ocean circulation and the carbon and nitrogen cycles.

We start the derivation of such a conservative tracer with the tracer conservation equation of two tracers, A and B, that are affected by the soft tissue pump only:

$$\Gamma(A) = J_{\text{soft}}(A) \tag{11}$$

$$\Gamma(B) = J_{\text{soft}}(B) \tag{12}$$

where J_{soft} denotes the source minus sink term due to the soft tissue pump. The operation Γ represents the transport and time rate of change:

$$\Gamma(T) = \frac{\partial T}{\partial t} + \vec{u} \cdot \nabla T - \nabla \cdot (D \cdot \nabla T) \tag{13}$$

where T represents any tracer concentration, ∇ the graident operator in three dimensions, $\vec{u}$ the velocity field, and D the eddy diffusivity tensor.

The Redfield ratio concept implies that

$$J_{\text{soft}}(A) = r_{A:B} J_{\text{soft}}(B) \tag{14}$$

We can use this relationship to eliminate the $J_{\text{soft}}(A)$ term from equation 11 by subtracting $r_{A:B}$ times equation 12 from it, that is,

$$\Gamma(A) - r_{A:B}\Gamma(B) = J_{\text{soft}}(A) - r_{A:B} J_{\text{soft}}(B) = 0 \tag{15}$$

Since we assumed a constant stoichiometric ratio $r_{A:B}$ and since the transport and time rate of change operator Γ is linear, the left-hand side of equation 15 can be combined to give $\Gamma(A - r_{A:B}B) = 0$. This permits us to define a new tracer A^*,

$$A^* = A - r_{A:B}B \tag{16}$$

with conservative properties $\Gamma(A^*) = 0$.

Some of these derived conservative tracers are, in principle, analogous to other conservative circulation tracers such as temperature and salinity. However, these derived conservative tracer often have very unique distributions making them very attractive for distinguishing water masses that have otherwise very similar temperature and salinity properties (Broecker et al., 1985b).

The second advantage of studying such derived quasiconservative tracers is that they are very helpful in investigating processes that do not follow the stoichiometry of equation 4. These processes can be boundary condition processes such as air–sea gas exchange, atmospheric deposition, river input, and sediment processes, but also interior processes that create sources and sinks, much as nitrogen fixation and denitrification.

3. Biogeochemical–Physical Interactions of Nitrogen, Phosphorus, and Oxygen

The soft tissue pump represents the dominant control of the distribution of inorganic nitrogen and phosphorus in the ocean by explaining over 99% of the variability in N and P (Fig. 9.9*c*). However, we have also seen in Fig. 9.9*c* that there exist deviations from this tight 16 : 1 relationship between the two tracers that must be caused by processes that have a distinctly different stoichiometry, such as N_2 fixation and denitrification.

Nitrogen fixation is the biologically catalyzed conversion of dinitrogen gas (N_2) to organic nitrogen. Only a very limited number of organisms, the diazotrophs, are capable of performing this reaction (Falkowski, 1997). The most important species is *Trichodesmium* spp. (Capone et al., 1997), but a number of other species have also been identified (Villareal and Carpenter, 1989; Zehr et al., 2000). Denitrification is a particular form of respiration, in which nitrate instead of oxygen is used as a terminal electron acceptor. This pathway occurs only under anaerobic conditions (no oxygen present) (Hattori, 1983). By contrast to N_2 fixation, a relatively large number of microorganisms are capable of using denitrification as a respiratory process (Falkowki, 1997).

Early research on the magnitude of N_2 fixation and denitrification suggested that their rates were relatively small and that they did not contribute greatly to the availability of nitrogen needed for phytoplankton growth. A growing body of evidence now suggests that N_2 fixation and denitrification are far larger and that the ocean nitrogen cycle is more dynamic than previously thought (Codispoti, 1989; Carpenter and Romans, 1991; Galloway et al., 1995; Michaels et al., 1996; Gruber and Sarmiento, 1997). Current estimates of N_2 fixation and denitrification in the ocean suggest that the oceanic residence time of fixed nitrogen is only about 3000 years (Gruber and Sarmiento, 1997). The large dynamics of the ocean nitrogen cycle and the evidence that a substantial fraction of the nitrogen present in the surface ocean comes from N_2 fixation (Karl et al., 1997) has greatly increased the scientific interest in studying these processes over the last few years. This interest is fueled further by the possibility that imbalances between the two processes can change the oceanic inventory of this nutrient in the ocean on relatively short time scales (Codispoti, 1989). Since fixed nitrogen is regarded as one of the major limiting nutrient for photosynthesis (Codispoti, 1989; Tyrrell, 1999), changes in the concentration of fixed nitrogen may have profound effects on photosynthesis and net rates of biological export of carbon from the surface ocean and hence on atmospheric CO_2 (Falkowski, 1997; Broecker and Henderson, 1998; see Fig. 9.10).

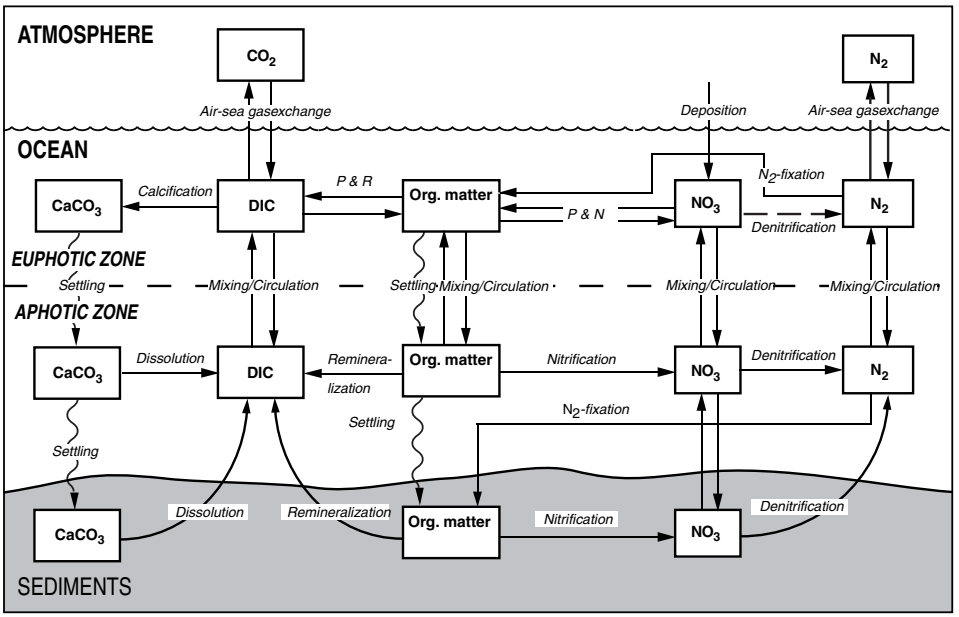

Fig. 9.10. Schematic diagram of the marine carbon and nitrogen cycles. The ocean is divided into an upper sunlit zone (euphotic zone), where carbon is on net consumed by biological processes, and an aphotic zone, where carbon is on net released. The marine nitrogen cycle is dominated by the nitrogen uptake and release associated with the carbon fixation and remineralization. However, N_2 fixation and denitrification can affect the amount of fixed nitrogen in the ocean. Surface deposition also constitutes a small source of fixed nitrogen. P & R denotes photosynthesis and respiration; P & N denotes photosynthesis and nitrification.

However, it is interesting to note that despite the fact that N_2 fixation and denitrification are two independent processes with very different controlling factors, the two processes appear to balance each other relatively well; otherwise, the slope of a plot of N versus P would be very different from 16 : 1 and the intercept very different from zero (see Fig. 9.9*c*). This indicates that there must be a negative feedback mechanism that precludes either one of these processes from running away. The most likely factor is phosphate itself in conjunction with oxygen (Codispoti, 1989; Tyrrell, 1999; Lenton and Watson, 2000).

In this section we use the quasiconservative tracer approach highlighted in Sidebar 9.2 to investigate the role of N_2 fixation and denitrification in decoupling N and P from each other. We define a tracer N^*, which reflects deviations of N from a 16 : 1 stoichiometric relationship with P (see Fig. 9.9*c*). This approach builds on an earlier quasiconservative tracer NO (Broecker, 1974), which has been used by a number of investigators to study denitrification in the ocean (Naqvi et al., 1982). We will show that the distribution of N^* is not random but reflects sources and sinks of fixed nitrogen in the ocean due to N_2 fixation and denitrification. The interpretation of this tracer is greatly aided by the fact that N_2 fixation and denitrification are often spatially and temporally separated. We also show that one can estimate rates of N_2 fixation and denitrification by combining N^* with tracers reflecting the ventilation age of waters. The concept of N^* is explained in more detail in Sidebar 9.3. We

first investigate the distribution of N^* and then discuss the role of N_2 fixation and denitrification in turn. We then investigate what may determine the observed close correspondence between N and P. This discussion will be of great relevance for our general theme of biogeochemical–physical interactions, since the factors controlling the relative rates of these two processes involve a complex interplay between ocean dynamics, nitrogen, phosphorus, and oxygen and therefore serve as a good example for illustrating such interactions.

3.1. Large-Scale Distribution of N^*

The net effect of nitrogen fixation on the large-scale distribution of N and P is to elevate the concentration of N without changing the concentration of P. This is because over sufficiently large scales (e.g., a scales of ocean basins) the uptake of P by the diazotrophs in the upper ocean [$J_{\text{up nf}}$(P) in Sidebar 9.3] is approximately balanced by the release of the P as the organic matter produced by these organisms is remineralized in the deeper layers of the ocean. Thus, we can identify regions of N_2 fixation by investigating regions where N^* concentrations are elevated relative to the local background. The net effect of denitrification is nearly opposite to that of N_2 fixation. Therefore, areas where N^* is smaller than the background can be identified as areas of active denitrification. It should be pointed out that the absolute value of N^* is arbitrary. Negative (positive) values of N^* cannot be directly associated with denitrification (N_2 fixation). Only deviations from conservative behavior are meaningful in identifying regions of denitrification and N_2 fixation.

Figure 9.11 shows a section of N^* following the same stations from the North Atlantic through the Southern Ocean into the North Pacific, as shown for N (Fig. 9.4*a*). This section reveals that N^* has a remarkable large-scale spatial coherence, which is a strong indication that the N^* signals are not caused by measurement noise

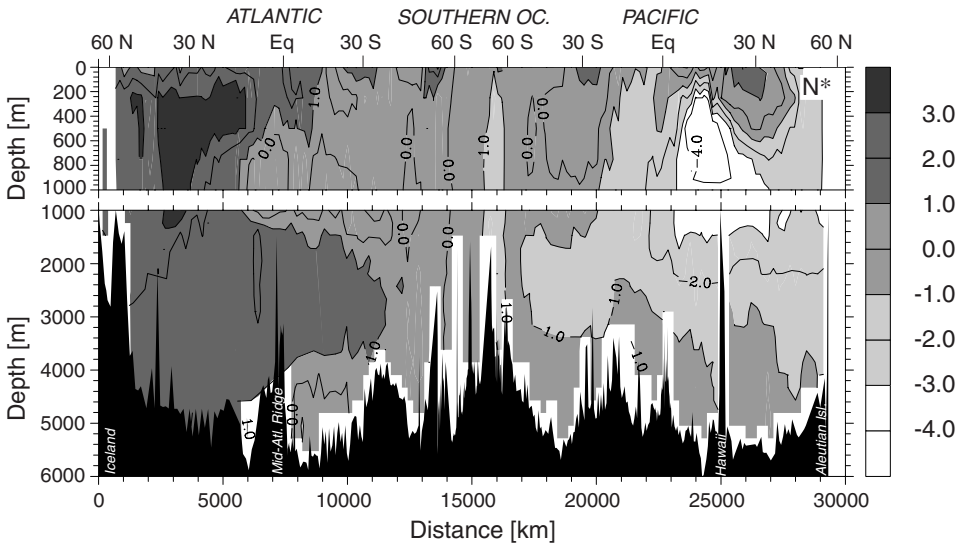

Fig. 9.11. Same as Fig. 9.3, except for N^* (μmol kg^{-1}). See text and Sidebar 9.3 for a definition and explanation of N^*.

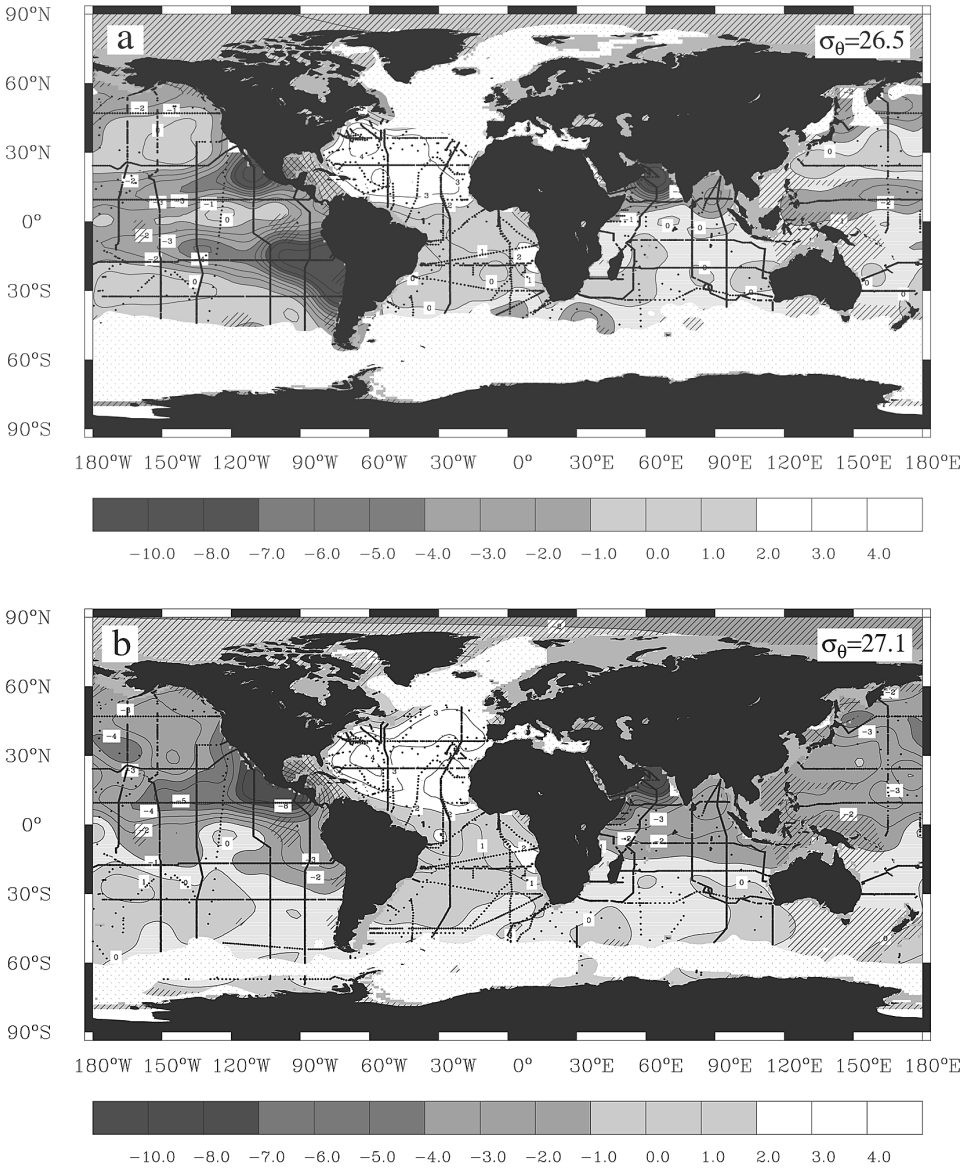

Fig. 9.12. Plots of the objectively analyzed distribution of N^* (μmol kg^{-1}) on isopycnal surfaces in the Global Ocean. (*a*) N^* on the $\sigma_\theta = 26.50$ surface. This surface is characteristic of subtropical mode waters, such as the 18° water in the North Atlantic. (*b*) N^* on the $\sigma_\theta = 27.10$ surface representing subpolar mode waters. Solid circles denote the stations; stippling denotes areas where the waters of this potential density are not present in winter time (determined from the NOAA NESDIS atlas; Levitus et al., 1994; Levitus and Boyer, 1994b). Crosshatched areas are regions where the estimated error in objectively analyzed N^* is greater than 0.7 μmol kg^{-1}.

but are linked to specific processes. The second observation to note is that N^*, in contrast to the distribution of almost all other tracers, shows no surface-to-deep gradients but exhibits a gradual decrease from the North Atlantic over the Southern Ocean into the Pacific Ocean. The lowest concentrations of N^* exist in the Arabian Sea (Fig. 9.12). This indicates that from a global perspective, the Atlantic Ocean acts as a net source of fixed nitrogen to the world ocean, and the Indian Ocean acts as a net sink, whereas the Pacific lies in between. The next outstanding features in the section (Fig. 9.11) are a large maximum of N^* in the thermocline of the North Atlantic and an extended minimum of N^* in the thermocline of the Pacific Ocean. A second positive anomaly of N^* can be found in the near-surface waters of the North Pacific, although this feature is substantially less pronounced than the North Atlantic maximum.

SIDEBAR 9.3
Concept of N^*

We derive here an equation for N^* following Deutsch et al. (2001). This derivation is slightly more general than that originally proposed by Gruber and Sarmiento (1997). We start with the continuity equations for N and P,

$$\Gamma(\mathrm{N}) = J_{\mathrm{soft}}(\mathrm{N}) + J_{\mathrm{denitr}}(\mathrm{N}) + J_{\mathrm{diazo\ remin}}(\mathrm{N}) \tag{17}$$

$$\Gamma(\mathrm{P}) = J_{\mathrm{soft}}(\mathrm{P}) + J_{\mathrm{denitr}}(\mathrm{P}) + J_{\mathrm{diazo\ remin}}(\mathrm{P}) + J_{\mathrm{up\ nf}}(\mathrm{P}) \tag{18}$$

The operator Γ represents the transport and time rate of change (see equation 13). The J terms denote the sources minus sinks due to (in order of appearance) the soft tissue pump, denitrification, remineralization of N-rich organic matter from nitrogen fixers, and the uptake of P by nitrogen fixers. We assume that the N sink and P source due to denitrification have a constant N/P ratio, $r_{\mathrm{denitr}}^{\mathrm{N:P}} = -104$ (Gruber and Sarmiento, 1997), given by the reaction equation of denitrification coupled with the remineralization of organic matter:

$$\begin{aligned} &\mathrm{C_{106}H_{175}O_{42}N_{16}P} + 104\mathrm{NO_3^-} \\ &\quad = 4\mathrm{CO_2} + 102\mathrm{HCO_3^-} + 60\mathrm{N_2} + 36\mathrm{H_2O} + \mathrm{HPO_4^{2-}} \end{aligned} \tag{19}$$

We can relate the N and P source terms of denitrification by $J_{\mathrm{denitr}}(\mathrm{N}) = r_{\mathrm{denitr}}^{\mathrm{N/P}} J_{\mathrm{denitr}}(\mathrm{P})$ and those of the soft tissue pump by $J_{\mathrm{soft}}(\mathrm{N}) = r_{\mathrm{soft}}^{\mathrm{N/P}} J_{\mathrm{soft}}(\mathrm{P})$. Then the N and P continuity equations can be combined as $\Gamma(\mathrm{N}) - r_{\mathrm{soft}}^{\mathrm{N/P}}\Gamma(\mathrm{P})$ to yield

$$\begin{aligned} \Gamma(\mathrm{N}^*) = J_{\mathrm{denitr}}(\mathrm{N}) - \frac{r_{\mathrm{soft}}^{\mathrm{N/P}}}{r_{\mathrm{denitr}}^{\mathrm{N/P}}} J_{\mathrm{denitr}}(\mathrm{N}) + J_{\mathrm{diazo\ remin}}(\mathrm{N}) \\ - r_{\mathrm{soft}}^{\mathrm{N/P}} [J_{\mathrm{diazo\ remin}}(\mathrm{P}) + J_{\mathrm{up\ nf}}(\mathrm{P})] \end{aligned} \tag{20}$$

Substituting stoichiometric N/P values of $r_{\mathrm{soft}}^{\mathrm{N/P}} = 16$ and $r_{\mathrm{denitr}}^{\mathrm{N/P}} = -104$, and adding a constant 2.90 μmol kg^{-1} to the definition of N^* to give a global mean of 0 gives

$$N^* = N - 16P + 2.90\ \mu\text{mol kg}^{-1}, \tag{21}$$

$$\Gamma(N^*) = 1.15 J_{\text{denitr}}(N) + J_{\text{diazo remin}}(N) - 16[J_{\text{diazo remin}}(P) + J_{\text{up nf}}(P) \tag{22}$$

How can we interpret variations in N^*? The first comment to make is that N^* is conserved under any process that consumes or releases N and P in a stoichiometric ratio $r_{\text{soft}}^{N/P}$. There are thus no sources or sinks of N^* in equation 22 due to the normal biological pump. Second, processes that introduce N and P in a ratio less than $r_{\text{soft}}^{N/P}$ are N^* sinks and will be revealed by low N^* anomalies. Such will be the case for denitrification, which is represented by the first terms on the right-hand side of equation 22. Processes that introduce N and P in a ratio above $r_{\text{soft}}^{N/P}$ are sources of N^* and will be revealed by high-N^* anomalies. This is the case for the N_2 fixation, which is represented by the remaining terms in equation 22.

To investigate the N^* distribution in more detail, we turn to two global maps that show the N^* distribution on two isopycnal surfaces (Fig. 9.12). The shallower surface (potential density $\sigma_\theta = 26.50$) represents subtropical mode waters (mean depth of about 300 m), and the deeper surface ($\sigma_\theta = 27.10$) reflects subpolar mode waters and lies at a mean depth of about 800 m. These maps reveal that the N^* maximum in the North Atlantic extends across the entire basin. These maps also show that the N^* minimum zone seen in the section at 150°W in the Pacific (Fig. 9.11) is associated with two intense N^* minimum zones in the eastern Tropical Pacific. Another strong minimum of N^* can be found in the Arabian Sea and to a lesser degree in the Bay of Bengal. We discuss the N^* maxima in Section 3.2 and the N^* minima in Section 3.3. As noted above, the N^* maxima are indicative of N_2 fixation.

3.2. Nitrogen Fixation

Patterns and Rates of N_2 Fixation

A more detailed inspection of the N^* maximum in the subtropical North Atlantic (Fig. 9.12) reveals that the concentration of N^* increases as waters move from the outcrop region in the northeastern part of the gyre into the center. Gruber and Sarmiento (1997) showed how one can estimate a formation rate of N^* by combining these increases with an estimate of how these waters age along their pathways. Since the thermocline waters of the North Atlantic are well ventilated, we can safety assume that there is no denitrification occurring and that the entire N^* signal is caused by the remineralization of N-rich organic material from diazotrophs [the uptake term $J_{\text{up nf}}(P)$ is zero, since we are only investigating the distribution of N^* in the interior of the ocean]. Therefore, the N^* formation rate can be translated into a N_2 fixation rate (see equation 22) by assuming a N/P ratio for the composition of N-rich organic material from diazotrophs. Gruber and Sarmiento (1997) used a ratio of 125 for the N/P ratio of diazotrophic organic matter [based on measurements reported by Karl et al. (1992)] and computed a N_2 fixation rate of about 28 Tg N yr^{-1} for the entire subtropical North Atlantic. This estimate is not very sensitive to the exact value chosen for this ratio, as long as it is significantly larger than 16 : 1. Recent laboratory experiments (D. Capone, personal communication, 1999) indicate that the N/P ratio in *Trichodesmium* varies between 40 and 130, depending on nutrient availability.

This N_2 fixation estimate turns out to be more than order of magnitude higher than previous estimates based on *Trichodesmium* abundance and direct rate measurements in the same region (Capone and Carpenter, 1982) but is supported by another geochemical N_2 fixation estimate by Michaels et al. (1996). The high geochemical rate estimates are supported further by the observation that the $^{15}N/^{14}N$ ratios of nitrate and organic matter in the thermocline of the subtropical gyre of the North Atlantic are very near atmospheric ratios, suggesting that a substantial fraction of the nitrogen present comes from the atmosphere by N_2 fixation (J. Montoya, unpublished data). More recent direct rate experiments of N_2 fixation in *Trichodesmium* colonies from the Bermuda Atlantic Time-Series Study (BATS) site near Bermuda by Orcutt et al. (2001) support significantly higher fixation rates than older studies suggested (Carpenter and Price, 1977), but still smaller than the geochemical estimates. However, N_2 fixation is known to occur not only in *Trichodesmium* but in a number of additional species (Villareal and Carpenter, 1989; Zehr et al., 2000). Their quantitative contribution to large-scale N_2 fixation is presently unknown. An alternative possibility is that the N^* signal in the subtropical gyre of the North Atlantic is not due to local N_2 fixation, but reflects the well-characterized high N_2 fixation in the Caribbean (Carpenter, 1983; Carpenter and Romans, 1991), which exports this excess nitrogen as dissolved organic nitrogen (DON) that then gets remineralized within the gyre. This would require substantial gradients in DON between the Caribbean and the North Atlantic subtropical gyre. Presently available DON data are insufficient to investigate this hypothesis (D. Hansell, personal communication, 2000).

Gruber and Sarmiento (1997) tentatively extrapolated their North Atlantic N_2 fixation estimate to the global ocean using the abundance of *Trichodesmium* as an indicator. They arrived at a global N_2 fixation estimate of about 110 Tg N yr^{-1}, with about 50 Tg N yr^{-1} occurring in the Pacific and 30 Tg N yr^{-1} being added in the Indian Ocean. Is this extrapolation consistent with the observed distribution of N^* in the other basins?

Interpretations of the N^* distribution in the Pacific and Indian Oceans is more difficult because of the existence of strong denitrification sites adjacent to the places where one expects to find the N_2 fixation signals. In the subtropical North Pacific, where N_2 fixation is well documented (Karl et al., 1997) the N^* maximum exists just near the surface and does not extend into the thermocline as is the case in the subtropical North Atlantic. This is likely a result of the eroding effect by waters that obtain extremely low N^* values in the eastern Pacific and are then advected westward in the main thermocline (Fig. 9.12).

Rather than trying to separate the N_2 fixation signal from the denitrification signal, Deutsch et al. (2001) decided to estimate N_2 fixation in the Pacific by establishing a nitrogen budget for this basin. By estimating the N transport across enclosing sections, total rates of denitrification, surface deposition, and river fluxes and assuming steady state, the N_2 fixation rate can be estimated by difference. They arrived at a N_2 fixation estimate of about 59 Tg N yr^{-1}, which is consistent with the extrapolation of Gruber and Sarmiento (1997). N_2 fixation is probably not distributed uniformly over the Pacific Ocean. If the near-surface distribution of N^* is taken as an indication of where this fixation is most likely taking place, two regions emerge: the northwestern Pacific and the southwestern Pacific. This distribution is roughly consistent with observations of *Trichodesmium* abundance (Capone and Carpenter, 1982; Carpenter, 1983; Carpenter and Capone, 1992), isotopic abundance of ^{15}N (Wada and Hattori,

1991), remote sensing (Dupoy et al., 2000), and dissolved organic nitrogen concentrations (Hansell and Feely, 2000).

In the Indian Ocean, near-surface values of N^* are slightly elevated (Gruber and Sarmiento, 1997). As these elevated values are located just above some of the lowest N^* values found anywhere in the world oceans, they could indicate rather strong N_2 fixation. Observations of *Trichodesmium* abundance (Carpenter, 1983) and a few direct rate measurements [reported in Capone et al. (1997)] appear consistent with such a conclusion. However, no basin-scale estimate of N_2 fixation has yet been attempted for the Indian Ocean.

Table II summarizes the pelagic N_2 fixation estimates. It also lists estimates of other sources of fixed nitrogen to the ocean. These other sources, primarily river input, bring the total N input into the ocean to about 185 Tg N yr^{-1} in preindustrial times and to about 235 Tg N yr^{-1} in present times.

Controls on N_2 Fixation

What are the factors controlling the pattern and rates of pelagic N_2 fixation? *Trichodesmium* colonies grow and fix N_2 successfully only at temperatures about 20°C (Capone et al., 1997). Additional factors playing an important role are the ambient concentration of O_2 and nitrate, as well as light levels. Since the fixation of N_2 is a very energy consuming process, *Trichodesmium* reduces its fixation rate drastically when it can take up fixed nitrogen directly from seawater. As the energy comes from sunlight, *Trichodesmium* dwells best at high insolation near the ocean surface (Capone et al., 1997). High rates of turbulence in the upper ocean has negative effects both through mixing, thereby reducing the average light level a particular colony is exposed to, and through physical destruction of the fragile colonies. These environmental factors are very successful in explaining why there are high rate of N_2 fixation in the tropics and in the subtropical gyres in contrast to the low rates found in the high latitudes. However, these factors fail to explain why N_2 fixation appears to be high in the North Atlantic, Arabian Sea, and western North Pacific, and low in the South Atlantic and eastern South Pacific, since few differences exist between these regions with regard to the controlling factors mentioned above. Therefore, other factors need to be considered, such as the delivery of essential trace metals by dust.

A major difference between these regions is the delivery of dust from the atmosphere to the surface ocean. The subtropical North Atlantic receives about one order of magnitude more dust than the South Atlantic, and almost two orders of magnitude more than the eastern South Pacific (Duce et al., 1991; Tegen and Fung, 1994; Mahowald et al., 1999). The deposition of dust represents the most important pathway for the delivery of a number of biologically important trace metals to the surface waters of the low latitudes (Fung et al., 2000; Lefèvre and Watson, 1999). The most important elements for biology among these trace metals are iron, manganese, cobalt, zinc, copper, and molybdenum, since these elements are frequently used as reaction centers of many vital enzymes. We restrict our discussion here to iron since it has recently received most attention, but it should be kept in mind that the other trace metals also have the potential to be limiting (Morel and Hudson, 1985). *Trichodesmium* has a relatively high requirement for iron, since the nitrogenase enzyme that is responsible for breaking the N_2 bond during N_2 fixation uses iron as its core (Reuter et al., 1992). This makes this organism sensitive to variations in the supply of iron. As the dust/iron ratio appears to be relatively constant (Duce et al., 1991),

TABLE II
Estimated Sources and Sinks in the Global Marine Nitrogen Budget[a]

Process	Preindustrial (Tg N yr^{-1})	Current (Tg N yr^{-1})
Sources		
Pelagic N_2 fixation	117 ± 40[b]	117 ± 40[b]
Benthic N_2 fixation	15 ± 10[c]	15 ± 10[c]
River input (DON)	20 ± 10[d]	34 ± 10[d]
River input (PON)	21 ± 10[e]	42 ± 10[e]
Atmospheric deposition	15 ± 5[f]	30 ± 5[f]
Total sources	188 ± 44	238 ± 44
Sinks		
Benthic denitrification	85 ± 20[g]	95 ± 20[g]
Water column denitrification	80 ± 20[h]	80 ± 20[h]
Sedimentation	15 ± 5[i]	25 ± 10[i]
N_2O loss	4 ± 2[j]	4 ± 2[j]
Total sinks	184 ± 29	204 ± 30

Source: Updated from Gruber and Sarmiento (1997).

[a] Uncertainty estimates based on ranges given in the literature. DON, dissolved organic nitrogen; PON, particulate organic nitrogen.

[b] Atlantic: Gruber and Sarmiento (1997); Pacific: Deutsch et al. (2001); Indian: extrapolation; see Gruber and Sarmiento (1997).

[c] Based on Capone (1983).

[d] Based on Meybeck (1982), Duce et al. (1991) and Galloway et al. (1995).

[e] Reduced from the value given by Codispoti and Christensen (1985) to account for the organic N loss from the ocean to the atmosphere.

[f] Based on Duce et al. (1991) and Galloway et al. (1995).

[g] Based on Codispoti and Christensen (1985). Galloway et al. (1995) and the assumption that half of the anthropogenic PON river flux is denitrified.

[i] Based on Wollast (1991) and the assumption that half of the anthropogenic PON river flux is sedimented.

[j] Based on Prather et al. (1994) and Suntharalingam and Sarmiento (2000).

the strong variations of dust supply over the different regions reflect directly strong variations of the supply of iron to the surface ocean.

The observed pattern of N_2 fixation and the distribution of N^* appear to be consistent with iron playing an important role for controlling N_2 fixation. If this is correct, rates of N_2 fixation could have varied quite strongly in the past, since it is known that the deposition of dust onto the surface ocean during glacial periods was at least twice the amount of today's deposition (Mahowald et al., 1999). This led Broecker and Henderson (1998) and Falkowski (1997) to hypothesize that dust-induced variations in the rate of N_2 fixation contributed substantially to the CO_2 drawdown during glacial periods. However, the evidence for iron limitation of N_2 fixation is largely circumstantial. Results from many iron addition experiments that have been carried out so far are inconclusive, and recent analysis of iron content in natural populations

of *Trichodesmium* reveals neither a significantly higher iron requirement nor a geographical pattern in cellular iron content consistent with patterns of iron deposition (Sanudo-Willhelmy, personal communication; Hood et al., 2000).

3.3. Water-Column Denitrification

We turn now to the N^* minima observed in the N^* distributions (Figs. 9.11 and 9.12), indicative of denitrification. We focus on water-column denitrification, since this process leads to the main N^* signals that we observe in the open ocean. However, N^* is also influenced by benthic denitrification, especially near the continental shelf regions (Christensen et al., 1987; Devol, 1991). This can be seen in Fig. 9.12, where N^* exhibits minimum concentrations all along the eastern shelf of North America, a region where benthic denitrification is known to occur (Seitzinger and Giblin, 1996).

Pattern and Rates of Denitrification

The strong N^* minima in the eastern tropical North Pacific (ETNP) and eastern tropical South Pacific (ETSP) (Fig. 9.12) coincide with oxygen minimum zones (Fig. 9.13), where water column denitrification has been well studied since Brandhorst (1959) noted the existence of a secondary nitrite maximum due to denitrification [see Hattori (1983) for a review]. The existence of strong N^* minima within these known denitrification regions provides confirmation of our interpretation of N^* as a tracer reflecting N_2 fixation and denitrification. The cores of the two N^* minima have long tails that reach far westward into the center of the Pacific. The shape and position of these tails, together with their high O_2 concentrations, suggest that these features are the result of westward advection of the N^* signals in the North and South Equatorial Currents. These waters slowly lose their signature as they mix with eastward-moving waters in the equatorial undercurrent system and as they entrain subtropical waters, both having elevated N^* concentrations.

Codispoti and Richards (1976) estimated total denitrification in the ETNP to be about 19 Tg N yr^{-1} on the basis of in situ measurements of denitrification rates and extrapolation of these measurements to the entire denitrification zone. Applying the same technique, Codispoti and Packard (1980) arrived at an estimate of about 23 Tg N yr^{-1} for the ETSP. Given the difficulty of extrapolating a few individual rate measurements, the uncertainty of these estimates could be relatively large. This problem can be avoided using N^*, which integrates denitrification over space and time and is therefore less susceptible to short-term variability. Deutsch et al. (2001) followed this approach and used the disappearance of N^* in these regions together with water age from CFC observations to estimate integrated denitrification in these two regions. They found a water column denitrification of about 22 Tg N yr^{-1} for the ETSP and of about 26 Tg N yr^{-1} for the ETNP, in good agreement with the extrapolation of direct rate measurements.

The third strong minimum in the N^* distribution occurs in the Arabian Sea, another well-known oxygen minimum zone (Fig. 9.13) with high rates of water column denitrification (Naqvi et al., 1982, 1987; Mantoura et al., 1983). Low concentrations of N^* are also found in the Bay of Bengal, where denitrification has been less studied (Naqvi et al., 1978). Hattori (1983) speculated that the Bay of Bengal may contribute to oceanic denitrification, as very low oxygen concentrations are found there. However, no active denitrification has yet been found (Howell et al., 1997). Rates of

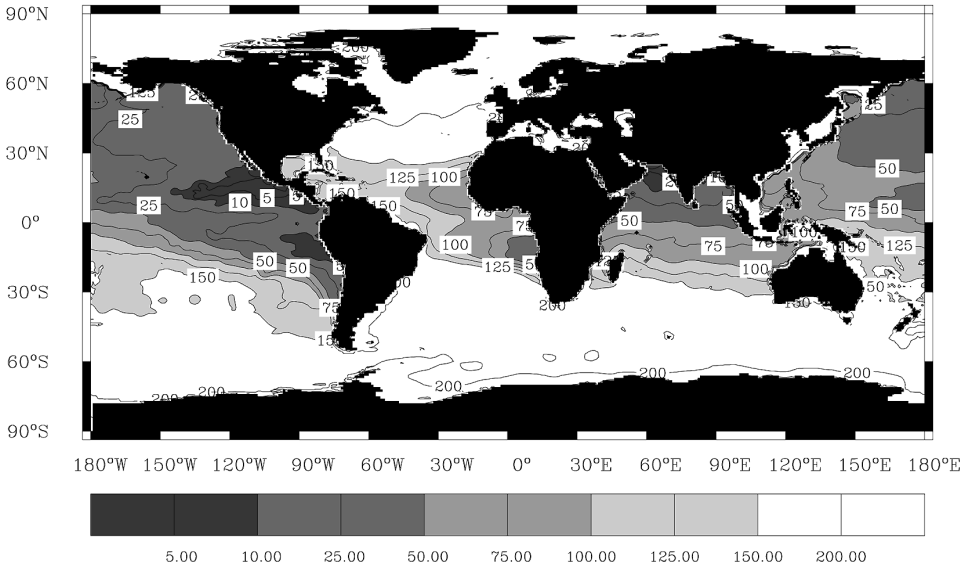

Fig. 9.13. Global distribution of the dissolved oxygen concentration (μmol kg^{-1}) at the depth of the vertical oxygen minimum. [Based on the 1° gridded oxygen data of Levitus and Boyer (1994a).]

denitrification in the Arabian Sea have been estimated following various techniques. Most recently, Howell et al. (1997) used NO, a geochemical tracer similar to N^*, to arrive at an integrated denitrification of about 21 Tg N yr^{-1}. This compares favorably with extrapolation of direct rate measurements (Naqvi and Shailaja, 1993) and box models (Naqvi, 1987).

Table II summarizes the global pelagic denitrification rates. Additional 10 Tg N yr^{-1} are added to account for pelagic denitrification in smaller areas, such as the eastern tropical Atlantic (Christensen et al., 1987). This table also shows that about an equal amount of fixed nitrogen is lost due to benthic denitrification, which occurs primarily in shelf sediments. Sedimentation and a small loss of N_2O to the atmosphere bring the total sinks of fixed nitrogen in the ocean to about 184 Tg N yr^{-1} in preindustrial times and about 204 Tg N yr^{-1} in present times.

Controls on Water Column Denitrification

Since the energy yield for the oxidation of organic matter is smaller when nitrate is used as terminal electron acceptor instead of oxygen, water column denitrification is essentially limited to the oxygen depleted zones of the open ocean. We therefore have to understand the mechanisms that generate these oxygen depletion zones if we want to understand the processes that control the pattern and rates of water column denitrification.

As we have seen in Section 2, the distribution of oxygen in the ocean is determined by air–sea gas exchange at the surface, ocean circulation and mixing, and the photosynthesis–respiration cycle of organic matter. In the interior of the ocean, the condition for the generation of an oxygen-depletion zone is therefore simply given when the supply of oxygen by ocean transport is smaller than the oxygen demand from the remineralization of organic matter. In the present ocean, only a few oxygen-depletion

zones exist in the open ocean (Fig. 9.13): the ETSP and ETNP in the Pacific and the Arabian Sea. The common characteristic of these three regions is high surface export production coupled with slow rates of water renewal in the subsurface ocean.

The high rates of export in these regions are linked to high rates of upwelling of nutrient-rich waters into the surface waters, thereby promoting high surface productivity. The low ventilation of subsurface waters in the eastern tropical Pacific can be explained on the basis of theories of the thermocline ventilation (see, e.g., Pedlovsky, 1987). The conservation of potential vorticity (a measure of the angular momentum of a fluid parcel) requires that the interior of a density surface can be advectively ventilated only along streamlines that intersect the outcrop. However, the entire density surface cannot be reached by these streamlines, resulting in a shadow zone that is being ventilated only by diffusion (Luyten et al., 1983). As diffusion is much less effective than advection in ventilating, waters in the shadow zones are relatively stagnant. The oxygen minimum zones in the eastern tropical Pacific are such shadow zones, as are the southeastern part of the North Atlantic subtropical gyre and the northeastern part of the South Atlantic subtropical gyre (Kawase and Sarmiento, 1985). Figure 9.13 shows that the two latter regions also have very low oxygen concentrations, but are not anoxic. Since the levels of productivity (Laws et al., 2000) and rates of water renewal in the Atlantic are relatively similar to those in the Pacific, this difference is probably caused by the fact that waters in the Atlantic Ocean are generally younger and hence contain, on average, higher O_2 concentrations. This therefore provides a higher supply of O_2 for the same rate of ventilation.

The conditions that lead to the formation of the oxygen minimum zone in the Arabian Sea are less clear (Naqvi, 1987; Morrison et al., 1999), since the Arabian Sea is not a shadow zone. However, the thermocline structure and circulation of the Arabian Sea is very unique (Wyrki, 1973). The Arabian Sea is characterized by a semiannual reversal in wind stress associated with the monsoon, water mass intrusions from marginal seas, and the absence of a subtropical convergence zone and deep-water formation. The core of the oxygen minimum zone is located within the salinity maximum of Persian Gulf water. Measurements of CFC indicate that these waters are only two to eight years old (Howell et al., 1997). This is much younger than the CFC ages found in the ETSP and ETNP (Deutsch et al., 2001). Thus, to create the intense oxygen depletion zone found in the Arabian Sea, either the oxygen demand must be substantially higher than that created in the ETSP and ETNP or the source waters must already have very low O_2 concentrations. Warren (1994) suggested that export production in the Arabian Sea is not anomalously large, concluding that the latter mechanism must be the cause of anoxia in the Arabian Sea. A newer study by Smith et al. (1998) disputes this conclusion and suggests that low ventilation and high biological production conspire to create suboxic waters.

Denitrification can respond strongly and rapidly to changes in physical forcing (changing ventilation) and changes in the supply of organic material as observationally confirmed in the Arabian Sea (Naqvi et al., 1990) and in the ETSP (Codispoti et al., 1986). This makes it likely that rates of denitrification could have varied substantially in the past. Analyzing sediment cores underlying the eastern Pacific and Arabian Sea, Altabet et al. (1995) and Ganeshram et al. (1995) found drastically reduced rates of denitrification during the last glacial period. This led them and Ganeschram et al. (2000) to hypothesize that reduced denitrification in these two zones resulted in an increased fixed-N inventory in the ocean and contributed to the glacial–interglacial

CO_2 drawdown. Although these observations clearly support the conclusion of lower water column denitrification during the last glacial period, they do not necessarily imply a higher N inventory. This is only the case if N_2 fixation stayed constant or increased.

3.4. Dynamic Homeostasis

Given that we just learned that the rates of N_2 fixation and water column denitrification are controlled by entirely different processes, it is surprising that the preindustrial and present marine N budget appears to be in relatively close balance (see Table II). This approximate balance is particularly difficult to explain when considering how strongly and rapidly each of these two processes can respond to changes in its controlling factors and mechanisms. Evidently, denitrification and N_2 fixation are more strongly linked together as first appears to be the case.

As it turns out, this question is tied to the question of whether nitrate or phosphate is limiting oceanic primary production (Smith, 1984; Codispoti, 1989; Tyrrell, 1999). One point of view is that N is the limiting nutrient, as evidenced by the existence of a small excess P in the surface waters of most of the low-latitude ocean and the enhancement of production when N is added to the ocean, as opposed to little effect when P is added (Ryther and Dunstan, 1971; Codispoti, 1989). The second point of view is that although the first point of view might be correct on short time scales, phosphate is the limiting nutrient on longer time scales (Broecker and Peng, 1998). According to this argument, the N content of the ocean is linked to that of P, since the N content can be adjusted by N_2 fixation and denitrification. Two negative feedback processes have been proposed that ensure this adjustment of N to P (Redfield, 1958; Codispoti, 1989). The first feedback process is based on denitrification (Codispoti, 1989). When denitrification increases, the N content of the ocean decreases, thereby on average reducing the supply of N to the surface ocean. This results in a smaller export production, leading to a smaller oxygen demand in the thermocline. As a consequence, denitrification decreases, closing the negative feedback loop.

The second feedback loop links surface N_2 fixation to the small excess of P that is generally observed in low-latitude surface waters (Tyrrell, 1999). This proposed mechanism builds on the assumption that N_2 fixers have a lower growth rate than that of normal phytoplankton (Capone et al., 1997). They can thrive, however, in the case when nitrate gets depleted in the surface ocean before phosphate, since they can circumvent nitrogen limitation. Therefore, if N becomes scarce relative to P, N_2 fixation would go up and resupply the N to the ocean. This process continues until the diazotrophic organisms effectively reduce their habitat until N_2 fixation is back in balance with denitrification.

Although these two feedback loops provide a possible answer to our question, many details remain unclear. For instance, the observation of high N_2 fixation in the North Atlantic is inconsistent with the second feedback mechanism, because in this ocean basin, P runs out before N (Wu et al., 2000). Therefore, according to this hypothesis, there should be no habitat for diazotrophs, which is clearly not the case (Carpenter and Romans, 1991). Conversely, over most of the low latitudes of the Pacific and Indian Oceans, N is depleted before P, yet diazotrophs are not as abundant as they should be according to this hypothesis (Carpenter, 1983). Clearly, other factors in addition to P, such as iron, must play an important role.

Lenton and Watson (2000) recently investigated these two feedback loops in a simple feedback model of ocean biogeochemical cycles. They find that these two feedback loops are indeed very effective in keeping nitrate close to the Redfield ratio with phosphate, as long as other factors, such as iron, do not limit N_2 fixation to a substantial degree. They find that in the case of strong iron limitation of N_2 fixation, increasing the phosphate input into the ocean can cause phosphate to deviate above the Redfield ratio to nitrate. Thus, under certain circumstances, nitrate can become the ultimate limiting nutrient even over geological time scales. But in all other cases, phosphate is controlling the amount of fixed nitrogen in the ocean.

It needs to be pointed out that both feedbacks operate on the time scale of whole ocean overturning (i.e., approximately 1000 years). This implies that on time scales shorter than this, imbalances between N_2 fixation and denitrification can exist and significantly alter the N content of the ocean. A second point to make is that these proposed feedback mechanisms do not necessarily imply that the N content of the ocean has to be exactly 16 times the P content; they imply only a rough Redfieldian stoichiometry. Therefore, the existence of negative feedback loops that couple the N content of the ocean to that of P are not at odds with the possibility that variations in the N content of the ocean contributed to the glacial interglacial CO_2 variations (Falkowski, 1997; Broecker, 1998). These feedback loops just confine the marine N inventory to within relative narrow boundaries set by the ocean inventory of P.

4. Ocean Carbon Pumps

We noted in the introduction that the surface concentration of DIC is lower than that of the deep ocean by more than 10%. Based on the WOCE global survey data, this vertical gradient in salinity normalized DIC (sDIC) amounts to about 270 μmol kg^{-1} (Fig. 9.14). This vertical gradient has major consequences for atmospheric CO_2. If the ocean were allowed to be mixed uniformly, atmospheric CO_2 would almost reach twice its preindustrial concentration. It is thus of considerable importance to understand what gradient makers act to maintain the DIC gradient in the face of ocean circulation and mixing, which generally tend to homogenize these gradients. We have seen in Fig. 9.9*a* that most of the variations of sDIC in the oceans are associated with P with stoichiometry of about 117 : 1, indicating that the soft tissue pump is the most important process controlling the distribution of sDIC in the ocean. There also exist, however, substantial deviations of sDIC from the stoichiometric relationship with P that must be due to processes that have stoichiometric ratios distinctly different from that of the soft tissue pump. These processes that decouple sDIC from P are (1) the biogenic formation and dissolution of calcareous material ($CaCO_3$), (2) air–sea gas exchange, and (3) the uptake of anthropogenic CO_2 from the atmosphere.

The role of these three processes in contributing to the observed sDIC variations will be the main emphasis of this section. We particularly focus on the role of air–sea gas exchange, since we will find that its influence—contrary to expectation—seems to be relatively small. This is especially surprising when contrasted with oxygen, whose distribution seems to be strongly affected by air–sea gas exchange (compare Fig. 9.9*a* with 9.9*b*). As we will see, the main reason for the small imprint of air–sea gas exchange on sDIC is because temperature-driven exchanges of CO_2 across the air–sea interface and biologically driven CO_2 fluxes work in opposite direction for CO_2, therefore strongly reducing the combined impact of air–sea gas exchange. By

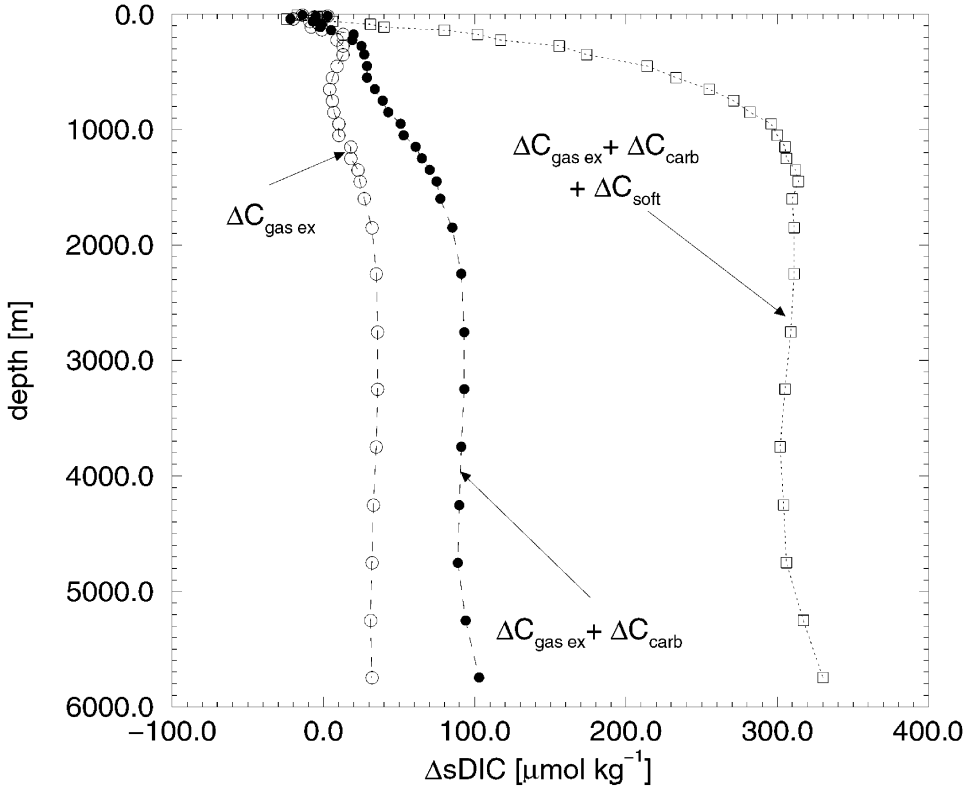

Fig. 9.14. Global mean profiles of the carbon pump components. (Based on data from the JGOFS/WOCE/NOAA global survey.)

contrast, these two driving factors work in the same direction for O_2, leading to a very strongly imprinted air–sea gas exchange signal for O_2. Before we can attempt to build the arguments to understand this conclusion, we need to briefly review the processes controlling air–sea gas exchange and $CaCO_3$ cycling, which requires the introduction of a few concepts of inorganic carbon chemistry in seawater.

4.1. Review of Air–Sea Gas Exchange and $CaCO_3$ Cycling

CO_2 exchanges across the air–sea interface whenever the partial pressure of CO_2 in the surface ocean is out of equilibrium with that in the overlying atmosphere. The partial pressure of CO_2 in the surface ocean is controlled by the solubility of CO_2 and by the concentration of gaseous CO_2 in the ocean (Henry's law). The solubility itself is highly sensitive to changes in temperature and to a lesser degree to changes in salinity. The concentration of gaseous CO_2 is in turn influenced by the fact that it reacts with seawater to form bicarbonate (HCO_3^-) and carbonate (CO_3^{2-}) ions. The sum of the concentrations of CO_2, HCO_3^{2-}, and CO_3^{2-} is equal to DIC (DOE, 1994):

$$\mathrm{DIC} = [CO_2] + [HCO_3^-] + [CO_3^{2-}]. \tag{23}$$

A measure of the extent to which CO_2 has reacted with water to form CO_3^{2-} and HCO_3^- is the concentration of total alkalinity (Alk), which represents approximately the contribution of CO_3^{2-} and HCO_3^- to the charge balance of seawater:

$$[\mathrm{Alk}] \approx [\mathrm{HCO_3^-}] + 2\,[\mathrm{CO_3^{2-}}]. \tag{24}$$

This means that the higher the Alk concentration for a given temperature, salinity, and DIC concentration, the more complete is the reaction of CO_2 with water to form CO_3^{2-} and HCO_3^-, leading to a low gaseous CO_2 concentration and hence low pCO_2. The sensitivity of pCO_2 to changes in DIC is opposite. The higher the DIC concentration for a given temperature, salinity, and Alk concentration, the higher is the concentration of gaseous CO_2 and hence pCO_2 (Baes, 1982). As the solubility of CO_2, like most gases, is substantially larger at low temperatures, pCO_2 decreases with decreasing temperatures for the same DIC and Alk. Because deep waters are cold and surface waters warm, the temperature sensitivity of the CO_2 solubility contributes to the surface to deep gradient in DIC, and hence this effect is commonly referred to as the *solubility pump* (Volk and Hoffert, 1985).

The exchange of CO_2 across the air–sea interface is relatively slow. It takes about a year for a 50-m-deep surface mixed layer to equilibrate with the atmosphere after a perturbation, whereas the equilibrium time for oxygen is only a few weeks (Broecker and Peng, 1974). The reason for this long equilibrium time relative to oxygen is the fact that CO_2 has to equilibrate with the total pool of DIC. The CO_2 molecule accomplishes that by reaction with the CO_3^{2-} ion, which constitutes about 10% of the total DIC pool. This leads to a slowdown of the air–sea gas exchange reaction of approximately a factor of 10 relative to oxygen. Nevertheless, the residence time of waters near the surface appears to be long enough so that the ocean pCO_2 is usually larger than 80% of saturation (Takahashi et al., 1997, 1999).

The invasion of anthropogenic CO_2 into the ocean represents another process we have to take into account. The net air–sea flux of CO_2 into the ocean is caused by a strong perturbation of the global carbon cycle by humankind through the burning of fossil fuels, cement production, and the changes in land use. As a consequence of these activities, atmospheric CO_2 has increased by more than 30% over the last two centuries (Keeling et al., 1995; Etheridge et al., 1996) and probably will continue to increase in the future (Houghton et al., 1996). The surface ocean takes up a fraction of the anthropogenic CO_2 from the atmosphere and transports it into the interior of the ocean. The rate-limiting step for this uptake is the surface to deep transport (Sarmiento et al., 1992), since air–sea gas exchange is rapid enough to keep up with the atmospheric CO_2 growth.

The second biological reaction of great importance for carbon cycling is the biogenic formation and dissolution of calcite or aragonite:

$$\mathrm{Ca^{2+}} + \mathrm{CO_3^{2-}} \Leftrightarrow \mathrm{CaCO_3} \tag{25}$$

Due to the double charge of the carbonate ion, the formation and dissolution of mineral calcium carbonate changes Alk twice as much as it changes DIC (Stumm and Morgan, 1981). Upon death of these organisms, these shells sink and eventually dissolve, either in the water column or in the sediments, except for a small fraction

buried permanently (Milliman, 1993). Because the concentration of Ca^{2+} is relatively constant, the dissolution of $CaCO_3$ is governed primarily by the difference between the in situ concentration of CO_3^{2-} and the saturation concentration of CO_3^{2-}, which itself is mainly controlled by pressure (Millero, 1983). The net effect of the biogenic formation and dissolution of $CaCO_3$ is a net downward transport of DIC and Alk from the surface ocean into the deeper ocean. This process thus adds to the biological pump and is often termed the *carbonate pump* (Volk and Hoffert, 1985).

SIDEBAR 9.4
Estimation of Carbon Pump Components

We begin with the conservation equations for DIC, Alk, and phosphate, P:

$$\Gamma(\mathrm{DIC}) = J_{\mathrm{soft}}(\mathrm{DIC}) + J_{\mathrm{carb}}(\mathrm{DIC}) \tag{26}$$

$$\Gamma(\mathrm{Alk}) = J_{\mathrm{soft}}(\mathrm{Alk}) + J_{\mathrm{carb}}(\mathrm{Alk}) \tag{27}$$

$$\Gamma(\mathrm{P}) = J_{\mathrm{soft}}(\mathrm{P}) \tag{28}$$

where J_{soft} denotes the source term due to the soft tissue pump and J_{carb} denotes the source term due to the carbonate pump. The operator Γ represents the transport and time rate of change (see equation 13). Please note that gas exchange enters as a boundary condition and is therefore not included in equation 26. The J terms of the soft tissue pump of DIC and P are related to each other by the stoichiometric ratio $r_{\mathrm{C/P}}$. The influence of the soft tissue pump on Alk (Brewer, 1978) is equal to the change in nitrate, which in turn is related to a change in P by the stoichiometric ratio $r_{\mathrm{N/P}}$.

$$J_{\mathrm{soft}}(\mathrm{DIC}) = r_{\mathrm{C/P}} J_{\mathrm{soft}}(\mathrm{P}) \tag{29}$$

$$J_{\mathrm{carb}}(\mathrm{DIC}) = \tfrac{1}{2} J_{\mathrm{carb}}(\mathrm{Alk}) \tag{30}$$

$$J_{\mathrm{soft}}(\mathrm{Alk}) = -J_{\mathrm{soft}}(\mathrm{NO_3^-}) = -r_{\mathrm{N/P}} J_{\mathrm{soft}}(\mathrm{P}) \tag{31}$$

Substituting these relationships (equations 29 to 31 into equations 26 and 27) and eliminating the J_{soft} and J_{carb} results in

$$\Gamma(\mathrm{DIC}) - r_{\mathrm{C/P}}\Gamma(\mathrm{P}) - \tfrac{1}{2}[\Gamma(\mathrm{Alk}) + r_{\mathrm{N/P}}\Gamma(\mathrm{P})] = 0 \tag{32}$$

Since we assumed constant stoichiometric ratios, the DIC, Alk, and P equations are linear, and therefore the transport and time rate of change operators Γ can be combined to give $\Gamma(\mathrm{DIC} - r_{\mathrm{C/P}}\mathrm{P} - \frac{1}{2}[\mathrm{Alk} + r_{\mathrm{N/P}}\mathrm{P})]$. This allows us to define a tracer C^*.

$$\mathrm{C}^* = \mathrm{DIC} - r_{\mathrm{C/P}}\mathrm{P} - \tfrac{1}{2}(\mathrm{Alk} + r_{\mathrm{N/P}}\mathrm{P}) + \mathrm{const} \tag{33}$$

with conservative properties; that is, C^* has no biological or chemical sources or sinks in the ocean [$\Gamma(\mathrm{C}^*) = 0$] (Gruber et al., 1999). Since we have removed the

effects of biological processes, the variations in C^* are governed only by air–sea gas exchange, including the uptake of anthropogenic CO_2.

The value of the constant is arbitrary, but for the purpose of our discussion here it is convenient to choose it such that the global mean surface value of C^* is zero. This is the case if we set the constant equal to $r_{C/P}P^o - \frac{1}{2}(Alk^o - r_{N/P}P^o) - DIC^o$, where P^o, Alk^o, and DIC^o are constant reference values, chosen here to be ocean surface mean values (i.e., 2320 μmol kg^{-1} for Alk^o, 0.07 μmol kg^{-1} for P^o, and 2034 μmol kg^{-1} for DIC^o. In addition, we normalize C^* to a constant salinity, S^o, in order to remove the influence of evaporation and precipitation.

This gives

$$sC^* = \frac{S^o}{S}\,[DIC - r_{C/P}\,\Delta P - \tfrac{1}{2}(\Delta Alk + r_{N/P}\,\Delta P)] - DIC^o \tag{34}$$

where $\Delta P = P - (S/S^o)P^o$ and $\Delta Alk = Alk - (S/S^o)Alk^o$. This definition of sC^* is equivalent to the tracer $\Sigma CO_2{}^*$ employed by Broecker and Peng (1992) to study large-scale meridional transport of carbon in the oceans. Strictly speaking, the salinity normalization introduces small nonlinear terms, so that $\Gamma(sC^*)$ is not exactly zero anymore. However, since salinity varies by less than 5% over most of the ocean, these nonlinearities are very small and can therefore be neglected.

The contribution of the potential soft tissue pump, ΔC_{soft}, and that of the potential carbonate pump, ΔC_{carb}, can be identified in equation 34 as the second and last terms inside the brackets on the right-hand side, that is,

$$\Delta C_{soft} = \frac{S^o}{S}\,r_{C/P}\,\Delta P \tag{35}$$

$$\Delta C_{carb} = \frac{S^o}{S}\,\tfrac{1}{2}\,(\Delta Alk + r_{N/P}\,\Delta P) \tag{36}$$

In Section 4.5, we explain how we can estimate the amount of anthropogenic CO_2 in the oceans using tracers derived from C^*. This permits us to remove the anthropogenic CO_2 component from sC^* and investigate the gas exchange pump in the preindustrial ocean.

$$\Delta C_{gas\ ex} = sC^* - \Delta C_{ant} \tag{37}$$

4.2. *Pump Separation*

We use the concept of quasiconservative tracers to separate the carbonate and gas exchange pumps from the soft tissue pump, as well as to distinguish the anthropogenic CO_2. Our strategy is very similar to that used by Broecker and Peng (1992), who investigated the uptake of CO_2 from the atmosphere in the North Atlantic and its subsequent transport across the equator. The details of the separation are given in Sidebar 9.4.

We describe the effect of the soft tissue pump, ΔC_{soft} by using phosphate as an

indicator just as we did for nitrate (see Sidebar 8.3). For the contribution of the carbonate pump, ΔC_{carb}, we can use alkalinity (Alk) as an indicator, since its distribution is dominated by this pump. Finally, we estimate the gas exchange pump, $\Delta C_{gas\ ex}$, by taking the difference between the observations and the two biological pumps. A complication is that we have to take into account the invasion of anthropogenic CO_2 from the atmosphere. We use the method of Gruber et al. (1996) to estimate this contribution, ΔC_{ant}, directly from observations, as discussed in more detail below. Since we are interested primarily in surface-to-deep gradients, we look only at deviations from surface mean concentrations. We thus consider the following separation:

$$\Delta sDIC_{pi} = sDIC - \Delta C_{ant} - DIC^{o} = \Delta C_{soft} + \Delta C_{carb} + \Delta C_{gas\ ex} \tag{38}$$

where $\Delta sDIC_{pi}$ is the preindustrial (pi) sDIC concentration relative to a reference concentration DIC^{o} chosen here as the mean surface ocean sDIC in preindustrial times.

It is important to note that the gas exchange pump, as we define it here, consists itself of two different components, one driven primarily by heat fluxes (thermal component, $\Delta C^{therm}_{gas\ ex}$) [with a small component driven by freshwater fluxes (Murnane et al., 1999)] and one driven by changes in surface carbon chemistry as a consequence of biology (biological component, $\Delta C^{bio}_{gas\ ex}$):

$$\Delta C_{gas\ ex} = \Delta C^{bio}_{gas\ ex} + \Delta C^{therm}_{gas\ ex} \tag{39}$$

The solubility pump (Volk and Hoffert, 1985), as commonly understood to be that part of the DIC variations that is driven by heat and freshwater fluxes, is therefore equivalent to the thermal component of the gas exchange pump, $\Delta C^{therm}_{gas\ ex}$.

It is important to recognize that the soft tissue pump and the carbonate pumps that we infer from P and Alk are the DIC distribution the ocean would have in the absence of air–sea gas exchange. They thus can be thought of as the "potential" biological pumps. The effect of air–sea exchange is to reduce the magnitude of the DIC variations induced by biological processes. Unfortunately, we cannot separate $\Delta C_{gas\ ex}$ rigorously into its two components on the basis of observations. However, we will use model results to illustrate the role of these two gas exchange components.

We discuss each of these pumps in turn, beginning with the soft tissue pump. The major focus of the discussion is on the contribution of the gas exchange pump to the DIC distribution, because this pump reveals some interesting features that serve as good examples to illustrate physical–biogeochemical interactions, particularly when contrasted with oxygen.

4.3. Biological Pumps

Figure 9.14 shows that the potential soft tissue pump is the most important one, being responsible for about 220 μmol kg^{-1} (70%) of the preindustrial surface-to-deep gradient of about 315 μmol kg^{-1}. The potential carbonate pump accounts for approximately 60 μmol kg^{-1} (20%) of the observed gradient. However, it is important to be reminded that these are estimates of the contributions of the biological pumps in the absence of air–sea gas exchange and that air–sea gas exchange will tend to reduce

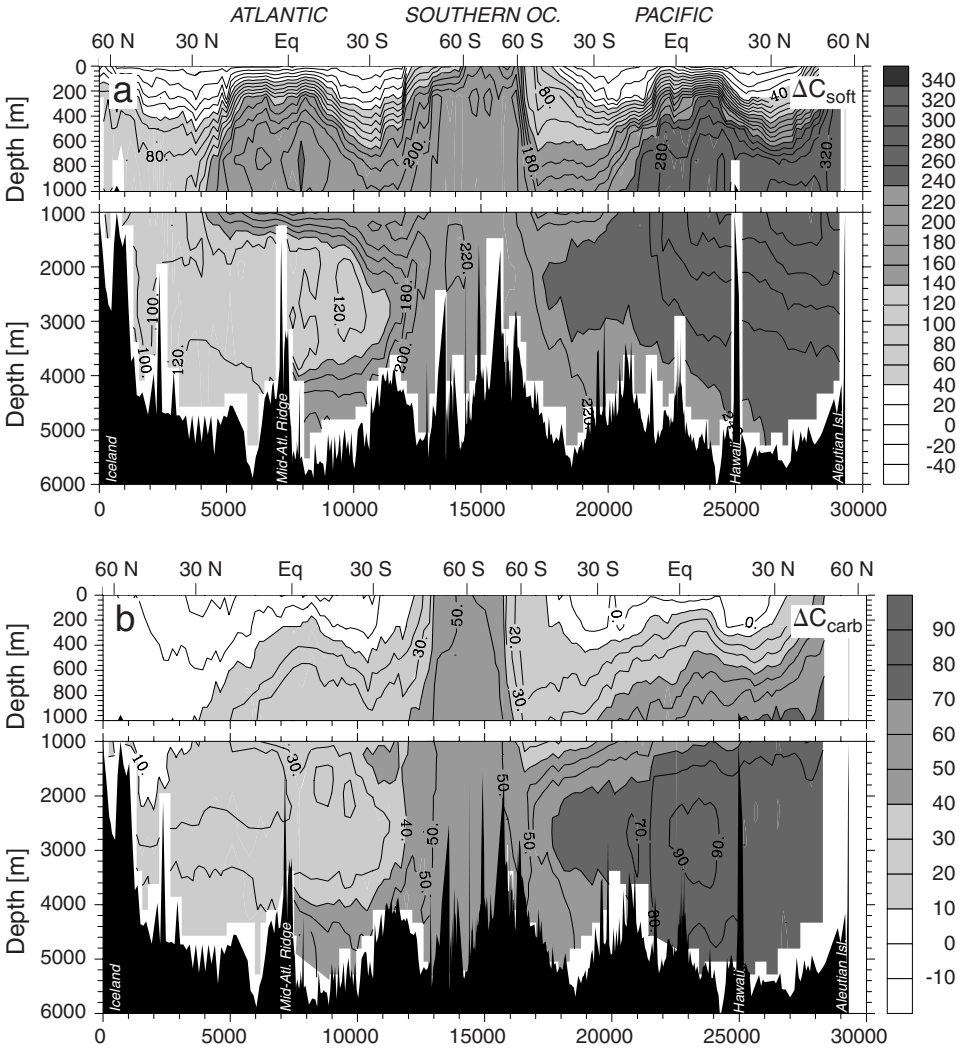

Fig. 9.15. Same as Fig. 9.3, but (*a*) for the soft tissue pump component of DIC (ΔC_{soft}) (μmol kg^{-1}), (*b*) for the the carbonate pump component of DIC (ΔC_{carb}) (μmol kg^{-1}) and (*c*) for the preindustrial gas exchange pump component of DIC ($\Delta C_{gas\,ex}$) (μmol kg^{-1}). See text and Sidebar 9.4 for details.

the effect of biology by allowing some of the deep-ocean CO_2 to escape through outcrops in the high latitudes.

The dominance of the soft tissue pump in creating the vertical gradient in $\Delta sDIC_{pi}$ is a direct consequence of the strong correlation observed between DIC and P (Fig. 9.9*a*). The substantially smaller contribution of the carbonate pump is consistent with the observation that the expert of $CaCO_3$ out of the surface ocean is about four to five times smaller than that of organic carbon (Broecker and Peng, 1982; Milliman, 1993; Milliman and Droxler, 1996). Figures 9.15*a* and *b* show the contribution of the biological pumps in more detail along the same section as DIC was presented in Fig.

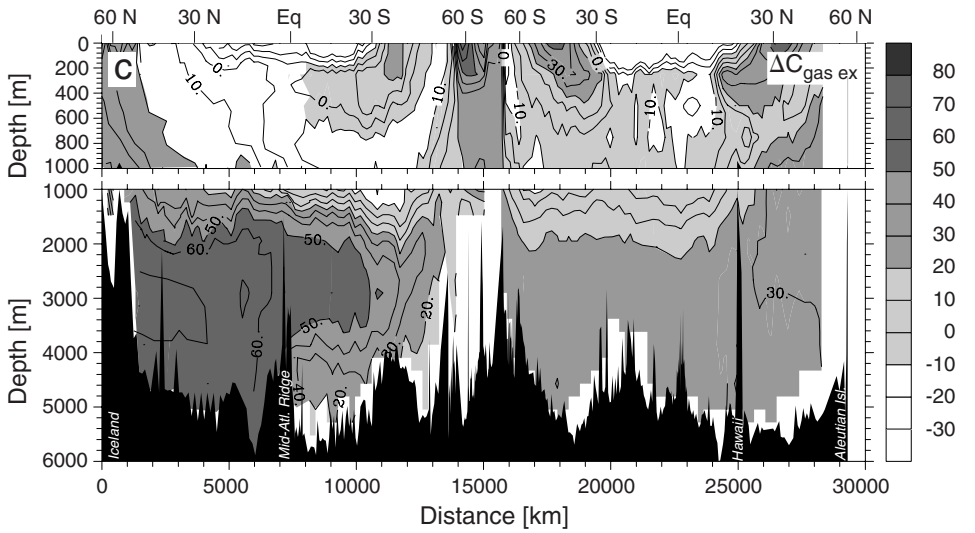

Fig. 9.15. Continued.

9.3*a*. As the contribution of the soft tissue pump is essentially a scaled version of the phosphate distribution, its distribution bears no new information. The contribution of the carbonate pump shows a pattern similar to that of the soft tissue pump, with surface depletion in the low latitudes, high concentrations in the surface waters of the Southern Ocean, and gradually increasing concentration along the flow path of the lower limb of the Great Conveyor Belt. However, there are a number of notable differences, of which two stand out.

First, the strong vertical gradients in ΔC_{soft} observed in the upper thermocline of the low latitudes are almost completely absent in the ΔC_{carb} distribution. Although this upper ocean gradient accounts for almost the entire surface-to-deep gradient in the soft tissue component, ΔC_{soft}, the contribution of the carbonate pump component, ΔC_{carb}, to the vertical variability of $\Delta sDIC_{pi}$ in the main thermocline is relatively small (<40 μmol kg^{-1}). The second difference to note is that the vertical maximum of ΔC_{carb} occurs significantly deeper than that of ΔC_{soft}.

The difference between ΔC_{soft} and ΔC_{carb} is particularly striking in the Atlantic basin, where ΔC_{carb} gradually increases all the way to the bottom, whereas ΔC_{soft} shows a pronounced maximum in intermediate waters at around 1000 m. The maximum in ΔC_{carb} shoals from the Atlantic to the Indian and Pacific Oceans but still occurs significantly deeper than the maximum in ΔC_{soft}. This indicates that the formation and dissolution of calcium carbonate is a process that is to some degree independent from the formation and remineralization of organic matter. With regard to dissolution, there exists a general consensus that the saturation state of seawater with respect to $CaCO_3$ represents the most important driver for $CaCO_3$ dissolution (Keir, 1980; Broecker and Peng, 1982; Jahnke et al., 1994). Surface waters are supersaturated with respect to $CaCO_3$, whereas deep waters are generally undersaturated. However, the depth where waters change from being supersaturated to being undersaturated [called the *saturation horizon* (Broecker and Takahashi, 1977)] is variable. The saturation horizon with respect to calcite lies at about 4000 m in the North Atlantic

and shoals gradually southward to about 3000 m in the South Atlantic (Broecker and Takahashi, 1977; Archer, 1996). The calcite saturation horizon shoals further as waters move northward into the Indian and Pacific Oceans. In the North Pacific, this horizon lies as shallow as 500 m (Archer, 1996).

It is interesting to note that the distribution of the calcite saturation horizon is largely shaped by the soft tissue pump. The saturation state of seawater with respect to $CaCO_3$ is essentially controlled by the concentration of the CO_3^{2-} ion, which can be approximated by the difference between Alk and DIC ($CO_3^{2-} \approx$ Alk $-$ DIC) (see equations 23 and 24). Using this approximation we can estimate the contribution of the soft tissue and carbonate pumps to variations in CO_3^{2-}, since we know the contribution of these pumps to variations in DIC and Alk. The net surface-to-deep gradient in (Alk $-$ DIC) from the carbonate pump is about 60 μmol kg^{-1} (2 $\times$ 60 μmol kg^{-1}), whereas the surface-to-deep gradient in (Alk $-$ DIC) from the soft tissue pump is about -190 μmol kg^{-1} (220/6.6 μmol kg^{-1} $-$ 220 μmol kg^{-1}). Thus, the soft tissue pump is clearly the dominating controlling factor for the distribution of CO_3^{2-} and hence also for the saturation horizon.

The spatial distribution exhibited by ΔC_{carb} is largely consistent with the observed variation of the calcite saturation horizon. Comparably little addition of DIC from the dissolution of $CaCO_3$ particles is found above the saturation horizon, whereas substantial amounts can be found below this horizon. However, the gradients are much smoother than one might expect if there were no dissolution occurring in supersaturated waters. This lack of strong gradients is certainly caused in part by the smoothing effect of ocean circulation and mixing. However, there exists increasing evidence that a sizable fraction of the sinking flux of $CaCO_3$ is dissolving well above the saturation horizon (Milliman et al., 1999). This evidence comes in part from many observations that show that the vertical $CaCO_3$ flux captured by sediment traps decreases with depth well above the saturation horizon (Martin et al., 1993). Shallow-water dissolution of $CaCO_3$ is further supported by measurements of the in situ concentration of $CaCO_3$ particles, which indicate a rapid decrease with depth (Bishop et al., 1986) and measurements of surface ocean calcification rates that are several times larger than the measured $CaCO_3$ fluxes at 1000 m depth (Balch and Kilpatrick, 1996). The exact mechanisms that drive this dissolution are presently not well understood, but Milliman et al. (1999) speculate that dissolution inside zooplankton guts and respiratory-driven dissolution within particles might be important. In addition, dissolution in sediments and diffusion of the products back into the overlying waters might also contribute to the existence of ΔC_{carb} signals above the saturation horizon (Emerson and Bender, 1981).

Processes in the sediments are important to consider for the $CaCO_3$ cycle for two reasons. First, a significant fraction of the surface export production of $CaCO_3$ reaches the sediment surface and is transformed there [about 40% according to Milliman and Droxler (1996)]. Second, observations and model studies have shown that the $CaCO_3$ saturation state of pore waters is often much lower than the saturation state of the overlying waters (Emerson and Bender, 1981; Archer et al., 1989; Berelson et al., 1994). The reason for this decoupling between dissolution and the saturation state of the overlying seawater is the remineralization of organic matter in the sediments which can strongly decrease the CO_3^{2-} content in the porewaters (identical to the effect of ΔC_{soft} on the position of the saturation horizon, explained above) (Berger, 1970; Emerson and Bender, 1981; Hales and Emerson, 1996). This effect is particu-

larly strong if the amount of organic matter reaching the sediment is approximately equal to or bigger than the amount of $CaCO_3$ being deposited (Archer, 1991, 1996). The magnitude of respiratory-driven dissolution of $CaCO_3$ is not very well established. Sediment model results suggest that 40 to 70% of the sediment dissolution could occur at or above the calcite saturation horizon (Hales et al., 1994; Archer, 1996), whereas budget calculations by Milliman (1993) indicate a far smaller contribution of only about 20%.

4.4 Gas Exchange Pump

We turn now to the gas exchange pump. Figure 9.14 reveals that the contribution of the gas exchange pump to the global mean vertical profile of $\Delta sDIC_{pi}$ amounts to only about 35 μmol kg^{-1} (10%). This is very different from what we might expect if we assumed that the main driving factor for the air–sea exchange of CO_2 is the exchange of heat across the air–sea interface and if we further assumed that CO_2 exchanges as quickly as heat. We can estimate the expected DIC gradient due to this process using the observed surface to deep temperature gradient of about 18°C and employing a temperature sensitivity of the DIC solubility of about 9 μmol kg^{-1} per degree temperature change (Takahashi et al., 1993). This yields an expected surface to deep gradient in DIC of about 155 μmol kg^{-1}, more than five times our estimate (Fig. 9.16). The small imprint of gas exchange on CO_2 is even more puzzling when we contrast it with the very large imprint this process has on the distribution of O_2 (Fig. 9.9*b*).

Consideration of $\Delta C_{gas\ ex}$ in the various ocean basins reveals additional puzzles (Fig. 9.15*c*). Hidden in the small global mean surface to deep difference of $\Delta C_{gas\ ex}$, we find a very large imprint of the gas exchange pump in the deep Atlantic associated with NADW. The deep Pacific has much smaller and vertically more uniform values of $\Delta C_{gas\ ex}$. What are the reasons for the Atlantic having such a large air–sea exchange imprint, whereas the deep Pacific is lacking it? This question is linked to one of the currently intensively debated research topics in global carbon cycle research. Since deep waters in the Atlantic flow southward, this high-$\Delta C_{gas\ ex}$ signal in the deep Atlantic provides, in principle, an oceanic conduit for transporting CO_2 from the northern hemisphere into the southern hemisphere (Broecker and Peng, 1992, 1993; Keeling and Peng, 1995). In the preindustrial steady state, such as oceanic southward transport had to be compensated by a northward transport in the atmosphere. This would have required the existence in preindustrial times of a south-to-north concentration gradient in atmospheric CO_2. Accurate knowledge of such a preindustrial interhemispheric gradient in atmospheric CO_2 is of prime importance for atmospheric inverse studies that attempt to determine the present sources and sinks of anthropogenic CO_2 in the global carbon cycle (Keeling et al., 1989; Tans et al., 1990; Ciais et al., 1995; Fan et al., 1999).

We start our discussion by addressing the puzzle of the small global mean contribution of the gas exchange pump and consider the Atlantic gas exchange signal afterward. As we will see, however, the underlying cause for these two patterns is the same. It is the interaction of large-scale ocean circulation, slow kinetics of air–sea gas exchange, ocean biology, and heat fluxes that determine how strongly the gas exchange pump influences the distribution of DIC in the ocean.

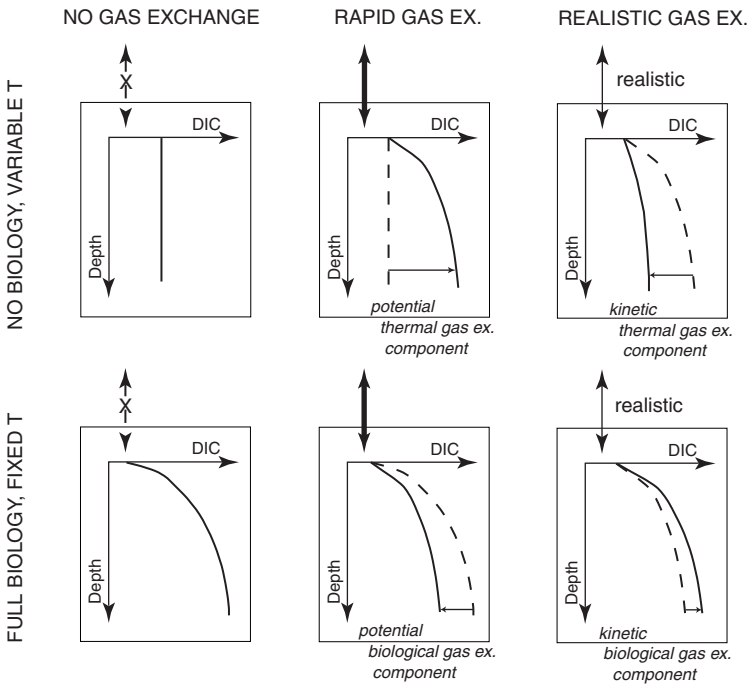

Fig. 9.16. Hypothetical vertical profiles of DIC in a series of thought experiments to elucidate the contributions from the two thermal gas exchange components (top row) and from the two biological gas exchange components (bottom row). The top row depicts the DIC distribution in an abiological ocean with realistic temperature distribution and various gas exchange scenarios. The bottom row shows the DIC distributions in a biological ocean with fixed temperature distribution and various gas exchange scenarios. The potential gas exchange pump components are the changes in the DIC distributions that occur when one goes from an ocean without air–sea gas exchange to one with infinitely fast gas exchange. The kinetic gas exchange components are then the changes in DIC that are caused by replacing the infinitely fast gas exchange with a realistic one. The main point to note is that the thermal and biological gas exchange pump components have a tendency to operate in opposite direction. This is the main reason why the gas exchange pump component is relatively small.

Global Mean

The key to understanding the vertical variations in $\Delta C_{gas\,ex}$ is to recall that not just heat fluxes control the exchange of CO_2 across the air–sea interface but that biological processes also play an important role (see equation 39). It is the opposing effects of the heat fluxes and biological processes, as explained below, that leads to the small contribution of the gas exchange pump. The second important key is the fact that the exchange of CO_2 across the air–sea interface is slow relative to the residence time of waters near the surface. This prevents the full expression of both the heat fluxes and the biological changes on the respective gas exchange fluxes.

We begin by separating the gas exchange pump into potential biological and thermal components ($\Delta C^{bio.\,pot}_{gas\,ex}$, $\Delta C^{therm.\,pot}_{gas\,ex}$), which indicate the tendency that would be achieved only if gas exchange was infinitely rapid; and into two kinetic components ($\Delta C^{bio.\,kin}_{gas\,ex}$, $\Delta C^{therm.\,kin}_{gas\,ex}$), which describe the changes from the infinitely rapid exchange to the case with realistic air–sea gas exchange.

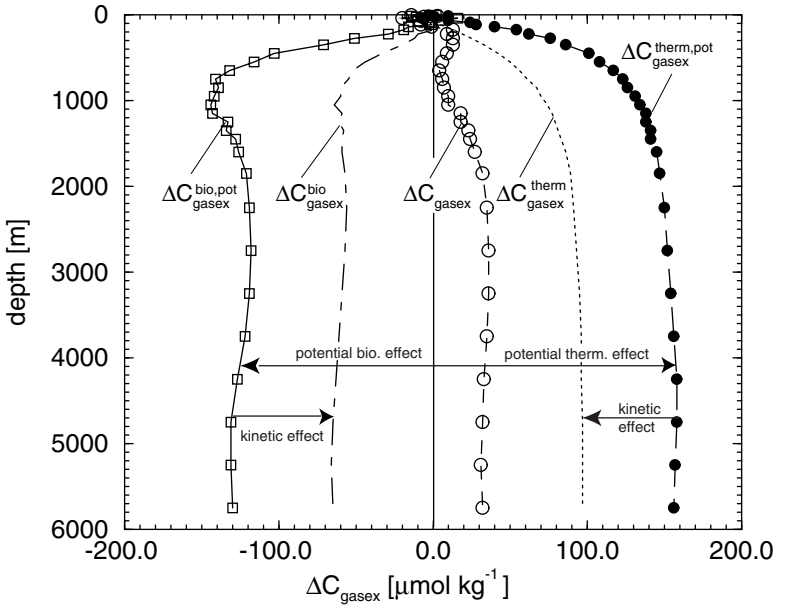

Fig. 9.17. Global mean profiles of the two biological and the two thermal gas exchange pump components. The potential $\Delta C^{therm}_{gas\,ex}$ has been calculated assuming that surface DIC is in equilibrium with the atmosphere using a constant salinity normalized total alkalinity. The potential $\Delta C^{bio}_{gas\,ex}$ has been computed from AOU, taking into account a change in the surface Alk concentration due to biology on the basis of preformed surface alkalinity estimates (Gruber et al., 1996). The kinetic $\Delta C^{therm}_{gas\,ex}$ profile is taken from the model of Murnane et al. (1999), and the kinetic $\Delta C^{bio}_{gas\,ex}$ is calculated by difference.

$$\Delta C_{gas\,ex} = \Delta C^{bio.\,pot}_{gas\,ex} + \Delta C^{bio.\,kin}_{gas\,ex} + \Delta C^{therm.\,pot}_{gas\,ex} + \Delta C^{therm.\,kin}_{gas\,ex} \tag{40}$$

The sum of the two biological components is equal to $\Delta C^{bio}_{gas\,ex}$ and the sum of the two thermal components is equal to $\Delta C^{therm}_{gas\,ex}$ (see equation 39).

The role of each of these four gas exchange components can be better understood following two thought experiments: In order to assess $\Delta C_{gas\,ex}$, we start with an ocean with realistic temperature distribution, but without biology. Without air–sea gas exchange, this ocean would have a uniform DIC distribution. We then turn on infinitely rapid air–sea exchange and let the ocean fully equilibrate with a fixed atmosphere of 280 ppm (Fig. 9.16). The difference between this case and the no-gas-exchange case is the contribution of the potential $\Delta C^{therm}_{gas\,ex}$ pump (also called a potential solubility pump (Murnane et al., 1999). The potential $\Delta C^{therm}_{gas\,ex}$ component can be estimated directly from data by computing the DIC equilibrium concentration and assuming constant salinity normalized total alkalinity. The resulting mean global surface-to-deep gradient of $\Delta C^{therm.\,pot}_{gas\,ex}$ amounts to about 155 μmol kg^{-1} (Fig. 9.17).

What happens if we then use a realistic air–sea gas exchange? As it takes about 10 months to equilibrate DIC in a 50-m-deep surface layer with the atmosphere (Broecker and Peng, 1974), and typical residence times of surface waters are between a few days to a few years, the CO_2 system in surface waters generally does not achieve equilibrium with the atmosphere. Therefore, the potential thermal gas

exchange pump cannot be achieved fully, resulting in a reduced vertical DIC gradient (Fig. 9.16), the difference being the kinetic $\Delta C^{therm}_{gas\ ex}$ effect. Unfortunately, we cannot estimate the kinetic $\Delta C^{therm}_{gas\ ex}$ component directly from observations, but simulations by Murnane et al. (1999) indicate that the slow kinetics of CO_2 exchange reduces $\Delta C^{therm}_{gas\ ex}$ from the potential $\Delta C^{therm}_{gas\ ex}$ of 155 μmol kg^{-1} to about 100 μmol kg^{-1}, suggesting that the slow kinetics of air–sea gas exchange plays an important role.

We do a second thought experiment to elucidate the influence of biology on air–sea gas exchange. We start with an isothermal ocean with fully expressed soft tissue and carbonate pumps and no air–sea gas exchange (Fig. 9.16). Infinitely rapid air–sea gas exchange is then turned on until surface waters are fully equilibrated with a fixed atmosphere of 280 ppm. In this case, CO_2 would behave very similarly to O_2 and the interior distribution of DIC would be similar to $r_{C/O_2} \times$ AOU, except for a small change caused by surface variations in Alk. The potential $\Delta C^{bio}_{gas\ ex}$ contribution is the difference between these two cases (Fig. 9.16) and amounts to about -130 μmol kg^{-1} (Fig. 9.17).

When we then use a realistic air–sea gas exchange instead, the reduction of the imprint of the biological pumps is smaller, leading to a vertical gradient from the biological pumps and the biological $\Delta C_{gas\ ex}$ pump that is somewhere between the fully expressed pumps and the potential $\Delta C^{bio}_{gas\ ex}$ case (Fig. 9.16). This means that the kinetic $\Delta C^{bio}_{gas\ ex}$ is positive, (i.e., it increases the surface to deep gradient in DIC) (Fig. 9.17). As was the case for the kinetic $\Delta C^{therm}_{gas\ ex}$ contribution, it is currently not possible to estimate the kinetic $\Delta C^{bio}_{gas\ ex}$ contribution directly from data. However, adopting the estimate $\Delta C^{therm}_{gas\ ex}$ estimated by Murnane et al. (1999) suggests that the kinetic effect for the biological component of $\Delta C_{gas\ ex}$ is substantial and around 60 μmol kg^{-1}, resulting in a $\Delta C^{bio}_{gas\ ex}$ component of only about -70 μmol kg^{-1} (Fig. 9.17).

Although the exact values of the kinetic components are not known, the overall conclusion is very clear. The small imprint that air–sea gas exchange has on the vertical DIC distribution ($\Delta C_{gas\ ex}$) is a consequence of generally opposing tendencies of $\Delta C^{bio}_{gas\ ex}$ and $\Delta C^{therm}_{gas\ ex}$. The magnitude of these two components depends on the magnitude of biological fluxes and heat fluxes that create potential gas exchange fluxes and the kinetics of air–sea exchange that determines to what degree these two potential pumps are realized. If the simulations by Murnane et al. (1999) are approximately correct, it appears that in the present ocean, a relatively small fraction of the potential gas exchange pumps are expressed.

The situation is very different for oxygen. Like CO_2, the solubility of O_2 increases with decreasing temperature. However, the contribution of the soft tissue pump to variations in O_2 is opposite to that of DIC. The biological contribution to air–sea gas exchange thus generally enhances the oxygen fluxes caused by heat fluxes. This fact and the more rapid air–sea exchange kinetics of O_2 relative to CO_2 leads to a much larger influence of the air–sea gas exchange pump on the large-scale distribution of oxygen in comparison to DIC.

Atlantic versus Pacific

The large $\Delta C_{gas\ ex}$ imprint in the deep Atlantic can be understood following arguments similar to those used to understand the global mean distribution of $\Delta C_{gas\ ex}$. However, this time it is more instructive to trace the different water masses back to

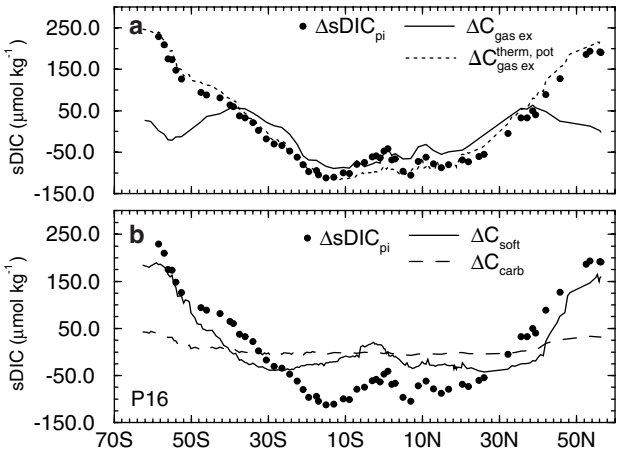

Fig. 9.18. Meridional variations of the ocean carbon pumps in the surface waters of the Pacific. (*a*) Surface concentrations of $\Delta C_{gas\,ex}$ and $\Delta sDIC_{pi}$. Also shown is the potential $\Delta C^{therm}_{gas\,ex}$ concentration. (*b*) Surface concentrations of ΔC_{soft} and ΔC_{carb}. The observations of $\Delta sDIC_{pi}$ are repeated for comparison. (Data from WOCE cruise P16.)

the places where they were last in contact with the atmosphere and obtained their air–sea gas exchange signal. What we will see below is that over most of the world ocean, $\Delta C_{gas\,ex}$ has a relatively small expression because of cancellation of the thermal gas exchange pump by the biological gas exchange pump. The North Atlantic, which has a very weak expression of the biological gas exchange effect, is the one exception to this. The deep $\Delta C_{gas\,ex}$ signal that we see is thus an expression of the thermal gas exchange pump.

The $\Delta C_{gas\,ex}$ signal in the deep Atlantic is associated with NADW, and since this water is formed in the northern North Atlantic, we have to look at surface-water properties there. To better understand the peculiarities of the North Atlantic, it is helpful to contrast this basin with the surface distribution in the Pacific.

Figure 9.18*a* shows surface ocean concentrations of $\Delta C_{gas\,ex}$, calculated from equation 37, as a function of latitude in the Pacific Ocean, and Fig. 19*a* shows the same for the Atlantic. Also plotted are the potential $\Delta C^{therm}_{gas\,ex}$ (equal to the equilibrium DIC concentration) and the observed DIC concentrations. The first point we note is that $\Delta C_{gas\,ex}$ shows more variations at the sea surface than we have seen in the water column. However, differences in $\Delta C_{gas\,ex}$ between the temperate latitudes where most of the thermocline waters are formed and the polar latitudes of the southern hemisphere, where most of intermediate and deep waters of the Indian and Pacific Oceans have their sources, are relatively small (e.g., maximally about 50 μmol kg^{-1}). This is consistent with our observation of a very small vertical gradient in $\Delta C_{gas\,ex}$, since the Indian and Pacific Oceans dominate the global mean profile.

By contrast to the Pacific, the $\Delta C_{gas\,ex}$ signal in the North Atlantic increases continuously toward the north, reaching higher levels than found in the northern North Pacific and in the far south of the Southern Ocean. Although this explains where the signals observed in the interior come from, it does not explain why the different regions have such a different surface expression of $\Delta C_{gas\,ex}$.

If air–sea gas exchange were infinitely fast and there were no biology, $\Delta C_{gas\,ex}$

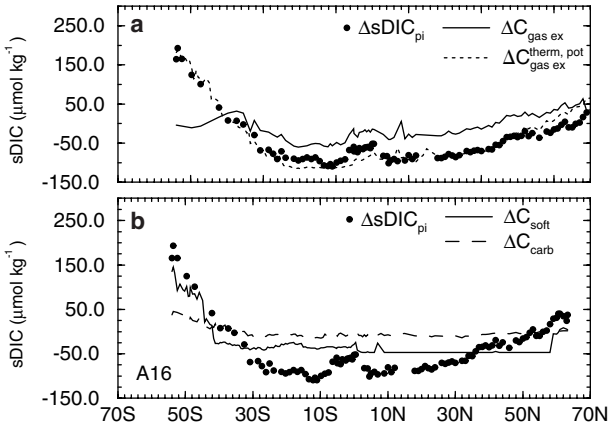

Fig. 9.19. Same as Fig. 9.18 except for surface waters of the Atlantic. (Data from the OACES NATL93 and SAVE cruises.)

would follow the potential $\Delta C^{therm}_{gas\ ex}$ concentration shown in Figs. 9.18*a* and 9.19*a*. In such a case, waters that flow from high latitudes to low latitudes, and vice versa, would need to exchange large amounts of CO_2 to the atmosphere to account for the large temperature sensitivity of DIC. Although it appears that $\Delta C_{gas\ ex}$ in the Atlantic Ocean indeed follows the potential $\Delta C^{therm}_{gas\ ex}$ distribution throughout the ocean basin $\Delta C_{gas\ ex}$ in the Pacific deviates strongly from it in the high latitudes. This small high-to-low latitude gradient in $\Delta C_{gas\ ex}$ indicates that much less CO_2 is exchanged with the atmosphere in this basin. Such a conclusion could be explained with the relatively slow rate of air–sea gas exchange. Nevertheless, this is surprising since despite this, surface water DIC is everywhere relatively close to equilibrium with the atmosphere. This can only be the case if other processes play also a role in controlling air–sea gas exchange.

The solution is revealed in Figs. 9.18*b* and 9.19*b*, which show the contribution of the two biological pumps to surface ocean DIC variations. It turns out that the surface waters in the Southern Ocean contain large amounts of DIC that stem from the remineralization of organic matter and the dissolution of $CaCO_2$ (high ΔC_{soft} and ΔC_{carb}). This is a consequence of upwelling processes, which bring intermediate and deep ocean waters with high ΔC_{soft} and ΔC_{carb} to the surface, and a relatively inefficient biological pump that is not able to remove these biological signals as rapidly as they are brought up.

When these waters are transported from the Southern Ocean to low latitudes, biological production removes almost all of this "excess" ΔC_{soft} and ΔC_{carb}, reducing DIC accordingly. This reduction is apparently of very similar magnitude as the required change in DIC to accommodate the temperature change. Therefore, these waters have to exchange only limited amounts of thermally driven CO_2 with the atmosphere to remain near equilibrium with the atmosphere. This is equivalent to saying that, in the Pacific and in the South Atlantic, the biologically driven CO_2 fluxes compensate to a large degree for the thermally driven CO_2 fluxes.

In the North Atlantic, the contribution of ΔC_{soft} and ΔC_{carb} to surface DIC variations are much smaller, indicating a much smaller biological compensation for the

thermally driven CO_2 fluxes. This creates a strong tendency for the North Atlantic to take up CO_2 from the atmosphere. The reason for this different behavior of the North Atlantic is the thermohaline circulation, which feeds low-nutrient surface waters from the subtropics into the NADW formation region. On the way, these waters are giving off large amounts of heat, leading to a strong cooling of these waters (Schmitz, 1996). These waters remain sufficiently long near the surface, so that the slow kinetics of air–sea gas exchange does not impede the uptake of substantial amounts of CO_2 from the atmosphere. This uptake from the atmosphere can occur because the cooling occurs without excessive entrainment of nutrients from below as is happening in the Southern Ocean. This is because the nutrient content of the thermocline is relatively low as a result of the nutrient export by the NADW. An additional factor contributing to the low ΔC_{soft} and ΔC_{carb} signals in the North Atlantic in comparison with the Southern Ocean might be the large difference in the deposition of dust from the atmosphere. In the Southern Ocean, the observational evidence is steadily increasing that the low atmospheric deposition of iron is preventing the complete drawdown of nutrients, thus creating the largest high-nutrient, low-chlorophyll (HNLC) regions (Martin et al., 1990, 1991; deBaar et al., 1995; Boyd et al., 2000). The delivery of iron to the North Atlantic is almost an order of magnitude higher (Duce et al., 1991; Tegen and Fung, 1994) and appears to be sufficient to allow nearly complete drawdown of nutrients (and hence ΔC_{soft} and ΔC_{carb}. This example illustrates how the interaction of biological processes with large-scale ocean circulation and possibly the biogeochemical cycles of iron can lead to quite unexpected results.

Surface Fluxes

A complementary way to study the role of the thermal and biological gas exchange pumps is to look at their role in shaping the spatial patterns of the air–sea exchange flux. As observations do not allow the separation into these two gas exchange components, we use the model results of Murnane et al. (1999) as an illustration. Figure 9.20 shows the meridional pattern of the zonally integrated air–sea gas exchange as predicted by this model. The patterns exhibited by the thermal gas exchange pump are related to the transport of heat and water within the ocean and its exchange with the atmosphere. In the high latitudes, surface waters lose heat to the atmosphere and consequently take up CO_2 from the atmosphere. In the equatorial regions, colder waters that are upwelled to the surface are warmed up, which leads to a loss of CO_2 to the atmosphere. The correlation of the air–sea exchange fluxes of CO_2 with the heat fluxes are modified, however, by the relatively slow air–sea exchange of CO_2 compared to heat. This shows up particularly in the equatorial region, where the peak of the CO_2 gas exchange is much wider than would be predicted by the heat exchange alone.

The biological pump represents, to a first approximation, a closed loop within the ocean. Waters that are brought to the surface contain an excess of inorganic carbon relative to these surface waters. At the same time, these waters also contain an excess of nutrients. Biological uptake at the surface is generally fast enough to strip out all or most of the nutrients and the excess CO_2 before CO_2 is lost to the atmosphere. Only in regions where the biological uptake is inefficient will CO_2 escape into the atmosphere. A good diagnostic of such regions is high surface nutrient concentrations, which occur in the Southern Ocean, the equatorial Pacific, and the North Pacific. The Southern Ocean, characterized by the highest surface ocean nutrient concentration,

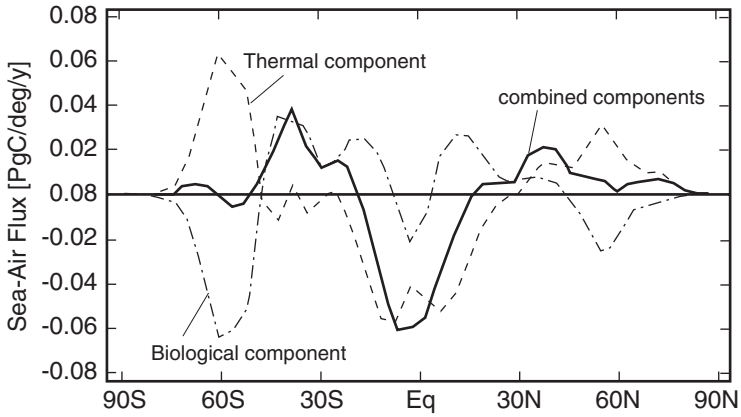

Fig. 9.20. Zonally averaged CO_2 air–sea gas exchange fluxes for the thermal, biological, and combined gas exchange pumps scenarios in the Princeton Ocean Biogeochemistry Model. Note that in the high-latitude regions the thermal and biological components of the gas exchange pumps tend to cancel each other, whereas at the equator they tend to reinforce each other. (Adapted from Murnane et al., 1999.)

also represents the region with the highest loss of CO_2 to the atmosphere associated with the biological pump. The loss in this region almost compensates the uptake of CO_2 from the atmosphere as a consequence of the thermal gas exchange pump, leaving only a small residual air–sea exchange flux in the combined pump scenario (Fig. 9.20). This is exactly the same compensation that we alluded to before when trying to explain the low vertical $\Delta C_{gas\ ex}$ signal in the observations. The loss of CO_2 in the high latitudes and near the equator due to the biological pump is compensated by a net uptake of CO_2 in the midlatitudes, so that the global net exchange is zero as required. Simulations of the contribution of the carbonate pump to the variation in the biological pump shows it to be generally small (Murnane et al., 1999).

The pattern of the zonally integrated air–sea exchange due to the combined pumps represents the sum of the patterns generated by the gas exchange and biological pumps. Since the two pumps almost cancel each other in the Southern Ocean, the equatorial outgassing region represents the largest source of CO_2 to the atmosphere. This primarily thermally driven outgassing is compensated in the midlatitudes by the primarily biologically driven uptake of CO_2 from the atmosphere.

4.5. Anthropogenic CO_2

We have assumed so far that we know the amount of anthropogenic CO_2 in the ocean and that we therefore can subtract it from the observed DIC distribution. However, the exact determination of the anthropogenic CO_2 signal in the ocean is far from trivial and subject to intense scientific debate.

The most direct means to estimate the oceanic uptake of anthropogenic CO_2 is to measure the increase of DIC in the oceans over time. This is a daunting task, given the large spatiotemporal variability observed in DIC and given that the maximum signal of anthropogenic CO_2 in the oceans is expected to be only about 65 μmol kg^{-1}, with a present rate of increase of about 1 μmol kg^{-1} per year. We are also lacking historical DIC measurements that are accurate enough to establish a reliable

base line of DIC concentrations in the past with a few exceptions (see, e.g., Sabine et al., 1999; Peng et al., 1998). Furthermore, no natural archive exists that would permit reconstruction of ocean DIC concentrations, such as we have for atmospheric trace gases in the form of ice core records.

Thus, the amount of anthropogenic CO_2 that has entered the ocean must be obtained by less direct means. The approach most commonly employed so far has been the use of ocean models designed to take into account not only the thermodynamic capacity of seawater but also the two rate-limiting steps, air–sea gas exchange and vertical transport. However, there exists a more direct strategy, in which the anthropogenic CO_2 signal is extracted from DIC observations in the water column. Brewer (1978) and Chen and Millero (1979) were the first to point out that the anthropogenic CO_2 can be estimated by correcting the measured DIC in a water sample for the changes that occurred due to the remineralization of organic matter and the dissolution of $CaCO_3$ since it lost contact with the atmosphere and by subtracting preformed preindustrial DIC. However, the Brewer and Chen–Milero approach never found general acceptance, since the uncertainties associated with the estimates were regarded as too large (Shiller, 1981, 1982; Broecker et al., 1985a). However, Gruber et al. (1996) showed that this approach can be improved by introducing a few important modifications.

Data Reconstruction

The approach described by Gruber et al. (1996) employs a quasiconservative tracer, ΔC^*, which is related to the C^* tracer used 0above for separating the different pump components from the observed variations of DIC (see equation 33). To extract the anthropogenic (CO_2 component from the observations, Gruber et al. (1996) looked only at deviations of C^* from preindustrial preformed concentration of C^* (i.e., the C^* concentration a water parcel had when it was last at the surface in contact with the preindustrial atmosphere). This preindustrial C^* concentration is estimated using information about the age of the water parcel estimated from age tracers [such as fluorochlorocarbons (CFC)] and assuming that the degree of CO_2 saturation has not changed over time as a result of the anthropogenic perturbation.

Goyet et al. (1999) recently introduced another new technique, in many ways similar to that of Gruber et al. (1996), but containing a number of distinct differences (Coatanoan et al., 2001). The main differences are the more detailed consideration of mixing effects, but foregoing the information contained in the age tracers and assuming instead that the anthropogenic CO_2 follows a predescribed depth distribution. This approach has been applied so far only in the northern Indian Ocean, where it resulted in about 40% lower inventories of anthropogenic CO_2 in comparison to the approach developed by Gruber et al. (1996) and employed by Sabine et al. (1999) (Coatanoan et al., 2001). As the anthropogenic CO_2 estimates based on the Gruber et al. (1996) technique are the only ones currently available on the global scale, we employ those for our discussion here, but it is important to note that these estimates have uncertainties on the order of 20% associated with them.

Figure 9.21 shows the distribution of anthropogenic CO_2 along the North Atlantic–Southern Ocean–North Pacific section, based on the data of Gruber (1998) for the Atlantic, of Sabine et al. (1999) for the Indian Ocean, and of Feely et al. (1999) for the Pacific. The large-scale distribution of anthropogenic CO_2 is as expected for a tracer that has invaded the ocean from the surface. Highest ΔC_{ant} concentrations

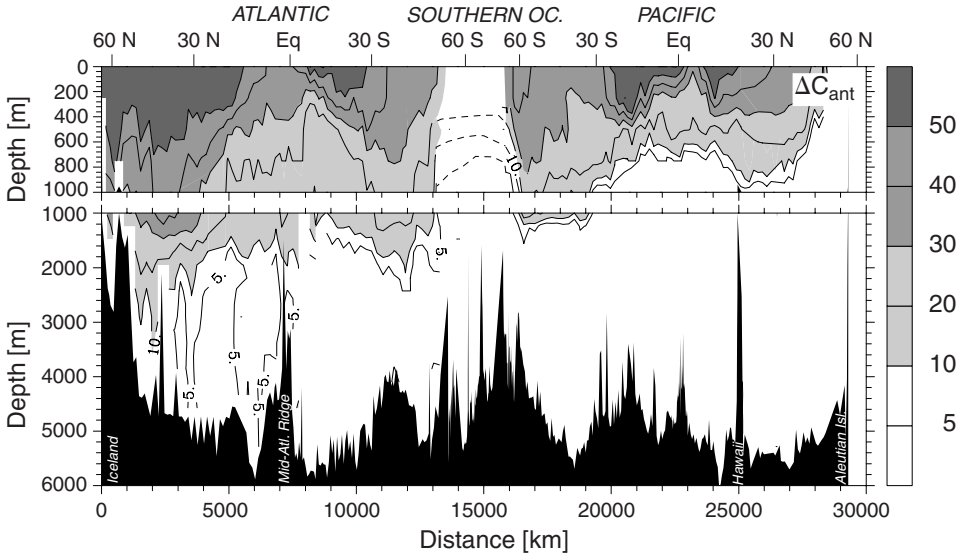

Fig. 9.21. Same as Fig. 9.3, except for anthropogenic CO_2 (μmol kg^{-1}). (Data from Gruber, 1998; Sabine et al., 1999; Feely et al. 1999.)

are found near the surface and the concentrations decrease slowly as depth increases. However, there exist substantial differences in the surface concentrations as well as in the vertical penetration of the anthropogenic CO_2 signal.

The near-surface concentrations of ΔC_{ant} are highest in the tropical to subtropical regions (40 to 60 μmol kg^{-1}) and decrease toward the high latitudes (20 to 30 μmol kg^{-1}). This initially surprising result is a consequence of the fact that low-latitude waters have a larger holding capacity for anthropogenic CO_2 than high-latitude waters (Takahashi et al., 1980). These surface concentrations are generally very similar to the concentrations expected under the assumption that these waters were able to track the anthropogenic CO_2 perturbation in the atmosphere (Gruber, 1998; Sabine et al., 1999). The somewhat lower anthropogenic CO_2 content in the surface waters of the Southern Ocean compared to these expectations indicate that these waters are not able to track the atmosphere completely. This is presumably the result of three factors: the short residence time of these surface waters, substantial dilution of deep and bottom waters by subsurface mixing with old waters, and effective inhibition of air–sea gas exchange by sea ice, especially during water (Poisson and Chen, 1987).

Figure 9.21 also reveals substantial meridional differences in vertical penetration of the anthropogenic CO_2 signal. In the tropics, ΔC_{ant} rapidly decreases with depth, whereas the vertical penetration of the signal is much deeper in the subtropical and temperate latitudes. The symmetry between the two hemispheres breaks down farther toward the poles. In the North Atlantic north of 60°N, deep vertical penetration of ΔC_{ant} is found with concentrations above 10 μmol kg^{-1} down to the bottom. In contrast, the vertical penetration of anthropogenic CO_2 in the Southern Ocean is very shallow. Little vertical penetration of anthropogenic CO_2 can be found in the North Pacific. Since anthropogenic CO_2 can be regarded as a conservative tracer,

not affected by biological processes, its distribution in the interior is determined by ocean transport only.

The shallow vertical penetration in the tropics and the deeper penetration in the subtropical and temperate zones reflect primarily the structure and ventilation of the thermocline. The contrast between the North Atlantic, Southern Ocean, and North Pacific requires more discussion. The high concentrations of anthropogenic CO_2 associated with NADW are not a surprise given the fact that NADW represents a recently ventilated water mass (Broecker et al., 1985b; Smethie, 1993; Doney and Jenkins, 1994), but why do the waters in the Southern Ocean contain so little anthropogenic CO_2, even though deep-water formation is well known to occur in the Weddell Sea, Ross Sea, and in other shelf areas around Antarctica (Gordon et al., 1993; Broecker et al., 1999)? As discussed above, surface waters in the Southern Ocean appear to have not fully tracked the atmospheric CO_2 increase. This deficit in anthropogenic CO_2 is then aggravated as the sinking water entrains large amount of old waters (Orsi et al., 1999) containing little or no anthropogenic CO_2, leading to only a small ΔC_{ant} signal in the AABW (Poisson and Chen, 1987). The reason for the low vertical penetration of anthropogenic CO_2 in the North Pacific is the absence of deep-water formation in this region. The densest water formed in the North Pacific originates from the Sea of Okhotsk, but does not penetrate deeper than approximately 1000 m.

Role of Biology

What is the role of biology in the oceanic uptake of anthropogenic CO_2? This topic has been the source of many misunderstandings and false claims (Broecker, 1999b; Longhurst, 1991a, b; Sarmiento, 1991), so a short discussion seems appropriate here.

So far in our discussion on anthropogenic CO_2, we have neglected the marine biota. This is somewhat counterintuitive, because we know that the marine biota is responsible for a large fraction of the surface-to-deep gradient in DIC. Why, then, does the biological pump not also transport anthropogenic CO_2 from the surface into the interior of the ocean? The first point to make here is that the downward transport of carbon in organic material is compensated in a steady state by an equally large upward transport of DIC, resulting in a zero net transport [except for the small fraction that goes into the sediments and is replaced by river input (Sarmiento and Sundquist, 1992)]. Our neglect of the biological pumps is based on the assumption that they have been operating in steady state before the start of the anthropogenic CO_2 perturbation of the carbon cycle and that they have continued to do so ever since (Broecker, 1991b).

Two lines of evidence support this hypothesis. First, atmospheric CO_2 has remained remarkably stable for at least 3000 years before the eighteenth century (Etheridge et al., 1996; Indermühle et al., 1999), indicating that the fluxes controlling the surface ocean total carbon content were in balance. Second, according to the present consensus, marine phytoplankton is controlled by nutrients (including micronutrients), light, grazing, and vertical stability of the water column (Falkowski et al., 1998), but not by the concentration of CO_2 dissolved in seawater (Falkowski, 1994). This view has been challenged, however, by Riebesell et al. (1993), who showed that the growth rate of three marine diatom species increased as the concentration of CO_2 increased as a result of the anthropogenic perturbation. Although the significance of these laboratory experiments for natural phytoplankton assemblages is controversial (Hein and Sand-Jensen, 1997), there exists more evidence that coral

reef-forming organisms (Gattuso et al., 1989; Kleypas et al., 1999) and plantonic calcifiers (Riebesell et al., 2000) will decrease their $CaCO_3$ precipitation rates as CO_2 increases. However, according to the model simulations of Kleypas et al. (1999), the reduction of the calcification rates should have been relatively small so far (but will become significant in the future) and therefore should not have had a large impact on the steady-state assumption of the biological pumps. We therefore assume that the biological pumps have not influenced the past oceanic uptake of anthropogenic carbon, but rather, acted as a natural background process continuing to work as in preindustrial times.

Murnane et al. (1999) recently carried out a simulation of oceanic uptake in two models, one of which contains just the solubility pump and a second combined simulation that includes the biological pumps. The combined simulation takes up 5% less anthropogenic CO_2. This is because the biological pumps reduce the surface alkalinity and hence storage capacity for anthropogenic CO_2. If the solubility simulation used the same surface alkalinities as the combined model, both would take up the same amount of anthropogenic CO_2.

One cannot assume, however, that the steady-state operation of the biological pumps will continue forever into the future. Future climate changes, associated with the buildup of greenhouse gases in the atmosphere, might modify the biological pump driven fluxes, which could then feed back on the atmospheric composition (Baes and Killough, 1986; Sarmiento, 1991). Alterations of the biological pumps, for instance, have been proposed as a possible cause for the dramatic changes in atmospheric CO_2 between the glacial and interglacial periods (Broecker, 1982; Sarmiento and Toggweiler, 1984; Siegenthaler and Wenk, 1984; Boyle, 1988; Martin, 1990; Keir, 1991; Broecker and Henderson, 1998). It is extremely difficult at present to assess how the biological pump will respond to future climate changes. Results from some first attempts are the topic of the next section.

Future CO_2 Uptake

Manabe and Stouffer (1993) showed in a coupled ocean–atmosphere–ice model that the continued buildup of greenhouse gases in the atmosphere can lead to major reorganizations of the oceanic circulation. Most notable is the complete shutdown of the North Atlantic deep water formation that occurs between a doubling and quadrupling of the preindustrial atmospheric CO_2 concentration. The concentration at which this breakdown occurs is certainly model dependent. It has also been shown (Stocker and Schmittner, 1997) that the rate of increase of the radiative forcing plays a role. More subtle changes in ocean circulation, which nevertheless can have a large impact on the ocean biota, occur in these models already much earlier. How do these changes affect the future oceanic CO_2 uptake?

Sarmiento and LeQuéré (1996) and Sarmiento et al. (1998) demonstrate that the predicted changes in ocean circulation lead to a significant decrease of the oceanic uptake of anthropogenic CO_2 in models with CO_2 chemistry but no biology (Fig. 9.22). However, they also found that the biological pumps have the potential to largely offset the decreased uptake. Using very different models, Joos et al. (1999) and Matear and Hirst (1999) came to conclusions similar to those of Sarmiento et al. (1998). It has to be noted, however, that representation of the biological pumps in these models is very simplistic and that these simulations therefore have to be regarded as case studies rather than accurate predictions.

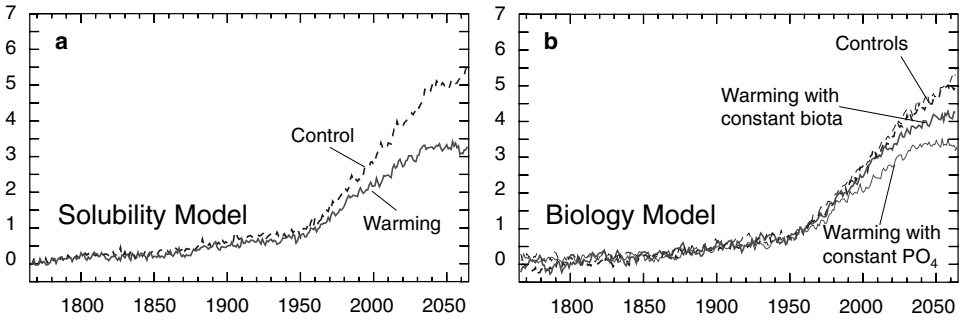

Fig. 9.22. Simulated oceanic uptake of anthropogenic CO_2 by the GFDL/Princeton coupled climate model. (*a*) Control run (dashed line) and ocean uptake for the solubility model only. (*b*) Control runs (dashed lines) and two scenarios for the biological pump. The thick solid line refers to a simulation where the soft tissue pump remained constant. The fine solid line corresponds to a scenario where the soft tissue pump was assumed to change in a manner to keep the surface nutrient concentration constant. In the control runs, the coupled climate model was run in a preindustrial climate and only atmospheric CO_2 was changed. In the warming scenarios, the climate model was externally forced with a time series of effective atmospheric CO_2, constructed from a business as usual scenario (IS92a), including the negative feedback from aerosols. (Adapted from Sarimento et al., 1998, with permission of *Nature*.)

These simulations demonstrate that while the biological pumps are unimportant for assessing the oceanic uptake of anthropogenic CO_2 in the past and present, these pumps might play an important role for the future uptake. However, very little is known about the possible response of the oceanic biota to climate change. To improve these predictions, one has to gain a clear understanding of the processes controlling all important steps of the oceanic biological pumps (e.g., surface production, respiration, export, and remineralization). As we have learned during our discussion of the marine carbon cycle, there are still considerable gaps in our understanding, even at a very fundamental level. However, while we cannot foresee the future, nature has in the past performed several experiments, from which we might learn something about the future. During glacial periods, atmospheric CO_2 has been about 80 to 100 ppm lower than during interglacial periods (Neftel et al., 1982; Petit et al., 1999). This large change must be related to dramatic changes in the oceanic carbon cycle, since the ocean is controlling atmospheric CO_2 on these time scales. However, the exact causes for this large drawdown are still unknown (Archer et al., 2000; Sigman and Boyle, 2000) despite 20 years of intense research. This glacial–interglacial CO_2 problem together with the question of how the marine carbon cycle will respond to future climate change thus represents two of the largest challenges for future carbon cycle research.

5. Concluding Remarks

We started out with the quest to understand the processes that lead to variations in the distribution of the major biogeochemical elements in the presence of ocean circulation and mixing that generally attempt to smooth these distributions. We learned that the dominant gradient maker by far is the photosynthetic uptake of inorganic constituents to form organic material in the surface ocean and the export and subsequent remineralization of this material in the deeper layers. The interaction of these processes with

large-scale ocean circulation (i.e., thermohaline circulation) then creates the typical large-scale distribution of biogeochemical tracers. We also learned that these interactions are often complex, involve many processes, and are seldom well understood. Unraveling these interactions is becoming more important as humankind is affecting the biogeochemical cycles on earth to an ever-increasing degree (Falkowski et al., 2000). For example, industrial N_2 fixation now exceeds the amount of biological N_2 fixation on earth, and the continuing use of fossil fuels will release large amounts of CO_2 into the atmosphere, probably leading to a doubling of the preindustrial CO_2 concentration by around 2050. We are thus faced at present with a situation where humankind in changing global biogeochemical systems in an unprecedented way, yet we are just beginning to understand how these systems operate.

Acknowledgments

This study would not have been possible without the careful and dedicated work of the scientists and personnel who were responsible for the collection and analysis of the tracer data that we relied on so heavily in this study. We are thankful for the rapid dissemination of these data to the public. The work of the Carbon Dioxide Information and Analysis Center (CDIAC) at Oak Ridge is much appreciated in this respect. N.G. has been supported by a NOAA Global Climate Change fellowship. Support for J.S. has been provided by NOAA Office of Global Programs through the Carbon Modeling Consortium.

References

Altabet, M. A., R. Francois, D. W. Murray and W. L. Prell, 1995. Climate-related variations in denitrification in the Arabian Sea from sediment $^{15}N/^{14}N$ ratios, *Nature*, **373,** 506–509.

Anderson, L. A., 1995. On the hydrogen and oxygen content of marine phytoplankton. *Deep-Sea Res. I*, **42**(9), 1675–1680.

Anderson, L. A. and J. L. Sarmiento, 1994. Redfield ratios of remineralization determined by nutrient data analysis. *Global Biogeochem. Cycles*, **8**(1), 65–80.

Archer, D., 1991. Modeling the calcite lysocline. *J. Geophys. Res.*, **96**(C9), 17037–17050.

Archer, D., 1996. A data-driven model of the global calcite lysocline. *Global Biogeochem. Cycles*, **10**(3), 511–526.

Archer, D., S. Emerson and C. R. Smith, 1989. Dissolution of calcite in deep-sea sediments: pH and O_2 results. *Geochim. Cosmochim. Acta*, **53,** 2831–2845.

Archer, D., A. Winguth, D. Lea and N. Mahowald, 2000. What caused the glacial/interglacial atmospheric pCO_2 cycles? *Rev. Geophys.*, **38**(2), 159–189.

Arrigo, K. R., D. H. Robinson, D. L. Worthen, R. B. Dunbar, G. R. DiTullio, M. VanWoert and M. P. Lizotte, 1999. Phytoplankton community structure and the drawdown of nutrients and CO_2 in the Southern Ocean. *Science*, **283,** 365–367.

Baes, C. F., 1982. Effects of ocean chemistry and biology on atmospheric carbon dioxide. In *1982 Carbon Dioxide Review*, W. C. Clark, ed. Oxford University Press, Oxford, pp. 189–211.

Baes, C. F. and G. G. Killough, 1986. Chemical and biological processes in CO_2-ocean models. In *The Changing Carbon Cycle*, J. R. Trabalka and R. E. Reichle, eds. Springer-Verlag, New York, pp. 329–347.

Balch, W. M. and K. A. Kilpatrick, 1996. Calcification rates in the equatorial Pacific along 140*w*. *Deep-Sea Res. II*, **43**(4–6), 971–993.

Berelson, W. M., D. E. Hammond, J. McManus and T. E. Kilgore, 1994. Dissolution kinetics of calcium carbonate in the equatorial Pacific sediments. *Global Biogeochem. Cycles*, **8**(2), 219–235.

Berger, W. H., 1970. Planktonic foraminifera: selective solution and the lysocline. *Marine Geol.*, **8,** 111–138.

Bishop, J. K. B., J. C. Stepien and P. H. Wiebe, 1986. Particulate, matter distributions, chemistry and flux in the Panama Basin: response to environmental forcing. *Prog. Oceanogr.*, **17,** 1–59.

Boulahdid, M. and J. F. Minster, 1989. Oxygen consumption and nutrient regeneration ratios along isopycnal horizons in the Pacific Ocean. *Mar. Chem.*, **26,** 133–153.

Boyd, P. W., A. J. Watson, C. S. Law, E. R. Abraham, T. Trull, R. Murdoch, D. C. E. Bakker, A. R. Bowie, K. O. Buesseler, H. Chang, M. Charette, P. Croot, K. Downing, R. Frew, M. Gall, M. Hadfield, J. Hall, M. Harvey, G. Jameson, J. Laroche, M. Liddicoat, R. Ling, M. T. Maldonado, R. M. McKay, S. Nodder, S. Pickmere, R. Pridmore, S. Rintoul, K. Safi, P. Sutton, R. Strzepek, K. Tanneberger, S. Turner, A. Waite and J. Zeldis, 2000. A mesoscale phytoplankton bloom in the polar Southern Ocean stimulated by iron fertilization. *Nature*, **407,** 695–702.

Boyle, E. A., 1988. Vertical oceanic nutrient fractionation and glacial/interglacial CO_2 cycles. *Nature*, **331,** 55–56.

Brandhorst, W., 1959. Nitrification and denitrification in the eastern tropical North Pacific. *J. Cons. Explor. Mer.*, **25,** 3–20.

Brewer, P. G., 1978. Direct observation of the oceanic CO_2 increase. *Geophys. Res. Lett.*, **5**(12), 997–1000.

Broecker, W. S., 1974. NO, a conservative water-mass tracer. *Earth Planet. Sci. Lett.*, **23,** 100–107.

Broecker, W. S., 1982. Glacial to interglacial changes in ocean chemistry. *Prog. Oceanogr.*, **11,** 151–197.

Broecker, W., 1991a. The great ocean conveyor. *Oceanography*, **4**(2), 79–89.

Broecker, W. S., 1991b. Keeping global change honest. *Global Biogeochem. Cycles*, **5**(3), 191–192.

Broecker, W. S., 1998. Paleocean circulation during the last deglaciation: a bipolar seesaw? *Paleoceanography* **13**(2), 119–121.

Broecker, W. S. and G. M. Henderson, 1998. The sequence of events surrounding Termination II and their implications for the cause of glacial–interglacial CO_2 changes. *Paleoceanography*, **13**(4), 352–364.

Broecker, W. S. and T.-H. Peng, 1974. Gas exchange rates between air and sea. *Tellus*, **26,** 21–35.

Broecker, W. S. and T.-H. Peng, 1982. *Tracers in the Sea*. Eldigio Press, Lamont-Doherty Geological Observatory of Columbia University, Palisades, N.Y.

Broecker, W. S. and T.-H. Peng, 1992. Interhemispheric transport of carbon dioxide by ocean circulation. *Nature*, **356,** 587–589.

Broecker, W. S. and T.-H. Peng, 1993. Interhemispheric transport of carbon through the ocean. In *The Global Carbon Cycle*, M. Heimann, ed. Springer-Verlag, New York, Vol. I, No. 15, pp. 551–570.

Broecker, W. S. and T. H. Peng, 1998. *Greenhouse Puzzles, 2nd ed.* Eldigio Press, Lamont-Doherty Earth Observatory of Columbia University, Palisades, N.Y.

Broecker, W. S. and T. Takahashi, 1977. Neutralization of fossil fuel CO_2 by marine calcium carbonate. In *The Fate of Fossil Fuel CO_2 in the Oceans*, N. Andersen and A. Malahoff, eds. Plenum Press, New York, p. 213.

Broecker, W. S., T. Takahashi and T.-H. Peng, 1985a. Reconstruction of past atmospheric CO_2 from the chemistry of the contemporary ocean: an evaluation. *Technical Report TRO 20*. U.S. Department of Energy, Washington, D.C.

Broecker, W. S., T. Takahashi and T. Takahashi, 1985b. Sources and flow patterns of deep-ocean waters as deduced from potential temperature, salinity, and initial phosphate concentration. *J. Geophys. Res.*, **90**(C4), 6925–6939.

Broecker, W. S., S. Peacock, S. Walker, R. Weiss, E. Fahrbach, M. Schroeder, U. Mikolajewicz, U. Mikolajewicz, R. Key, T.-H. Peng and S. Rubin. 1998. How much deep water is formed in the Southern Ocean? *J. Geophys. Res.*, **103**(C8), 15833–15843.

Broecker, W. S., S. Sutherland and T.-H. Peng, 1999. A possible 20th-century slowdown of Southern Ocean deep water formation. *Science*, **286,** 1132–1135.

Capone, D. G., 1983. Benthic nitrogen fixation. In *Nitrogen in the Marine Environment*, E. J. Carpenter and D. G. Capone, eds. Academic Press, San Diego, Calif., pp. 105–137.

Capone, D. G. and E. J. Carpenter, 1982. Nitrogen fixation in the marine environment. *Science*, **217,** 1140–1142.

Capone, D. G., J. P. Zehr, H. W. Paerl, B. Bergman and E. J. Carpenter, 1997. *Trichodesmium*, a globally significant marine cyanobacterium. *Science*, **276,** 1221–1229.

Carpenter, E. J., 1983. Nitrogen fixation by marine Oscillatoria (*Trichodesmium*) in the world's oceans. In *Nitrogen in the Marine Environment*, E. J. Carpenter and D. G. Capone, eds. Academic Press, San Diego, Calif., pp. 65–103.

Carpenter, E. J. and D. G. Capone, 1992. Nitrogen fixation in *Trichodesmium* blooms. In *Marine Pelagic Cyanobacteria: Trichodesmium and Other Diazotrophs*, E. J. Carpenter, ed. Kluwer Academic Publishers, Dordrecht, The Netherlands, pp. 211–217.

Carpenter, E. and C. Price, Nitrogen fixation, distribution, and production of *Oscillatoria (trichodesmium)* spp. in the western Sargasso and Caribbean seas. *Limnol. Oceanogr.*, **22,** 60–72.

Carpenter, E. J. and K. Romans, 1991. Major role of the cyanobacterium *Trichodesmium* in nutrient cycling in the North Atlantic Ocean. *Science*, **254,** 1356–1358.

Chen, C.-T. A. and F. J. Millero, 1979. Gradual increase of oceanic CO_2. *Nature*, **277,** 205–206.

Chipman, D., T. Takahashi, D. Breger, and S. Sutherland, 1994. Carbon dioxide, hydrographic, and chemical data obtained during the R/V *Meteor* cruise 11/5 in the South Atlantic and northern Weddell Sea areas (WOCE sections A-12 and A-21). *Carbon Dioxide Information and Analysis Center Data Report ORNL/CDIAC-55; NDP-045*. Oak Ridge National Laboratory, Oak Ridge, Tenn.

Chipman, D. W., T. Takahashi, S. Rubin, S. C. Sutherland and M. H. Koshlyakov, 1997. Carbon dioxide, hydrographic, and chemical data obtained during the R/V *Akademik Ioffe* cruise in the South Pacific Ocean (WOCE section S4P, February–April 1992). *Carbon Dioxide Information and Analysis Center Data Report ORNL/CDIAC-100: NDP-063*. Oak Ridge National Laboratory, Oak Ridge, Tenn.

Christensen, J. P., J. W. Murray, A. H. Devol and L. A. Codispoti, 1987. Denitrification in continental shelf sediments has major impact on the oceanic nitrogen budget. *Global Biogeochem. Cycles*, **1**(2), 97–116.

Ciais, P., P. P. Tans, M. Trolier, J. W. C. White and R. J. Francey, 1995. A large northern hemispheric terrestrial CO_2 sink indicated by the $^{13}C/^{12}C$ ratio of atmospheric CO_2. *Science*, **269,** 1098–1102.

Coatanoan, C., C. Goyet, N. Gruber, C. L. Sabine and M. Warner, 2001. Comparison of two approaches to quantify anthropogenic CO_2 in the ocean: results from the northern Indian Ocean. *Global Biogeochem. Cycles*, **15**(1), 11–25.

Codispoti, L. A., 1989. Phosphorus vs. nitrogen limitation of new and export production. In *Productivity of the Ocean: Present and Past*, W. H. Berger, V. S. Smetacek and G. Wefer, eds. Wiley, New York, pp. 377–394.

Codispoti, L. A. and J. P. Christensen, 1985. Nitrification, denitrification and nitrous oxide cycling in the eastern tropical South Pacific Ocean. *Mar. Chem.*, **16,** 277–300.

Codispoti, L. A. and T. T. Packard, 1980. Denitrification rates in the eastern tropical South Pacific. *J. Mar. Res.*, **38**(3), 453–477.

Codispoti, L. A. and F. A. Richards, 1976. An analysis of the horizontal regime of denitrification in the eastern tropical North Pacific. *Limnol. Oceanogr.*, **21**(3), 379–388.

Codispoti, L. A., G. E. Friederich, T. T. Packared, H. E. Glover, P. J. Kelly, R. W. Spinrad, R. T. Barber, J. W. Elkins, B. B. Ward, F. Lipschultz and N. Lostaunau, 1986. High nitrite levels off northern Peru: A signal of instability in the marine denitrification rate. *Science*, **233,** 1200–1202.

deBaar, H. J. W., J. T. M. deJong, D. C. E. Bakker, B. M. Löscher, C. Veth, U. Bathmann and V. Smetacek, 1995. Importance of iron for plankton blooms and carbon drawdown in the Southern Ocean. *Nature*, **373,** 412–415.

Deutsch, C. D., N. Gruber, R. M. Key, A. Ganachaud and J. L. Sarmiento, 2001. Denitrification and N_2 fixation in the Pacific Ocean. *Global Biogeochem. Cycles*, **15**(2), 483–506.

Devol, A. H., 1991. Direct measurements of nitrogen gas fluxes from continental shelf sediments. *Nature*, **349,** 319–321.

DOE, 1994. Handbook of methods for the analysis of the various parameters of the carbon dioxide system in sea water; version 2. *U.S. Department of Energy Technical Report ORNL/CDIAC-74*. Carbon Dioxide Information and Analysis Center, Oak Ridge National Laboratory, Oak Ridge, Tenn.

Doney, S. and W. Jenkins, 1994. Ventilation of the deep western boundary current and abyssal western North Atlantic: estimates from tritium and ^{3}He distributions. *J. Phys. Oceanogr.*, **24,** 638–659.

Duce, R. A., P. S. Liss, J. T. Merrill, E. L. Atlas, P. Buat-Ménard, B. B. Hicks, J. M. Miller, J. M. Prospero, R. Arimoto, T. M. Church, W. Ellis, J. N. Galloway, L. Hansen, T. D. Jickells, A. H. Knap, K. H. Reinhardt, B. Schneider, A. Soudine, J. J. Tokos, S. Tsunogai, R. Wollast and M. Zhou, 1991. The atmospheric input of trace species to the world ocean. *Global Biogeochem. Cycles*, **5**(3), 193–259.

Dupoy, C., J. Neveux, A. Subramaniam, M. R. Mullholland, J. P. Montoya, L. Campbell, E. J. Carpenter and D. G. Capone, 2000. Satellite captures *Trichodesmium* blooms in the southwestern tropical Pacific. *Eos Trans. AGU*, **81**(1), 15–16.

Emerson, S. R. and M. Bender, 1981. Carbon fluxes at the sediment–water interface of the deep-sea: calcium carbonate preservation. *J. Mar. Res.*, **39,** 139–162.

Etheridge, D. M., L. P. Steele, R. L. Langenfelds, R. J. Francey, J.-M. Barnola and V. I. Morgan, 1996. Natural and anthropogenic changes in atmospheric CO_2 over the last 1000 years from air in antarctic ice and firn. *J. Geophys. Res.*, **101,** 4115–4128.

Falkowski, P. G., 1994. The role of phytoplankton photosynthesis in global biogeochemical cycles. *Photosynth. Res.*, **39,** 235–258.

Falkowski, P. G., 1997. Evolution of the nitrogen cycle and its influence on the biological sequestration of CO_2 in the ocean. *Nature*, **387,** 272–275.

Falkowski, P. G., 2000. Rationalizing elemental ratios in unicellular algae. *J. Phycol.*, **36**(1).

Falkowski, P. G., R. T. Barber and V. S. Smetacek, 1998. Biogeochemical controls and feedbacks on ocean primary production. *Science*, **281,** 200–206.

Falkowski, P. G., R. J. Scholes, E. Boyle, J. Canadell, D. Canfield, J. Elser, N. Gruber, K. Hibbard, P. Högberg, S. Linder, F. T. Mackenzie, B. Moore III, T. Pederson, Y. Rosenthal, S. Seitzinger, V. Smetacek and W. Steffen, 2000. Integrated understanding of the global carbon cycle: a test of our knowledge. *Science*, **290,** 291–296.

Fan, S., T. L. Blaine and J. L. Sarmiento, 1999. Terrestrial carbon sink in the northern hemisphere estimated from atmospheric CO_2 difference between Mauna Loa and South Pole since 1959. *Tellus Ser. B.*, **51,** 863–870.

Feely, R. A., C. L. Sabine, R. M. Key, T.-H. Peng and R. Wanninkhof, 1999. The U.S. global CO_2 survey in the North and South Pacific Oceans: preliminary synthesis results. In *2nd International Symposium CO_2 in the Oceans, Extended Abstracts*, Center for Global Environmental Research, Tsukuba, Japan, pp. 20–01.

Fleming, R. H., 1940. The composition of plankton and units for reporting population and production. *Proc. Sixth Pacific Sci. Cong. Calif.*, **3,** 535–540.

Fung, I. Y., S. K. Meyn, I. Tegen, S. C. Doney, J. G. John and J. K. B. Bishop, 2000. Iron supply and demand in the upper ocean. *Global Biogeochem. Cycles*, **14,** 281–295.

Galloway, J. N., W. H. Schlesinger, H. Levy II, A. Michaels and J. L. Schnoor, 1995. Nitrogen fixation: anthropogenic enhancement–environmental response. *Global Biogeochem. Cycles*, **9**(2), 235–252.

Ganeshram, R. S., T. F. Pedersen, S. E. Calvert and J. W. Murray, 1995. Large changes in oceanic nutrient inventories from glacial to interglacial periods. *Nature*, **376,** 755–758.

Ganeshram, R. S., T. F. Pedersen, S. E. Calvert, G. W. McNeil and M. R. Fontugne, 2000. Glacial–interglacial variability in denitrification in the world's ocean: causes and consequences. *Paleoceanography*, **15**(4), 301–376.

Gattuso, J.-P. D. Allemand and M. Frankignoulle, 1989. Interactions between the carbon and carbonate cycles at organism and community levels in coral reefs: a review on processes, rates and environmental control. *Am. Zool.*, **39**(1), 160–183.

Goldman, J. C., J. J. McCarthy and D. G. Peavey, 1979. Growth rate influence on the chemical composition of phytoplankton in oceanic waters. *Nature*, **279,** 210–215.

Gordon, A. L., B. A. Huber, H. H. Hellmer and A. Ffield, 1993. Deep and bottom water of the Weddell Sea's western rim. *Science*, **262,** 95–97.

Goyet, C., P. R. Guenther, C. D. Keeling and L. D. Talley, 1996. Carbon dioxide, hydrographic, and chemical data obtained during the R/V *Thomas Washington* cruise TUNES 3 in the equatorial Pacific

(WOCE section P16C). *Carbon Dioxide Information and Analysis Center Data Report ORNL/CDIAC-96; NDP-060*. Oak Ridge National Laboratory, Oak Ridge, Tenn.

Goyet, C., C. Coatanoan, G. Eischeid, T. Amaoka, K. Okuda, R. Healy and S. Tsunogai, 1999. Spatial variation of total CO_2 and total alkalinity in the northern Indian Ocean: a novel approach for the quantification of anthropogenic CO_2 in seawater. *J. Mar. Res.*, **57,** 135–163.

Gruber, N., 1998. Anthropogenic CO_2 in the Atlantic Ocean. *Global Biogeochem. Cycles*, **12**(1), 165–191.

Gruber, N. and J. L. Sarmiento, 1997. Global patterns of marine nitrogen fixation and denitrification. *Global Biogeochem. Cycles*, **11**(2), 235–266.

Gruber, N., J. L. Sarmiento and T. F. Stocker, 1996. An improved method for detecting anthropogenic CO_2 in the oceans. *Global Biogeochem. Cycles*, **10**(4), 809–837.

Gruber, N., C. D. Keeling, R. B. Bacastow, P. R. Guenther, T. J. Lueker, M. Wahlen, H. A. J. Meijer, W. G. Mook and T. F. Stocker, 1999. Spatiotemporal patterns of carbon-13 in the global surface oceans and the oceanic Suess effect. *Global Biogeochem. Cycles*, **13**(2), 307–335.

Hales, B. and S. Emerson, 1996. Calcite dissolution in sediments of the Ontong–Java Plateau: in situ measurements of pore water O_2 and pH. *Global Biogeochem. Cycles*, **10**(3), 527–541.

Hales, B., S. Emerson and D. Archer, 1994. Respiration and dissolution in the sediments of the western North Atlantic: estimates from models of in situ microelectrode measurements of porewater oxygen and pH. *Deep-Sea Res. I*, **41**(4), 695–719.

Hansell, D. A. and R. A. Feely, 2000. Atmospheric intertropical convergence impacts surface ocean carbon and nitrogen biogeochemistry in the western tropical Pacific. *Geophys. Res. Lett.*, **27**(7), 1013–1016.

Hattori, A., 1983. Denitrification and dissimilatory nitrate reduction. In *Nitrogen in the Marine Environment*, E. J. Carpenter and D. G. Capone, eds., Academic Press, San Diego, Calif., pp. 191–232.

Hein, M. and K. Sand-Jensen, 1997. CO_2 increases oceanic primary production. *Nature*, **388,** 526–527.

Honjo, S., 1996. Fluxes of particles to the interior of the open oceans. In *Particle Flux in the Ocean*, V. Ittekkot, P. Schäfer, S. Honjo and P. J. Depetris, eds. Vol. 57 of *SCOPE*. Wiley, New York.

Hood, R. H., A. F. Michaels and D. G. Capone, 2000. The enigma of marine nitrogen fixation: answers on the horizon. *Eos Trans. AGU*, **81**(13), 133, 138, 139.

Houghton, J. T., L. M. Filho, B. A. Callander, N. Harris, A. Kattenberg and K. Maskell, 1996. *Climate Change 1995: The Science of Climate Change*. Intergovernmental Panel on Climate Change, Cambridge.

Howell, E. A., S. C. Doney, R. A. Fine and D. B. Olson, 1997. Geochemical estimates of denitrifications in the Arabian Sea and the Bay of Bengal during WOCE. *Geophys. Res. Lett.*, **24**(21), 2539–2552.

Hupe, A. and J. Karstensen, 2000. Redfield stoichiometry in Arabian Sea subsurface waters. *Global Biogeochem. Cycles*, **14**(1), 357–372.

Indermühle, A., T. F. Stocker, F. Joos, H. Fischer, H. J. Smith, M. Wahlen, B. Deck, D. Mastroianni, J. Tschumi, T. Blunier, R. Meyer and B. Stauffer, 1999. Holocene carbon-cycle dynamics based on CO_2 trapped in ice at Taylor Dome, Antarctica. *Nature*, **398,** 121–126.

Jahnke, R. A., D. B. Craven and J.-F. Gaillard, 1994. The influence of organic matter diagenesis on $CaCO_3$ dissolution at the deep-sea floor. *Geochim. Cosmochim. Acta*, **58**(13), 2799–2809.

Joos, F., G.-K. Plattner, T. F. Stocker, O. Marchal and A. Schmittner, 1999. Global warming and marine carbon cycle feedbacks on future atmospheric CO_2. *Science*, **284,** 464–467.

Karl, D. M., R. Letelier, D. V. Hebel, D. F. Bird and C. D. Winn, 1992. *Trichodesmium* blooms and new production in the North Pacific gyre. In *Marine Pelagic Cyanobacteria: Trichodesmium and Other Diazotrophs*. E. J. Carpenter, ed. Kluwer Academic Publishers, Dordrecht, The Netherlands, pp. 219–237.

Karl, D., R. Letelier, L. Tupas, J. Dore, J. Christian and D. Hebel. 1997. The role of nitrogen fixation in the biogeochemical cycling in the subtropical North Pacific Ocean. *Nature* 533–538.

Kawase, M. and J. L. Sarmiento, 1985. Nutrients in the Atlantic thermocline. *J. Geophys. Res.*, **90**(C5), 8961–8979.

Keeling, R. F. and T.-H. Peng, 1995. Transport of heat, CO_2 and O_2 by the Atlantic's thermohaline circulation. *Philos. Trans. R. Soc. London Ser. B*, **348,** 133–142.

Keeling, C. D., S. C. Piper and M. Heimann, 1989. A three dimensional model of atmospheric CO_2 transport based on observed winds. 4. Mean annual gradients and interannual variations. In *Aspects of Climate Variability in the Pacific and the Western Americas*, D. H. Peterson, ed. Geophysics Monograph Series, 55, American Geophysical Union, Washington, D.C., pp. 305–363.

Keeling, C. D., T. P. Whorf, M. Wahlen and J. v. d. Plicht, 1995. Interannual extremes in the rate of atmospheric carbon dioxide since 1980. *Nature*, **375,** 666–670.

Keir, R. S., 1980. The dissolution kinetics of biogenic calcium carbonates in seawater. *Geochim. Cosmochim. Acta*, **44,** 241–252.

Keir, R. S., 1991. The effect of vertical nutrient redistribution on surface ocean ^{13}C. *Global Biogeochem. Cycles*, **5**(4), 351–358.

Kleypas, J. A., R. W. Buddemeier, D. Archer, J.-P. Gattuso, C. Langdon and B. N. Opdyke, 1999. Geochemical consequences of increased atmospheric carbon dioxide on coral reefs. *Science*, **284,** 118–120.

Knauer, G. A., J. H. Martin and K. W. Bruland, 1979. Fluxes of particulate carbon, nitrogen and phosphorus in the upper water column of the northeast Pacific. *Deep-Sea Res.*, **26,** 445–462.

Laws, E. A., 1991. Photosynthetic quotients, new production and net community production in the open ocean. *Deep-Sea Res.*, **38**(1), 143–167.

Laws, E. A., P. Falkowski, E. Carpenter and H. Ducklow, 2000. Temperature effects on export production in the open ocean. *Global Biogeochem. Cycles*, **14**(4), 1231–1246.

Lefèvre, N. and A. J. Watson, 1999. Modeling the geochemical cycle of iron in the oceans and its impact on atmospheric CO_2 concentrations. *Global Biogeochem. Cycles*, **13**(3), 727–736.

Lenton, T. M. and A. J. Watson, 2000. Redfield revisited. 1. Regulation of nitrate, phosphate, and oxygen in the ocean. *Global Biogeochem. Cycles*, **14**(1), 225–248.

Levitus, S. and T. Boyer, 1994a. *NOAA Atlas NESDIS 2: World Ocean Atlas 1994*, Vol. 2, *Oxygen*. National Oceanic and Atmospheric Administration, Silver Spring, Md.

Levitus, S. and T. P. Boyer, 1994b. *NOAA Atlas NESDIS 3: World Ocean Atlas 1994*, Vol. 4, *Temperature*. National Oceanic and Atmospheric Administration, Silver Spring, Md.

Levitus, S., R. Burgett and T. Boyer, 1994. *NOAA Atlas NESDIS 3: World Ocean Atlas 1994*, Vol. 3, *Salinity*. National Oceanic and Atmospheric Administration, Silver Spring, Md.

Longhurst, A. R., 1991a. A reply to Broecker's charges. *Global Biogeochem. Cycles*, **5**(4), 315–316.

Longhurst, A. R., 1991b. Role of the marine biosphere in the global carbon cycle. *Limnol. Oceanogr.*, **36**(8), 1507–1526.

Luyten, J. L., J. Pedlovsky and H. Stommel, 1983. The ventilated thermocline. *J. Phys. Oceanogr.*, **13,** 292–309.

Mahowald, N., K. E. Kohfeld, M. Hansson, Y. Balkanski, S. P. Harrison, I. C. Prentice, M. Schulz and H. Rodhe, 1999. Dust sources and deposition during the Last Glacial Maximum and current climate: a comparison of model results with paleodata from ice cores and marine sediments. *J. Geophys. Res.*, **104,** 15895–15916.

Manabe, S. and R. J. Stouffer, 1993. Century-scale effects of increased atmospheric CO_2 on the ocean–atmosphere system. *Nature*, **364,** 215–218.

Mantoura, R. F. C., C. S. Law, N. J. P. Owens, P. H. Burkill, E. M. S. Woodward, R. J. M. Howland and C. A. Lewellyn, 1993. Nitrogen biogeochemical cycling in the northwestern Indian ocean. *Deep-Sea Res. II*, **40**(3), 651–671.

Martin, J. H., 1990. Glacial–interglacial CO_2 change: the iron hypothesis. *Paleoceanography*, **5**(1), 1–13.

Martin, J. H., G. A. Knauer, D. M. Karl, and W. W. Broenkow, 1987. Vertex: carbon cycling in the northeast Pacific. *Deep-Sea Res.*, **34**(2), 267–285.

Martin, H. M., R. Gordon and S. E. Fitzwater, 1990. Iron in Antarctic waters. *Nature*, **345,** 156–158.

Martin, J. H., S. E. Fitzwater and R. M. Gordon, 1991. Iron deficiency limits phytoplankton growth in antarctic waters. *Global Biogeochem. Cycles*, **4**(1), 5–12.

Martin, J. H., S. E. Fitzwater, R. M. Gordon, C. N. Hunter and S. J. Tanner, 1993. Iron, primary production and carbon–nitrogen flux studies during the JGOFS North Atlantic Bloom Experiment. *Deep-Sea Res. II*, **40**(1–2), 115–134.

Matear, R. J. and A. C. Hirst, 1999. Climate change feedback on the future oceanic CO_2 uptake. *Tellus Ser. B*, **51,** 722–733.

Meybeck, M., 1982. Carbon, nitrogen, and phosphorus transport by world rivers. *Am. J. Sci.*, **282,** 401–450.

Michaels, A. F., D. Olson, J. L. Sarmiento, J. Ammerman, K. Fanning, R. Jahnke, A. H. Knap, R. Lipschultz and J. Prospero, 1996. Inputs, losses and transformations of nitrogen and phosphorus in the pelagic North Atlantic Ocean. *Biogeochemistry*, **35,** 181–226.

Millero, F. J., 1983. Influence of pressure on chemical processes in the sea. In *Chemical Oceanography*, 2nd ed., J. P. Riley and R. Chester, eds. Academic Press, San Diego, Calif., vol. 8, Chap. 43, pp. 1–88.

Milliman, J. D., 1993. Production and accumulation of calcium carbonate in the ocean: budget of a nonsteady state. *Global Biogeochem. Cycles*, **7**(4), 927–957.

Milliman, J. D. and A. W. Droxler, 1996. Neritic and pelagic carbonate sedimentation in the marine environment: ignorance is not bliss, *Geol. Rundschau*, **85,** 496–504.

Milliman, J. D., P. J. Troy, W. M. Balch, A. K. Adams, Y.-H. Li and F. T. Mackenzie, 1999. Biologically mediated dissolution of calcium carbonate above the chemical lysocline? *Deep-Sea Res. I*, **46,** 1653–1669.

Minster, J. and M. Boulahdid, 1987. Redfield ratios along isopycnal surfaces: a complimentary study. *Deep-Sea Res.*, **34**(12), 1981–2003.

Morel, F. M. M. and R. J. M. Hudson, 1985. The geobiological cycle of trace elements in aquatic systems: Redfield revisited. In *Chemical Processes in Lakes*, W. Stumm, ed. Wiley, New York, pp. 251–281.

Morrison, J. M., L. A. Codispoti, S. L. Smith, K. Wishner, C. Flagg, W. D. Gardner, S. Gaurin, S. W. A. Naqvi, V. Manghnani, L. Prosperie and J. S. Gundersen, 1999. The oxygen minimum zone in the Arabian Sea during 1995. *Deep-Sea Res. II*, **46,** 1903–1931.

Murnane, R. J., J. L. Sarmiento and C. LeQuéré, 1999. The spatial distribution of air–sea fluxes and the interhemispheric transport of carbon by the oceans. *Global Biogeochem. Cycles*, **13,** 287–305.

Naqvi, S. W. A., 1987. Some aspects of the oxygen-deficient conditions and denitrification in the Arabian Sea. *J. Mar. Res.*, **45,** 1049–1072.

Naqvi, S. W. A. and M. S. Shailaja, 1993. Activity of the respiratory electron transport system and respiration rates within the oxygen minimum layer of the Arabian Sea. *Deep-Sea Res. II*, **40**(3), 687–695.

Naqvi, S., S. D. Souza and C. Reddy, 1978. Relationship between nutrients and dissolved oxygen with special reference to water masses in western Bay of Bengal. *Ind. J. Mar. Sci.*, **7,** 15–17.

Naqvi, S. W. A., R. J. Noronha and C. V. G. Reddy, 1982. Denitrification in the Arabian Sea. *Deep-Sea Res.*, **29**(4A), 459–469.

Naqvi, S. W. A., R. J. Noronha, K. Somasundrar and R. Sen Gupta, 1990. Seasonal changes in the denitrification regime of the Arabian Sea. *Deep-Sea Res.*, **37**(4), 593–611.

Neftel, A., H. Oeschger, J. Schwander, B. Stauffer and R. Zumbrunn, 1982. Ice core sample measurements give atmospheric CO_2 content during the past 40,000 yr. *Nature*, **295,** 220–223.

Nozaki, Y., 1997. A fresh look at elemental distribution in the North Pacific Ocean. *Eos Trans. AGU*, **78**(21), 221–223.

Oceanographic Data Facility (ODF), South Atlantic Ventilation Experiment (SAVE), 1992a. *Scripps Institute of Oceanography, Chemical, Physical and CTD Data Report. Legs 1–3*. Scripps, La Jolla, Calif.

Oceanographic Data Facility (ODF), South Atlantic Ventilation Experiment (SAVE), 1992b. *Scripps Institute of Oceanography, Chemical, Physical and CTD Data Report. Legs 4–5*. Scripps, La Jolla, Calif.

Orcutt, K. M., F. J. Lipschultz, K. Gundersen, R. Arimoto, J. R. Gallon, A. F. Michaels and A. H. Knap, 2001. Seasonal patterns and significance of N fixation by *Trichodesmium* at the Bermuda Time-Series (BATS) site. *Deep-Sea Res. II*, **48**(8–9), 1583–1608.

Orsi, A. H., C. Johnson and J. L. Bullister, 1999. Characteristics, circulation and production of Antarctic Bottom Water. *Prog. Oceanogr.*, **43,** 55.

Pedlovsky, J., 1987. *Geophysical Fluid Dynamics*. Springer-Verlag, New York.

Peng, T.-H., R. Wanninkhof, J. L. Bullister, R. A. Feely and T. Takahashi, 1998. Quantification of decadal anthropogenic CO_2 uptake in the ocean based on dissolved inorganic carbon measurements. *Nature*, **396,** 560–563.

Petit, J. R., J. Jouzel, D. Raynaud, N. I. Barkov, J.-M. Barnola, I. Basile, M. Bender, J. Chappellaz, M. Davis, G. Delaygue, M. Delmotte, V. M. Kotlyakov, M. Legrand, V. Y. Lipenkov, C. Lorius, L. Pépin, C. Ritz, E. Saltzman and M. Stievenard, 1999. Climate and atmospheric history of the past 420,000 years from Vostok ice core, Antarctica. *Nature*, **399,** 429–436.

Poisson, A. and C.-T. A. Chen, 1987. Why is there so little anthropogenic CO_2 in the Antarctic Bottom Water? *Deep-Sea Res.*, **34**(7), 1255–1275.

Prather, M., R. Derwent, D. Ehhalt, P. Fraser, E. Sanhueza and X. Zhou, 1994. In *Climate Change 94: Radiative Forcing of Climate Change*. Other trace gases and atmospheric chemistry. Intergovernmental Panel on Climate Change, Cambridge, pp. 77–126.

Redfield, A. C., 1958. The biological control of chemical factors in the environment. *Am. Sci.*, **46,** 205–221.

Redfield, A. C., B. H. Ketchum and F. A. Richards, 1963. The influence of organisms on the composition of sea-water. In *Composition of Sea Water*, M. N. Hill, ed. Vol. 2 of *The Sea*. Wiley-Interscience, New York, pp. 26–77.

Riebesell, U., D. A. Wolf-Gladrow and V. Smetacek, 1993. Carbon dioxide limitation of marine phytoplankton growth rates. *Nature*, **361,** 249–251.

Riebesell, U., I. Zondervan, B. Rost, P. D. Tortell, R. E. Zeebe and F. M. M. Morel, 2000. Reduced calcification of marine plankton in response to increased atmospheric CO_2. *Nature*, **407,** 364–367.

Rueter, J. G., D. A. Hutchins, R. W. Smith and N. L. Unsworth, 1992. Iron nutrition of *Trichodesmium*. In *Marine Pelagic Cyanobacteria: Trichodesmium and Other Diazotrophs*, E. J. Carpenter, ed. Kluwer Academic Publishers, Dordrecht, The Netherlands, pp. 289–306.

Ryther, J. G. and W. M. Dunstan, 1971. Nitrogen, phosphorus and eutrophication in the coastal marine environment. *Science*, **171,** 1008–1013.

Sabine, C. L., R. M. Key, K. M. Johnson, F. J. Millero, J. L. Sarmiento, D. W. R. Wallace and C. D. Winn, 1999. Anthropogenic CO_2 inventory of the Indian Ocean. *Global Biogeochem. Cycles*, **13**(1), 179–198.

Sambrotto, R. N., G. Savidge, C. Robinson, P. Boyd, T. Takahashi, D. M. Karl, C. Langdon, D. Chipman, J. Marra and L. Codispoti, 1993. Elevated consumption of carbon relative to nitrogen in the surface ocean. *Nature*, **363,** 248–250.

Sarmiento, J. L., 1991. Oceanic uptake of anthropogenic CO_2: the major uncertainties. *Global Biogeochem. Cycles*, **5**(4), 309–313.

Sarmiento, J. L. and C. LeQuéré, 1996. Oceanic carbon dioxide uptake in a model of century-scale global warming. *Science*, **274,** 1346–1350.

Sarmiento, J. L. and E. T. Sundquist, 1992. Revised budget for the oceanic uptake of anthropogenic carbon dioxide. *Nature*, **356,** 589–593.

Sarmiento, J. L. and J. R. Toggweiler, 1984. A new model for the role of the oceans in determining atmospheric pCO_2. *Nature*, **308,** 621–624.

Sarmiento, J. L., J. C. Orr and U. Siegenthaler, 1992. A perturbation simulation of CO_2 uptake in an ocean general circulation model. *J. Geophys. Res.*, **97**(C3), 3621–3645.

Sarmiento, J. L., T. M. C. Hughes, R. J. Stouffer and S. Manabe, 1998. Simulated response of the ocean carbon cycle to anthropogenic climate warming. *Nature*, **393,** 245–249.

Schmitz, W. J., 1996. On the world ocean circulation: Vol. II, *Technical Report WHOI-96-08*. Woods Hole Oceanographic Institution, Woods Hole, Mass.

Seitzinger, S. and A. Giblin, 1996. Estimating denitrification in North Atlantic continental shelf sediments. *Biogeochemistry*, **35**(1), 235–260.

Shaffer, G., 1996. Biogeochemical cycling in the global ocean. 2. New production, Redfield ratios, and remineralization in the organic pump. *J. Geophys. Res.*, **101**(C2), 3723–3745.

Shaffer, G., J. Bendtsen and O. Ulloa, 1999. Fractionation during remineralization of organic matter in the ocean. *Deep-Sea Res. I*, **46**(2), 185–204.

Shiller, A. M., 1981. Calculating the oceanic CO_2 increase: a need for caution. *J. Geophys. Res.*, **86**(C11), 11083–11088.

Shiller, A. M., 1982. Reply to comment by Chen et al., on "Calculating the oceanic CO_2 increase: a need for caution," by A. M. Shiller. *J. Geophys. Res.*, **87**(C3), 2086.

Siegenthaler, U. and T. Wenk, 1984. Rapid atmospheric CO_2 variations and ocean circulation. *Nature*, **308,** 624–626.

Sigman, D. M. and E. A. Boyle, 2000. Glacial/interglacial variations in carbon dioxide: searching for a cause. *Nature*, **407,** 859–869.

Smethie, W. M. J., 1993. Tracing the thermohaline circulation in the western North Atlantic using chlorofluorocarbons. *Progr. Oceanogr.*, **31,** 51–99.

Smith, S. V., 1984. Phosphorus versus nitrogen limitation in the marine environment. *Limnol. Oceanogr.*, **29**(6), 1149–1160.

Smith, S., M. Roman, K. Wishner, M. Gowing, L. Codispoti, R. Barber, J. Marra, I. Prusova and C. Flagg, 1998. Seasonal response of zooplankton to monsoonal revserals in the Arabian Sea. *Deep-Sea Res. II*, **45,** 2369–2404.

Stocker, T. F. and A. Schmittner, 1997. Influence of CO_2 emission rates on the stability of the thermohaline circulation. *Nature*, **388,** 862–865.

Stumm, W. and J. J. Morgan, 1981. *Aquatic Chemistry*, 2nd ed. Wiley-Interscience, New York.

Suntharalingam, P. and J. L. Sarmiento, 2000. Factors governing the oceanic nitrous oxide distribution: simulations with an ocean general circulation model. *Global Biogeochem. Cycles*, **14**(1), 429–454.

Takahashi, T., W. Broecker, S. Werner and A. E. Bainbridge, 1980. Carbonate chemistry of the surface waters of the world oceans. In *Isotope Marine Chemistry*, E. D. Goldberg, Y. Horibe and K. Saruhashi, eds. Uchida Rokakuho, Tokyo, pp. 291–326.

Takahashi, T., W. S. Broecker and S. Langer, 1985. Redfield ratio based on chemical data from isopycnal surfaces. *J. Geophys. Res.*, **90**(C4), 6907–6924.

Takhashi, T., J. Olafsson, J. G. Goddard, D. W. Chipman and S. C. Sutherland, 1993. Seasonal variation of CO_2 and nutrients in the high-latitude surface oceans: a comparative study. *Global Biogeochem. Cycles*, **7**(4), 843–878.

Takahashi, T., J. G. Goddard, S. Rubin, D. W. Chipman, S. C. Sutherland and C. Goyete, 1996. Carbon dioxide, hydrographic, and chemical data obtained in the central South Pacific ocean (WOCE sections P17S and P16S) during the TUNES-2-expedition of the R/V *Thomas Washington*, July–August 1991. *Carbon Dioxide Information and Analysis Center Data Report ORNL/CDIAC-86; NDP-054*. Oak Ridge National Laboratory, Oak Ridge, Tenn.

Takahashi, T., R. A. Feely, R. Weiss, R. H. Wanninkhof, D. W. Chipman, S. C. Sutherland and T. T. Takahashi, 1997. Global air–sea flux of CO_2: an estimate based on measurements of sea–air pCO_2 difference. In *Revelle Symposium: Proceedings of the National Academy of Science*, C. D. Keeling, ed. National Academy of Science, Washington, D.C., Vol. 94, pp. 8292–8299.

Takahashi, T., R. H. Wanninkhof, R. A. Feely, R. F. Weiss, D. W. Chipman, N. Bates, J. Olafsson, C. Sabine and S. C. Sutherland, 1999. Net sea–air CO_2 flux over the global oceans: An improved estimate based on the sea–air pCO_2 difference. In *2nd International Symposium. CO_2 in the Oceans, Extended Abstracts*. Center for Global Environmental Research, Tsukuba, Japan, pp. 9–15.

Tans, P. P., I. Y. Fung and T. Takahashi, 1990. Observational constraints on the global atmospheric CO_2 budget. *Science*, **247,** 1431–1438.

Tegen, I. and I. Fung, 1994. Modeling of mineral dust in the atmosphere: sources, transport and optical thickness. *J. Geophys. Res.*, **99,** 22897–22914.

Tyrrell, T., 1999. The relative influences of nitrogen and phosphorus on oceanic primary production. *Nature*, **400,** 525–531.

Villareal, T. A. and E. J. Carpenter, 1989. Nitrogen fixation, suspension characteristics, and chemical composition of rhizosolenia mats in the central Pacific gyre. *Bio. Oceanogr.*, **6,** 327–345.

Volk, T. and M. I. Hoffert, 1985. Ocean carbon pumps: analysis of relative strengths and efficiencies in ocean-driven atmospheric CO_2 changes. In *The Carbon Cycle and Atmospheric CO_2: Natural Variations Archean to Present*, E. T. Sundquist and W. S. Broecker, eds. Geophysics Monograph Series, 32, Washington, D.C., pp. 99–110.

Wada, E. and A. Hattori, 1991. *Nitrogen in the Sea: Forms, Abundance, and Rate Processes*. CRC Press, Boca Raton, Fla.

Warren, B. A., 1994. Context of the suboxic layer in the Arabian Sea. *Proc. Indian Acad. Sci.—Earth Planetary Sci.*, **103**(2), 301–314.

Wollast, R., 1991. The coastal organic carbon cycle: fluxes, sources and sinks. In *Ocean Margin Processes in Global Change*, R. Mantoura, J.-M. Martin and R. Wollast, eds. Wiley, New York, pp. 365–381.

Wu, J., W. Sunda, E. A. Boyle and D. M. Karl, 2000. Phosphate depletion in the western North Atlantic Ocean. *Science*, **289,** 759–762.

Wyrtki, K., 1973. The physical oceanography of the Indian Ocean. In *The biology of the Indian Ocean*. Springer-Verlag, New York, pp. 18–36.

Zehr, J. P., E. Carpenter and T. A. Villareal, 2000. New perspectives on nitrogen-fixing microorganisms in tropical and subtropical oceans. *Trends Microbiol.*, **8**(2), 68–73.

DO NOT PRINT

THIS PAGE INTENTIONALLY LEFT BLANK